# Microstructure Sensitive Design: A Tool for Exploiting Material Anisotropy in Mechanical Design

A Thesis

Submitted to the Faculty

of

Drexel University

by

Joshua Robert Houskamp

In partial fulfillment of the degree

of

Doctorate of Philosophy

November 2005

## Dedications

**I would like to dedicate my research to my parents who have always supported me.**

## Acknowledgements

Financial support for this work was provided by the Army Research Office, Proposal No. 42566-MS, Dr. David Stepp, Program Director.

The Koerner Family for their financial support.

My committee members: Dr. Kalidindi, Dr. Doherty, Dr. Lau, Dr. Zavaliangos, and Dr. Schoenfeld for their valuable advice.

Dr. Adams for his time and support.

My MMG research group, particularly for Dr. G. Proust, H Duvvuru, and M. Knezevic for their assistance in code development and programming.

My Friends and Colleagues for their support: Dr. G. Proust, Dr. J. Lyons, Dr. S. Mastro, H. Duvvuru, X. Wu, M. Knezevic, W. Wang, B. Woods, K. Behler, M. Birnkrant, J. Lee.

And especially my parents for their constant support.

# TABLE OF CONTENTS

## LIST OF TABLES

## LIST OF FIGURES

**ABSTRACT**

Microstructure Sensitive Design: Exploiting Material Anisotropy in Mechanical Design

Joshua R. Houskamp

Surya R. Kalidindi, Ph.D.

A new mathematical framework called Microstructure Sensitive Design (MSD) was recently developed to facilitate solutions to inverse problems in microstructure design where the goal is to identify the complete set of relevant microstructures that are predicted to satisfy a set of designer specified criteria for effective properties or performance. In this work, MSD has been successfully applied to a few design case studies involving polycrystalline metals and continuous fiber reinforced composites (CFRC). The solutions obtained are, as expected, strongly influenced by the selected homogenization theories. In the case studies presented here, elementary first-order theories are used for both the polycrystalline metals and the continuous fiber reinforced composites. In the composite case, elementary first-order theories spanning two length scales have been selected to obtain effective properties of continuous fiber reinforced composite material systems. Having selected these first-order theories, we proceeded to demonstrate the viability of applying the MSD framework to designing optimal orientation distributions in both polycrystalline metals and continuous fiber reinforced composites for the selected mechanical design problems. Specifically, the mechanical design case study used in this work involved maximizing the load carrying capacity of an orthotropic plate with a circular hole and loaded in in-plane tension. MSD results for this case study show a potential improvement of 27% in nickel polycrystals and 267%

improvement in AS4-Epoxy composites investigated in this study. Additionally the mechanical design of a pressure vessel containing a partially through axial flaw is examined; the potential improvement in energy dissipated during crack growth is 31%.

# CHAPTER 1. INTRODUCTION

In recent years, the discipline of materials science has witnessed the emergence of a grand challenge that had always implicitly defined this multidisciplinary field, namely, the ability to identify and process specific materials to yield microstructures that are predicted to meet or exceed multiple properties/performance criterion stipulated by the designer. Olson[1, 2] labeled this new paradigm as the "goals-means" approach where the target properties are used to define the processing routes to acquire the microstructure with those properties. This contrasts sharply with the traditional "cause and effect" approach that is driven mainly by innovations in processing, which typically focuses only a limited number of readily manufacturable microstructures. This inverted paradigm of materials design is especially critical for highly constrained design (HCD) applications, where the designer faces increasingly complex requirements with multiple property objectives/constraints and material anisotropy affecting system performance. It is in this context that a new microstructure design framework called Microstructure Sensitive Design (MSD) [3] was recently proposed.

MSD comprises a novel methodology to identify the best of all possible microstructures within a given mechanical and physical framework that meet the stipulated design performance requirements. Thus, information flow is in the 'inductive' direction: design objectives $\rightarrow$ properties $\rightarrow$ microstructure $\rightarrow$ processing. A dominant characteristic of MSD is its use of spectral representations in all aspects of the problem. These representations of microstructure can be used with established homogenization theory to estimate the effective properties of the material, and to frame the design requirements. The tensorial nature of spectral representations of microstructure and

microstructure/properties relations insures that an optimally compact and complete representation of microstructure is used – no more and no less than what is precisely needed for the representation of the problem. The reader is referred to earlier papers [3, 4] for further details of the technique, where the example of the optimal design of material microstructure for a compliant beam component and a hole in a plate were worked out in detail, respectively. This work details a fully integrated design methodology, and extends the MSD framework to a new material system.

MSD uses spectral representations of the distribution functions that characterize statistically the internal structure of a given material system, and formulates invertible quantitative linkages between these microstructure representations and their associated macroscale properties using existing homogenization theories or composite theories (often recast in a Fourier space).

Materials design is a broad area of research with several competing methodologies. Although many claim to be designing microstructures it is clearly evident that they lack the element of invertibility that is central to design. Many proposed "design" methodologies in current literature are simply forward models, or evaluation tools. In the interest of keeping this thesis concise the discussion on competing materials design methodologies will be restricted here to two approaches, which will be qualified as *novel engineering* materials design. Engineering Materials Design will be restricted to methodologies that have promise in the realm of engineering design. This definition will restrict the discussion of the several emerging nanotechnologies whereby materials are designed and built up atom by atom to have 'ideal' properties. While this may be a reality someday, it appears that this future is a long way off for any meaningful engineering

design. Similarly, this definition of design will prevent strictly forward models (multi-scale modeling) from being called design tools. While the multi-scale modeling tools are very useful tools in establishing forward models, multi-scale modeling does not yet have a framework that can determine the microstructure that is most useful for a particular design.

Under the restricted definition of design described above, two techniques currently exist that merit discussion here. These are the systems approach pioneered by Olsen [2, 5] and topology optimization methods [6-16], Of these techniques, the systems approach considers materials to be isotropic and therefore substantially limits the design space. Topology optimization largely considers the local states to be isotropic materials at the local state but the morphological arrangements of isotropic phases induce an effective anisotropic response at the macroscale [6-16].

An important distinguishing feature of MSD is that it rigorously accounts for the anisotropy of properties associated with the local state. Since materials are inherently anisotropic at the local state specifically with respect to mechanical properties, it is expected that the MSD methodology would prove to be much more beneficial for several engineered material systems. An additional advantage of MSD is the fact that it delineates a complete set of relevant material internal structures for a specified design problem; this will become apparent later with the discussion of property closures in Chapters 6 and with selected case studies Chapter 9.

The main focus of this thesis is to develop and evaluate the advantages and limitations of using an integrated MSD-FE Design Tool to design the internal structure of

a given materials system for meeting or exceeding targeted properties/performance criterion that can be applied to engineering design.

In this thesis, we will focus on continuous fiber reinforced composites and polycrystalline fcc metals. The treatment of discontinuously reinforced composites is expected to require the use of higher-order distribution functions in the statistical description of the material internal structure and is being pursued by others in the research group [17]. Furthermore, in the ensuing discussion, for clarity of presentation, we will present the mathematical framework of MSD for two specific classes of composites and one class of polycrystalline metals: (i) two-dimensional (2-D) composites, (ii) three-dimensional (3-D) composites, and (iii) cubic metals. Although the 2-D composite microstructures are essentially a subset of the 3-D composite microstructures, it will be seen that the Fourier basis required for the description of the complete set of 2-D composite microstructures is substantially simpler. It is hoped that this would help the reader in understanding better the mathematically complex concepts presented in this thesis. Chapter 3 will focus on the statistical description of the internal structure of fiber reinforced composites and cubic polycrystalline metals. Chapter 4 will present the delineation of microstructure hulls (the complete set of relevant microstructures) in Fourier space. The first-order homogenization relations selected for this first application of MSD to continuous fiber reinforced composites and polycrystalline metals are discussed in Chapter 5. These spectral representations will be used in Chapter 6 to formulate quantitative microstructure-property linkages in Fourier space and delineate the property closures (the complete set of all possible property combinations that could be achieved for a given material system). Chapter 7 discusses in

detail the components of the MSD tools with existing engineering design tools (FE). Chapter 8 discusses the integration and optimization methodologies. Case studies presented in Chapter 9 demonstrate the application of the MSD-FE design tool and presents results obtained in the MSD Framework for two simple design case studies.

# CHAPTER 2. MATERIALS DESIGN

The concept of materials design has been an emerging research topic for quite some time. Traditionally materials design has been driven by innovations in processing; this approach relies substantially on serendipity and exceptional observational skills (for example, the development of steel from iron and brass from bronze). However, the definition of materials design adopted here requires an intentional and informed approach to manipulating the material microstructure to obtain improved properties. The drive to design materials is driven by several factors: design better materials, better understand their behavior, design better structures with them, and shorten the development cycle from concept to implementation [18]. Computational materials design was identified to be specific area of opportunity for improvement, particularly where several material properties are often competing (i.e. strength and fracture toughness) [18]. Properties of materials are inherently linked to the microstructures and therefore present a grand opportunity for a design framework that can efficiently handle properties that are sensitive to the underlying microstructure.

Materials development has strong implications for the U.S. economy and considerations on national defense, and as such, the National Research Council has studied the effects of materials research and development. The cost of developing new materials is considerable but the failure to develop new and better materials can be even more costly, leading to a decline in the overall standing of the economy [18]. Materials development plays a strong role in the economy of the U.S. in addition to the national security [18]. Material design is a subject of interest among a wide group of parties including the Department of Defense, individual research groups [19, 20], as well as

companies that are more familiar to consumers such as Gillette [21], involved in a wide array of industries.

## 2.1. CURRENT DESIGN METHODS

Current engineered materials design methodologies may be grouped into three categories: topology optimization, a systems approach, and MSD. The details of the MSD framework will be addressed in subsequent chapters.

The most prevalent approach is topology optimization. In topology optimization, the problem is formulated as a material distribution problem and the focus is on the spatial arrangement of two to three, usually isotropic, phases resulting in macroscopically anisotropic materials. One of the phases under consideration is typically a void space which enhances the design space significantly, which means the designers may achieve properties ranging from no properties (void phase) to properties normally achieved by using bulk 'isotropic' materials. Initially published in 1988 by Bendsøe and Kikuchi [22] (currently) of the Technical University of Denmark and University of Michigan, respectively. The ideas of Bendsøe and Kikuchi lead the development Optistruct in 1994, [23] the software is available from Altair. The technique optimizes material placement in 2D and 3D space within the selected physical framework. Topology is an iterative optimization method in a discretized space and the performance is evaluated by finite element methods. Since 1994 there has been much activity in the area of topology optimization, several case studies have been successfully presented in literature and include materials with extreme thermal expansions [9, 24], piezoelectrics [11, 25], snap fit connectors [26], multiphysics actuators [27, 28], and negative Poisson's ratios [24].

Another approach called Materials by Design ®[5, 29] applies systems engineering concepts to materials design. Pioneered by Professor G. Olson in the Steel Research

Group at Northwestern University, this approach uses the link between microstructure (such as grain size and alloys) to affect the macroscopic properties (such as toughness and strength). The systems approach uses "reciprocity" to associate macroscopic properties with characteristic microstructure variables. The use of reciprocity for determining the microstructure variables is an imprecise definition that needs to be carefully applied in order to avoid considering non-physical material properties as design variables. This approach uses a set of forward models i.e. thermodynamic models, finite element methods (FEM), and solidification models to design materials. The set of forward models are empirically linked by the user using his or her judgment. The Materials by Design ® technique has largely assumed that the materials are isotropic and neglected anisotropy completely. The systems approach has had some notable successes in the design of stronger and tougher steel alloys [5]. The systems approach to materials design has been commercialized and is called Materials by Design ® by QuesTek.

At this point it may be worthwhile to also describe the current process typically used by mechanical designers. Most often, the typical designer relies upon compiled material databases [30-36] that generally provide only isotropic material properties. In rare cases, anisotropy may be considered in elasticity (for example for single crystals and for 3-D continuous reinforced composites). More enlightened designers use a systematic *materials selection* process in combination with iterative design on the geometry of the component usually using finite element methods (FEM). The most prevalent systematic materials selection database was developed by Ashby [30, 31]. He realized that knowledge designs often depend on more than one key material property. Ashby's approach was to plot properties of materials such that the designer has a visualization of

the combination of properties that are feasible from various materials. Although, these charts are useful for broad material comparisons, they cannot be used for highly constrained design since they are not refined enough to account the precise effect of the microstructure of a material on its properties and provide estimates of feasible property combinations. The charts were built using experimental data and are therefore limited to the set of materials and microstructures that have been experimentally tested. Therefore the charts do not reflect all of the feasible combinations of properties for a particular material system [37].

Microstructure Sensitive Design is a rigorous mathematical technique that has been recently developed by collaboration between Dr. B. Adams of Brigham Young University and Dr. S. R. Kalidindi of Drexel University. The MSD approach is a method that specifically accounts for material anisotropy and was initially published in 2001 [38]. It is a methodology that potentially can result in substantial gains in highly constrained designs. It presents a single unified mathematical framework that addresses microstructure representation, homogenization and performance of materials. The following chapters discuss the MSD framework and several applications of the methodology in detail.

Microstructure Sensitive Design is not in direct competition with either of the previously mentioned design techniques. The three techniques often address different often complimentary factors in materials design. Microstructure Sensitive Design in unique in that it addresses material anisotropy at the local state and how it affects the macroscale properties.

# CHAPTER 3. MSD FRAMEWORK

The starting point in MSD, is the statistical description of the material microstructure using local state distribution functions. The first order representation of statistics of microstructure is the 1-point distributions that reflect the probability density associated with realizing a specified local state (can be defined as an ordered series of several microstructural variables) in the neighborhood of a point thrown randomly into the microstructure (assumed to be a representative volume element of the material). Higher order descriptions, called *n*-point spatial correlation functions, are also possible [7, 39-42] [37], though neglected for the remainder of this work. These distributions are used to establish quantitative linkages between the microstructure and the bounds on their effective properties (using homogenization and/or statistical continuum theories) [37].

The MSD framework relies heavily upon spectral methods for representation of statistics of microstructures as well as effective properties and performance. The efficiency of MSD is derived from the fact that the Fourier basis used is already optimized to represent tensorial variables in the most economical way (i.e. the coordinate transformation properties expected from tensors are captured with the least number of terms in the Fourier expansion). It is worth noting that most physical properties of interest in design are tensorial in nature such as elasticity, plasticity, and thermal properties. The critical aspects of the MSD framework revolve around microstructure representation and homogenization methods (property estimates) which are discussed in detail in section 3.1 and Chapter 5.

## 3.1. MICROSTRUCTURE REPRESENTATIONS

Selection of the local descriptors of importance from the complex internal structure of a given material system for a given design problem is often the most difficult step. The

MSD framework described here relies heavily on the availability of robust physics-based models that can predict the macroscale properties for a specified material internal structure with reasonable or quantifiable accuracy. It is emphasized once again that the current focus of MSD is not on developing new physics in establishing the internal structure-property linkages, but in establishing these relationships using known physics in an invertible framework so that the problems of materials design can be addressed.

For this work, the local state, $h$, at any location in any material is adequately described by an ordered set of variables. The ordered variables may include phase, orientation, dislocation density, crosslink density, etc., for the materials of interest. For brevity the current examples are restricted to the phase ($\rho$) and orientation ($g$). The microstructure variables may readily be extended following the current framework for additional microstructural variables that are deemed to be important to the physics of the problem. For example a continuous fiber reinforced composites (CFRC) the phase denoted by $\rho$ and the orientation of the material frame denoted by $g$ constitutes the local state description, i.e. $h = (\rho, g)$ is shown in Figure 2. The examples involving polycrystalline metals described in this work are restricted to a single phase ($\rho = \text{constant}$), and therefore, the only microstructure variable considered in those examples is the local lattice orientation.

### 3.1.1. CONTINUOUSLY REINFORCED FIBROUS COMPOSITES

The local material frame is usually aligned along the principal axes of material anisotropy (in the present case it would be aligned with the fiber orientation). In the most general case, the local material frame is defined by a proper orthogonal rotation tensor, i.e. $g \in SO(3)$ ($SO(3)$ represents the set of all proper orthogonal tensors in the familiar

Euclidean 3-dimensional space). Additionally, materials often exhibit certain symmetries in the description of the local properties that are derived from the detail of the internal structure at the local scale. In order to take these into account and represent economically the local state space, a fundamental set or fundamental zone of local material frames is identified as $SO(3)/G^{\rho}$, where $G^{\rho}$ represents the symmetry subgroup associated with the selected local state descriptor, $\rho$.

Although the 2-D composite microstructures are essentially a subset of the 3-D composite microstructures, it will be seen that the Fourier basis required for the description of the complete set of 2-D composite microstructures is substantially simpler. It is also important to note that 2-D idealization for composites is much more common than the 3-D idealization. This comes largely from the processing methods commonly used, which often involve building composite laminates using thin single plies to build up a structure.

For the current example in composites we will restrict our attention to composite materials with only two phases: an anisotropic reinforcing fiber phase, *f*, and an isotropic matrix phase, *m*. Because of the isotropy of the matrix phase, it does not need a specification of material axes. However, the fiber reinforcement phase needs specification of a local material frame at any fiber location in the material system. As noted above, this would normally mean that the local material frame needs to be specified by a proper orthogonal tensor belonging to the fundamental set $SO(3)/G^{\rho}$. It will be further assumed here that the fiber phase has transversely isotropic mechanical properties with respect to the fiber axis. The local anisotropy in the fiber phase is then defined completely by the specification of a single material axis. In two dimensional (2-D)

composites where all fiber orientations are restricted to a single plane, the material axis can be specified by a single angle, $\theta \in [0,\pi)$ (see Figure 2). In three dimensional (3-D) composites, the material axis can be specified by an ordered pair of angles, $\phi \in [0,\pi), \beta \in [0,\pi)$ (see Figure 2).

In summary, the local state space representing the complete set of all possible distinct local states, for the 2-D and 3-D composite systems considered in this study, can be expressed as

$$\begin{aligned} &2-D:\ H_2 = H^m \cup H^{f2},\ H^m = \{m\},\ H^{f2} = \{(r,\theta)|\theta \in [0,\pi)\} \\ &3-D:\ H_3 = H^m \cup H^{f3},\ H^{f3} = \{(r,\phi,\beta)|\phi \in [0,\pi), \beta \in [0,\pi)\} \end{aligned} \tag{3.1}$$

where *H* represents the complete set of local states the composite may exhibit.

The required details of the spatial distribution of the local state in the internal structure of a given composite material system are fully dictated by the effective properties under consideration in a specific design problem and the homogenization theories selected for their estimation. Most composite (homogenization) theories utilize statistical descriptions of the spatial correlations of microstructure in establishing linkages between the internal structure and effective macroscale properties of a given material system. A rigorous framework exists for defining the necessary (normalized) distribution functions (see e.g. [12]), and these are usually referred to as the spatial correlation functions. The simplest of these are the 1-point (1-pt.) distribution that simply reflect the probability density of realizing a specific local state, *h*, in the immediate neighborhood of a point thrown randomly into the internal structure of the material, and is usually denoted as $f(h)$. The 1-pt. distribution essentially contains information about the volume fractions of the distinct local states in the microstructure, and does not reflect

any spatial correlations of these local states. The first order spatial correlations of the local states are actually captured by the 2-pt. correlation function, $f_2\left(h,h'|\mathbf{r}\right)$, which describes the probability density associated with finding the local states $h$ and $h'$ in the immediate neighborhood of the tail and the head of a vector $\mathbf{r}$ thrown randomly into the internal structure of the material. As mentioned earlier, in this first foray of MSD into composite material systems, we will restrict our attention to the 1-pt distributions and the associated first-order homogenization theories described in Section 5.1. Extension of MSD to include the 2-pt spatial correlation function, and the utilization of the advanced homogenization theories (also called statistical continuum theories [39, 43-46]) that use the 2-pt spatial correlations is still in its infancy [47].

The 1-pt distribution, *f(h)*, is usually defined as probability density (as opposed to defining directly the probability itself), because the local state space ($H$) is often a continuous space. For a continuous local state space the 1-pt distribution is defined such that

$$f\left(h\right)dh=\frac{dV_h}{V},\qquad \int_H f\left(h\right)dh=1 \tag{3.2}$$

where $dV_h/V$ denotes the volume fraction of the material that is associated with a local state that lies in the neighborhood $dh$ of $h$. It should be stressed here that $dh$ needs to be defined as an invariant measure of the local state space (see e.g. [48]). In the composite material systems being studied here, the local state space consists of some discrete local states (e.g. the separation of material into $m$ and $f$) and some continuous state spaces (see Eq. (3.1)). Therefore, the 1-pt statistics of the microstructure will be specified for these materials by a combination of volume fractions (for the discrete local states describing

the phase) and distribution functions (for the continuous local state space describing the material frame of the reinforcing fiber phase). For the idealized 2-D composites, the 1-pt statistics are specified by the set $\{V_f, f(\theta)\}$, where $V_f$ is the total volume fraction of the reinforcing phase, and *f(θ)* is suitably defined by Eq. (3.2). Likewise, for the 3-D composites, the 1-pt. statistics of the internal structure of the composite are described by $\{V_f, f(\phi,\beta)\}$.

We shall find it convenient in MSD to seek Fourier representations of the distributions described above. The orthonormal basis selected depends strongly on the description of the local state space. These can vary from the primitive indicator functions [49] to classical exponential functions [49] to spherical harmonics [48], depending on the specific application. Building on previous work [38], the following Fourier representations are adopted for the distributions described above for the 2-D and 3-D composite systems.

$$\begin{aligned} &2-D:\ f(\theta)=\sum_{l=-\infty}^{\infty} F_l e^{il\theta} \\ &3-D:\ f(\phi,\beta)=\sum_{l=0}^{\infty}\sum_{m=-l}^{l} F_l^m k_l^m(\phi,\beta) \end{aligned} \tag{3.3}$$

In the Fourier representations shown in Eq. (3.3), classical exponential functions were used for *f(θ)* and the surface spherical harmonic functions, $k_l^m(\phi,\beta)$ [48], were used for *f(ϕ,β)*. While other choices of Fourier basis are possible, it will be seen later that these choices of the Fourier basis produce the most economical representation of the internal structure-property relationships being sought. The coefficients $\{F_l\}$ and $\{F_l^m\}$ will be referred to as the Fourier coefficients of the material internal structure, and represent

uniquely the functions $f(\theta)$ and $f(\phi,\beta)$ as single points in their respective infinite dimensional Fourier spaces.

As mentioned earlier, certain material and processing symmetries arise in most problems. These symmetries not only reduce the local state space (Eq. (3.1)), but also reduce the number of terms needed in the Fourier representations shown in Eq. (3.3). In the problems under consideration here, the following symmetries reflect the fact that the assignment of local material axis at any fiber location can be accomplished in two equivalent ways (positive and negative directions along the fiber).

$$f(\theta+\pi)=f(\theta),\ f(\pi-\phi,\pi+\beta)=f(\phi,\beta) \tag{3.4}$$

Imposition of the symmetries in Eq. (3.4) compact the Fourier representations in Eq. (3.3) into the following forms:

$$\begin{aligned} &2-D:\ f(\theta)=\sum_{l=-\infty,2}^{\infty}F_l e^{il\theta} \\ &3-D:\ f(\phi,\beta)=\sum_{l=0,2}^{\infty}\sum_{m=-l}^{l}F_l^m k_l^m(\phi,\beta) \end{aligned} \tag{3.5}$$

the notation on the summation sign implies that $l$ is even and is a direct consequence of the continuous fiber assumption Eq. (3.4).

In addition to the implicit symmetries of the problem such as those in Eq. (3.4), one can impose additional symmetries on the problem dictated by other factors. For example, one can impose orthorhombic sample symmetry, i.e. only those internal structures that reflect orthorhombic sample symmetry (obtained by the processing or manufacturing routes) are to be considered in the design. In the case studies presented here, we will impose orthorhombic sample symmetry. This will impose the following requirements:

$$\begin{aligned} &2-D:\ f(\pi-\theta)=f(\theta) \\ &3-D:\ f(\phi,\beta)=f(\phi,\pi-\beta)=f(\pi-\phi,\pi-\beta)=f(\pi-\phi,\beta) \end{aligned} \tag{3.6}$$

These requirements further restrict the associated local state spaces and further compact the Fourier representations of the 1-pt. distributions as follows:

$$\begin{aligned} &2-D:\ H_2=H^m\cup H^{f2},\ H^m=\{m\},\ H^{f2}=\{(r,\theta)|\theta\in[0,\pi)\} \\ &3-D:\ H_3=H^m\cup H^{f3},\ H^{f3}=\{(r,\phi,\beta)|\phi\in[0,\pi/2],\beta\in[0,\pi/2]\} \end{aligned} \tag{3.7}$$

$$\begin{aligned} &2-D:\ f(\theta)=F_0+2\sum_{l=2,2}^{\infty}F_l\cos(l\theta) \\ &3-D:\ f(\phi,\beta)=\sum_{l=0,2}^{\infty}\sum_{\mu=-l}^{l}F_l^{\mu}\dot{k}_l^{\mu}(\phi,\beta) \end{aligned} \tag{3.8}$$

Note that the imposition of the orthorhombic sample symmetry precludes the need for the imaginary terms in the Fourier expansion of the distribution functions ($\dot{k}_l^{\mu}(\phi,\beta)$ are real-valued functions, while $k_l^m(\phi,\beta)$ are complex-valued functions [48]) and reduces dramatically the number of independent terms in the series expansion (M($l$)). This indicates that the number of these functions depends on the value of $l$ and these have been enumerated in [48]. Furthermore, the orthonormality of the Fourier basis, the normalization requirement of Eq. (3.2), and the requirement for an invariant measure of local state space, result in the derivation of the following expressions for the Fourier coefficients in Eq. (3.8).

$$\begin{aligned} &F_l=\int_{H^{f2}}f(\theta)\cos(l\theta)dh, \qquad dh=\frac{2}{\pi}d\theta \\ &F_l^{\mu}=\iint_{H^{f3}}f(\phi,\beta)\dot{k}_l^{\mu}(\phi,\beta), \quad dh=\frac{2}{\pi}\sin\phi d\phi d\beta \end{aligned} \tag{3.9}$$

Note that the invariant measures of local state space used in Eq. (3.9) have been normalized to yield $f(\theta) = f(\phi,\beta) = 1$ for material internal structures that contain a uniform

distribution of all the local states from their respective fundamental sets of local state space. For these special microstructures, it also follows from Eq. (3.9) that only the first Fourier coefficient (corresponding to *l = 0*) is non-zero and its value is equal to one.

### 3.1.2. POLYCRYSTALLINE METALS

Polycrystalline metals exhibit anisotropy that is very important scientifically as well as industrially. For example aluminum in deep drawing exhibits earring, that is nonuniform deformation that results in uneven edges at top of a deep drawn aluminum can, as shown in Figure 3. It is understandable that earring requires an extra trimming step to produce a final aluminum can which is costly and undesirable. The source of this anisotropy is in the distribution of the crystallographic orientations of the grains of the metal, schematically shown in Figure 4. As with the composite system, it is convenient to represent individual grain orientations with respect to a fixed reference frame (in this case the sample frame). In the polycrystalline metal, this requires a set of three rotations to transform the sample frame to the crystal frame. These rotations are commonly referred to as Euler angles; the notation used here is described by Bunge [48, 50] and most commonly used for textured materials. Figure 5 shows the set of rotations explicitly, i) rotation around the axis $Z_s$ (sample Z axis in Figure 5) of an angle $\varphi_1$, ii) rotation around the axis $X_s'$ (new axis obtained after first rotation of the axis $Z_s$) of an angle $\Phi$, iii) rotation around the axis $Z_s'$ (new axis $Z_s$ obtained after the second rotation of about $X_s'$) of an angle $\varphi_2$.

Mathematically, the coordinate transformation is described by an orthonormal rotation matrix $\mathbf{g}$.

$$\mathbf{e}^s = \mathbf{g}\mathbf{e}^c \tag{3.10}$$

where $\mathbf{e}^s$ and $\mathbf{e}^c$ are the basis vectors describing the sample frame and crystal frame, respectively. The rotation matrix $\mathbf{g}$ can be decomposed to describe each rotation mentioned previously as

$$\mathbf{g}_{\varphi_1} = \begin{pmatrix} \cos\varphi_1 & \sin\varphi_1 & 0 \\ -\sin\varphi_1 & \cos\varphi_1 & 0 \\ 0 & 0 & 1 \end{pmatrix} \tag{3.11a}$$

$$\mathbf{g}_{\Phi} = \begin{pmatrix} 1 & 0 & 0 \\ 0 & \cos\Phi & \sin\Phi \\ 0 & -\sin\Phi & \cos\Phi \end{pmatrix} \tag{3.11b}$$

$$\mathbf{g}_{\varphi_2} = \begin{pmatrix} \cos\varphi_2 & \sin\varphi_2 & 0 \\ -\sin\varphi_2 & \cos\varphi_2 & 0 \\ 0 & 0 & 1 \end{pmatrix} \tag{3.11c}$$

The overall rotation is described by the multiplication of the rotations as

$$\mathbf{g}^{\mathbf{T}} = \mathbf{g}_{\varphi_2}\mathbf{g}_{\Phi}\mathbf{g}_{\varphi_1} \tag{3.12}$$

$$\mathbf{g} = \begin{pmatrix} \cos\varphi_1\cos\varphi_2 - \sin\varphi_1\sin\varphi_2\cos\Phi & -\cos\varphi_1\sin\varphi_2 - \sin\varphi_1\cos\varphi_2\cos\Phi & \sin\varphi_1\sin\Phi \\ \sin\varphi_1\cos\varphi_2 + \cos\varphi_1\sin\varphi_2\cos\Phi & -\sin\varphi_1\sin\varphi_2 + \cos\varphi_1\cos\varphi_2\cos\Phi & -\cos\varphi_1\sin\Phi \\ \sin\varphi_2\sin\Phi & \cos\varphi_2\sin\Phi & \cos\Phi \end{pmatrix} \tag{3.13}$$

With no symmetry (triclinic) any lattice orientation can be represented within the bounds of $\Phi$ from 0 to $\pi$ and both $\varphi_1$ and $\varphi_2$ from 0 to $2\pi$. With the symmetries under consideration in this thesis some orientations would have multiple, equivalent representations.

The sample symmetry also influences the range of the Euler angles. The symmetry elements for the orthorhombic symmetry are three 2-fold symmetry axes parallel to each of the three sample axes; these symmetries reduce the range of $\varphi_1$ to a quarter of its original size, thus $\varphi_1$ varies from 0 to $\pi/2$. The crystal symmetry changes the range of the

two other angles $\Phi$ and $\varphi_2$. For example an n-fold symmetry axis reduces the Euler space by a factor n [51].

Cubic crystals have 24 distinct fundamental zones when we take into account the lattice symmetry. The orthorhombic sample symmetry will further reduce the size of the fundamental zone by a factor of 4. The fundamental zone most commonly used for a cubic-orthorhombic polycrystalline material is:

$$FZ = \left\{ (\phi_1, \Phi, \phi_2) \middle| 0 \le \phi_1 \le \frac{\pi}{2}, \cos^{-1}\left( \frac{\cos\varphi_2}{\sqrt{1+\cos^2\phi_2}} \right) \le \Phi \le \frac{\pi}{2}, 0 \le \phi_2 \le \frac{\pi}{4} \right\} \qquad (3.14)$$

The local state $h$ in Eq. 3.2 is then represented by only one parameter, the lattice orientation **g**. For these materials, the 1-point correlation function is referred to as the Orientation Distribution Function or simply as ODF and is denoted by f(**g**). The local state space H is, in this case, equivalent to the fundamental zone of the Euler space. The fundamental zone is dependent on the crystal and sample symmetries.

In this work, polycrystalline nickel was studied, which has a face centered cubic (fcc) crystal arrangement. The sample symmetry is taken to be orthorhombic (many of the typical processing operations used on metals such as rolling produce this symmetry) as is rolling is typically used to produce thin plates.

Fourier representations of the distributions described above for the cubic-orthorhombic microstructure systems is most efficiently done by generalized spherical harmonics that have the symmetries built in. Discussion of how the symmetries are

incorporated are given in detail in [50]. The $\dddot{T}_l^{\mu\nu}(g)$[1] will represent the basis functions that incorporate the symmetries. In spherical harmonics, the ODF is expressed as

$$f(g)=\sum_{l=0}^{\infty}\sum_{\mu=-l}^{M(l)}\sum_{\nu=-l}^{M(l)}\frac{F_l^{\mu\nu}\dddot{T}_l^{\mu\nu}(g)}{2l+1} \tag{3.15}$$

As is the case with the orthorhombic composites, the imposed orthorhombic symmetry precludes the need for imaginary terms in the Fourier expansion ($\dddot{T}_l^{\mu\nu}(g)$ are real valued functions while $T_l^{mn}(g)$ are complex valued functions [50]).The derivation for determining the Fourier coefficients is shown in Appendix D. The resulting expression for the Fourier coefficients for a given single crystal microstructure is

$$F_l^{\mu\nu}=(2l+1)\dddot{T}_l^{*\mu\nu}(g_i) \tag{3.16}$$

Note that an invariant measure has used to normalize $f(g)=1$ for the material internal structures that contain uniform distribution of all the local states. This special microstructure, directly following from Eq. (3.16) is such that only the first Fourier coefficient (corresponding to *l*=0) is nonzero and its value is equal to one. The physical realization of this would be a completely random textured polycrystalline metal, which results in completely isotropic material properties.

In concluding this chapter, the following connections were made between the distribution functions described above and their direct experimental measurement. First, it is important to note that these distributions are to be measured on a statistically relevant collection (ensemble) of samples, obtained with nominally similar manufacturing process

[1] Note the imposed symmetry is represented using a two-fold notation. The (:.) above the basis functions represent the cubic material symmetry (:), and orthorhombic processing symmetry (.).

or conditions. Second, each sample (also called the representative volume element or RVE) is expected to be sufficiently large in size that the measured distributions from the different samples of the ensemble are sufficiently close to each other (within a specified acceptable tolerance). Third, since most measurements probes used are unable to interrogate the interior of a material, one has to resort to some sort of automated serial sectioning [52-54] to reconstruct the internal structure of the material, and then extract the distributions described above from those reconstructions. The recent advances in 3-D X-ray tomography [55, 56] offer tremendous promise in this regard. Assuming that a three dimensional description of the material internal structure has been acquired using one of these techniques, the 1-pt distributions may be established as follows:

A large number of points could be thrown randomly into the internal structure and each point would then be associated with one of the possible local states. The local state space, H, should be discretized into several cells, such that each cell has the same invariant measure *dh*. For higher accuracy, the fundamental set should be discretized into a very large number of cells. However, the cell size should not be made smaller than the resolution limits of the measurement techniques used. Each material point can be associated with one of the discretized cells in the fundamental set of the local state space. From the fraction of points associated with each cell, the value of the distribution function for that cell can be computed using the first part of Eq. (3.2), and the integration in Eq. (3.9) permits computation of the Fourier coefficients.

# CHAPTER 4. MICROSTRUCTURE HULLS

The term microstructure hull is used to represent the complete set of distributions in the appropriate Fourier space that correspond to all physically realizable microstructures. In the realm of one point statistics of microstructure, the microstructure hull becomes an infinite dimensional convex space that contains the complete set of microstructures that are relevant to the physics of the problem. In the case studies that follow, the orientation descriptor of the local state was deemed to be the most important source of material property variability. It is recognized that there are other microstructure variables that affect properties as well, however most other material variables are either scalar quantities (the mathematical treatment presented can be easily extended) or the physics is less completely understood.

The complete set of microstructures to be considered for composite materials considered in this case is a two phase composite; considering an isotropic matrix and an anisotropic fiber phase. The matrix is isotropic and the 1-pt statistics of the matrix are completely determined by a single parameter, i.e. the volume fraction of the matrix. The fiber distributions in 2D and 3D have orientation dependence, and the range of microstructures that are physically realizable, are described in section (4.1). Likewise, polycrystalline metals are orientation dependent.. The detailed descriptions of the feasible microstructures are given in section (4.2).

## 4.1. COMPOSITE MICROSTRUCTURE HULL

As noted earlier, the focus here will be the 1-pt microstructure hull. In order to delineate the microstructure hull, it is convenient to start with certain special microstructures that are called “eigen” microstructures or “single-state” microstructures

in MSD. The local state distributions for these eigen microstructures are conveniently represented by Dirac functions:

$$f(h)=\delta(h-h_i),\quad \int_{H_i}\delta(h-h_i)dh=\begin{cases}1\ if\ h_i\in H_i\\ 0\ if\ h_i\notin H_i\end{cases}\quad \forall\ H_i\subset H \tag{4.1}$$

The distribution functions described in Eq. (4.1) imply that the eigen microstructures are allowed to possess only one local state. In practical terms, this means that a 2-D orthorhombic composite eigen microstructure is realized by assembling laminates with orientation $\theta$ and $-\theta$ in equal parts. Similarly an orthorhombic 3-D composite eigen microstructure can be realized by assembling a set of four unidirectional laminate systems that are selected specifically to satisfy the required elements of the orthorhombic symmetry group. The concept of eigen microstructures is repeated for polycrystalline metals as a decomposition of polycrystalline materials into a representative set of single crystals.

The complete set of all physically realizable 1-pt. distributions, ***M*****,** can now be represented as

$$M=\left\{f(h)\middle|f(h)=\sum_j\alpha_j\delta(h-h_j);\sum_j\alpha_j=1;\alpha_j>0;h_j\in H\right\} \tag{4.2}$$

Eq. (4.2) reflects the fact that any physically reliable microstructure has to be comprised of the elements of the set of eigen microstructures described earlier, and that this assemblage has to be accomplished in such a way that the volume fractions of the various eigen microstructures must be positive and add up to one.

Substituting the Dirac distributions of Eq. (3.9) into Eq. (4.1) yields the Fourier coefficients for the eigen microstructures. Let $\hat{M}$ represent the complete set of Fourier

coefficients for all eigen microstructures. This set for the idealized 2-D and 3-D composite materials considered here can be expressed as:

$$\begin{aligned} 2-D:\ \hat{M} &= \left\{ \hat{F}_l \middle| \hat{F}_l = \cos(l\theta); \theta \in ([0, \pi/2]) \right\} \\ 3-D:\ \hat{M} &= \left\{ \hat{F}_l^{\mu} \middle| \hat{F}_l^{\mu} = \dot{k}_l^{\mu}(\phi, \beta); \phi \in ([0, \pi/2]; \beta[0, \pi/2]) \right\} \end{aligned} \tag{4.3}$$

Using $\hat{M}$ together with Eq. (4.3), one can construct the complete set of Fourier coefficients corresponding to all physically realizable microstructures, referred to as microstructure hull in MSD and denoted as $\widetilde{M}$ .

$$\begin{aligned} 2-D: \tilde{M} &= \left\{ F_l \middle| F_l = \sum_j \alpha_j \hat{F}_l; \sum_j \alpha_j = 1; \alpha_j > 0; \hat{F}_l \in \hat{M} \right\} \\ 3-D: \tilde{M} &= \left\{ F_l^{\mu} \middle| F_l^{\mu} = \sum_j \alpha_j \hat{F}_l^{\mu}; \sum_j \alpha_j = 1; \alpha_j > 0; \hat{F}_l^{\mu} \in \hat{M} \right\} \end{aligned} \tag{4.4}$$

Equation (4.4) essentially defines $\widetilde{M}$ as a compact convex hull (region) in Fourier space, where the vertices of the convex hull are elements of $\hat{M}$ . Note that this compact convex hull exists in an infinite dimensional Fourier space. It can be shown that the projections of this convex hull in any of its finite dimensional subspaces are also convex. Figure 6 depicts the projection of the convex hull defined in Eq. (4.4) in the lower dimensions of their respective Fourier spaces. Note that any physically realizable idealized 2-D or 3-D composite material under consideration here is guaranteed a representation either on the surface or inside of the hulls depicted in Figure 6. The locations of a few selected microstructures are also shown. The eigen microstructures in this case happen to lie on the curved line segment ABC. Point D on the boundary of the microstructure hull is not an eigen microstructure. However, it lies exactly midway on the line joining Points A and C, and can therefore be realized by mixing the microstructures

corresponding to these points in equal volume fractions. Therefore, Point D corresponds to a 0/90 laminate composite. Similarly the interior points of the hull can be realized in a number of different ways. For example, Point O (at the origin) can be realized by mixing microstructures corresponding to points D and B in equal parts or by mixing microstructures corresponding to points E and F in equal parts. It should therefore be recognized that the interior points of the hulls shown in Figure 6 do not correspond to a single unique microstructure. Just as important, a distribution corresponding to a point outside the depicted hull in Figure 6 will not correspond to a physically realizable microstructure.

### 4.2. METAL POLYCRYSTALLINE MICROSTRUCTURE HULL

The polycrystalline hull is obtained in the same manner as the composite microstructure hull. Similarly the focus here will be on the 1-pt. polycrystalline microstructure hull. In order to delineate the microstructure hull; it is convenient to start once again with the "eigen" microstructures. In the context of polycrystalline metals, an eigen microstructure corresponds to a microstructure with a single orientation. i.e. a single crystal. The state distributions for these single crystals are represented in Eq. (4.1) where $h$ is replaced by $\mathbf{g}$.

The complete set of physically realizable 1-pt distributions, $M$, can be represented by

$$M = \left\{ f(g) \middle| f(g) = \sum_j \alpha_j \delta(g - g_j);\ \sum_j \alpha_j = 1; \alpha \geq 0;\ g \in FZ \right\} \tag{4.5}$$

Eq. (4.5) is analogous to Eq. (4.2) for composites, and reflects that any physically realizable microstructure has to be comprised of the elements of the set of all eigen microstructures, or equivalently that any polycrystal is made from a set of single crystals.

The assemblage of these single crystals is such that the volume fractions of the single crystals must be positive and sum to one.

By substituting the Dirac distributions of Eq. (3.16) into Eq. (4.1) yields the Fourier coefficients for the single state microstructures. Let $\hat{M}$ represent the complete set Fourier coefficients of single state microstructures. This set for cubic orthorhombic metals is expressed as[2]:

$$\hat{M} = \left\{ \hat{F}_l^{\mu\nu} \middle| \hat{F}_l^{\mu\nu} = (2l+1)\dot{\dot{T}}_l^{*\mu\nu}(g); g \in [FZ] \right\} \tag{4.6}$$

Using Eqns. (3.16) and (4.1) and making use of Eq. (4.6) one can now identify the complete set of Fourier coefficients corresponding to all physically realizable microstructures, referred to as microstructure hull in MSD and denoted as $\widetilde{M}$.

$$\widetilde{M} = \left\{ F_l^{\mu\nu} \middle| F_l^{\mu\nu} = \sum_j \alpha_j \hat{F}_l^{\mu\nu}; \sum_j \alpha_j = 1; \alpha_j \geq 0; \hat{F}_l^{\mu\nu} \in \hat{M} \right\} \tag{4.7}$$

Equation (4.7) defines $\widetilde{M}$ the compact convex hull for polycrystalline metals in Fourier space, where the vertices are elements of $\hat{M}$. Note that this compact convex hull exists in infinite dimensions in Fourier space. Figure 7 depicts the first three non-zero Fourier coefficients. Note that any physically realizable microstructure under consideration is guaranteed a representation either inside or on the surface of the hull in Figure 7.

In concluding this chapter, it is important to take away the message that the microstructure hull is i) convex and ii) contains all physically realizable 1-pt. distribution functions. Convexity is important because search algorithms in convex spaces are widely

[2] Note the change of indices on the spherical harmonics

known. The more important aspect is that the hull contains all 1-pt. distributions that may be obtained physically, and that if the 1-pt. distribution lies outside the hull, it cannot exist physically. The consequence of this is that the selection of microstructures is bounded to real microstructures and there is a method to determine whether a microstructure exists from its Fourier representation.

# CHAPTER 5. HOMOGENIZATION

Homogenization theories are commonly used in studies of composite materials that consist of domains of different local states (phases or orientation for composites and lattice orientation for polycrystalline metals). Homogenization is a method for addressing the effective (or continuum level) properties of material consisting of multiple local states or phases at their respective volume fractions. In this work the homogenization is based on the volume fractions and requires only one-point statistics of the microstructure, consistent with the previous chapter on microstructure representation.

The emphasis here is on formulating and exploring invertible microstructure-effective property linkages using known homogenization theories. We will therefore focus mainly on the mathematical framework of MSD, and in doing so we will limit ourselves to the currently used homogenization theories in composite textbooks and literature, ignoring their known inadequacies and limitations. It is envisioned that advanced homogenization theories, when they become available in the literature, can be readily incorporated into the general mathematical framework of MSD following the same techniques given in this chapter.

In general, any local property that has a dependence on the local state (e.g. lattice or fiber orientation) can be represented in the same Fourier space that was used to represent the statistics of the microstructure. Any general property may be represented as

$$
\begin{aligned}
&2-D_{\text{Composite}}: P(\theta) = P_0 + 2\sum_{l=2,2}^{\infty} P_l e^{il\theta} \\
&3-D_{\text{Composite}}: P(\phi,\beta) = \sum_{l=0,2}^{\infty}\sum_{m=-l}^{+l} P_l^m k_l^m(\phi,\beta) \\
&\textit{Polycrstalline Metal}: P(g) = \sum_{l=0}^{\infty}\sum_{m=-l}^{+l}\sum_{n=-l}^{+l} \frac{P_l^{mn} T_l^{mn}(g)}{2l+1}
\end{aligned}
\tag{5.1}
$$

for the 2-D and 3-D composites, and polycrystalline metals. Where $\{P_l\}$, $\{P_l^m\}$, and $\{P_l^{mn}\}$ represent the set of Fourier coefficients specific to the selected tensorial property. If the simple volume averaging homogenization rule (often corresponding to the upper bound theory) is selected for the macroscale effective property of the material, it can be expressed as

$$\langle P \rangle = \oint_H f(h) P(h) dh \tag{5.2}$$

It can be seen that the Fourier representation of the functions $P(h)$ and $f(h)$ will beneficial in the following sections, in evaluating the integral shown in Eq. (5.2), because of the orthonormality of the Fourier basis.

## 5.1. HOMOGENIZATION: COMPOSITES

Composites often consist of materials with very different material properties, such as the carbon (AS-4) fiber, epoxy matrix composite studied herein. The most commonly used homogenization scheme is the rule of mixtures, which suggest that the composite properties are represented by the proportion of the material present (treating the constituent materials as isotropic). This work specifically incorporates anisotropy, and therefore the homogenization schemes are necessarily altered. The homogenization scheme that was used for this study was a two level scheme; the first level estimates the effective properties of a single ply, the second level estimates the effective properties for the entire composite. The details for the homogenization scheme are given in the following sections.

The first order homogenization methods presented here however neglect physical features such as interface bonding. For more realistic material performances, significantly more sophisticated homogenization methods are required.

### 5.1.1. FIRST-ORDER ELASTICITY HOMOGENIZATION THEORIES

As mentioned earlier, our goal in this paper is to explore the application of MSD concepts to continuous fiber reinforced 2-D and 3-D composites using first-order theories for their effective elastic and failure behavior. It is also not the goal to present a comprehensive review of the currently used homogenization theories, but merely to summarize briefly the specific homogenization theories were selected (mainly for their simplicity) for this study.

For the 2-D and 3-D composite materials systems of interest here, it is convenient to consider a two-scale homogenization theory. In this approach (see e.g. [57, 58]), the composites are idealized to be comprised of a number of unidirectional reinforced laminate systems (see Figure 6), all of which contain the same amount of the reinforcing fiber phase (i.e. the volume fraction of the reinforcing fiber phase, $V_f$, in all of the constituent laminate systems is the same; only the fiber orientation is different in the various laminate subcomponents). For the present study, the following equations have been selected from earlier literature [59] to estimate the effective properties of a unidirectional laminate subcomponent:

$$\begin{aligned} &S_{11} = \left(E_m\left(1-V_f\right)+E_{f1}V_f\right)^{-1}, \qquad S_{22} = \left(E_m\Big/\left(1-\sqrt{V_f}\left(1-E_m/E_{f2}\right)\right)\right)^{-1}, \\ &S_{66} = \left(1-\sqrt{V_f}\left(1-G_m/G_{f12}\right)\right)\Big/G_m \quad S_{44} = \left(1-\sqrt{V_f}\left(1-G_m/G_{f23}\right)\right)\Big/G_m, \\ &S_{12} = \left(\nu_m\left(1-V_f\right)+\nu_{f12}V_f\right)\Big/\left(E_m\left(1-V_f\right)+E_{f1}V_f\right) \end{aligned} \tag{5.3}$$

where $S_{ij}$ are the five independent constants in the local elastic compliance and stiffness tensors of a unidirectional laminate assuming transverse isotropy (with the 1-axis aligned with the fiber orientation), $E_{f1}$, $E_{f2}$, $G_{f12}$, $G_{f23}$, and $\nu_{f12}$ are the five independent elastic constants of the fiber phase (again assuming transverse isotropy with respect to fiber axis), and $E_m$ and $G_m$ are elastic properties of the matrix phase (assuming isotropy). The

local compliance and stiffness tensors of the laminate subsystems in a given 2-D or 3-D composite can be prescribed completely using the $S_{ij}$ parameters described in Eq. (5.3) (see e.g. [60]). These local compliance and stiffness tensors can then be transformed into the global sample frame (see Figure 2) by the fourth-rank coordinate transformation law:

$$S_{abcd} = Q_{ap}Q_{bq}Q_{cr}Q_{ds}S^{l}_{pqrs}, \qquad C_{abcd} = Q_{ap}Q_{bq}Q_{cr}Q_{ds}C^{l}_{pqrs} \tag{5.4}$$

where the superscript $l$ denotes that the tensor components are expressed in the local reference frame (see Figure 2), and $Q_{ij}$ are the components of the transformation (rotation) matrix. The transformation matrices for the 2-D and 3-D composites of interest here can be expressed as:

$$\begin{aligned} 2-D: \quad [Q] &= \begin{bmatrix} \cos\theta & -\sin\theta & 0 \\ \sin\theta & \cos\theta & 0 \\ 0 & 0 & 1 \end{bmatrix} \\ 3-D: \quad [Q] &= \begin{bmatrix} \cos\Phi & -\sin\Phi & 0 \\ \sin\Phi\cos\beta & \cos\Phi\cos\beta & -\sin\beta \\ \sin\Phi\sin\beta & \cos\Phi\sin\beta & \cos\beta \end{bmatrix} \end{aligned} \tag{5.5}$$

Rigorous first-order bounds, commonly referred to as the Hill-Paul bounds [61, 62], will be employed in this study at the second scale of homogenization when obtaining the effective macroscale elastic properties of the multi-laminate composite material systems shown in Figure 2. The first-order bounds for certain components of the fourth-rank elastic stiffness tensor can be expressed as (without summation over repeated indices[3]) [63]

[3] The standard convention of implied summation over repeated indices is used, except where noted otherwise specifically.

$$\langle S\rangle_{abab}^{-1} \;\le\; C_{abab}^{*} \;\le\; \langle C\rangle_{abab}$$
$$\max(\langle C\rangle_{aabb}, \langle S\rangle_{aabb}^{-1}) - \sqrt{\Delta_a \Delta_b} \le C_{aabb}^{*} \le \min(\langle C\rangle_{aabb}, \langle S\rangle_{aabb}^{-1}) + \sqrt{\Delta_a \Delta_b} \tag{5.6}$$
$$\Delta_a = \langle C\rangle_{aaaa} - \langle S\rangle_{aaaa}^{-1}$$

where $\langle . \rangle$ denotes an ensemble or volume average[4] (here it is taken to refer to the volume average over the laminate subsystems), $C_{abcd}$ and $S_{abcd}$ denote the components of the laminate subsystem's elastic stiffness and compliance tensors in the sample reference frame (see Eq. (5.2)), and $C_{abcd}^{*}$ are the components of the effective elastic stiffness tensor in the sample reference frame.

As noted earlier, more advanced homogenization theories exist and are a topic of research in current literature. The scope of this study will, however, be limited to the first-order theories and the 1-pt. description of the microstructure distributions. Note also that the elementary homogenization theories selected here require evaluation of ensemble averages of various quantities over the microstructure. The ensemble average of any quantity, $A$, can be evaluated using 1-pt. distributions as

$$\langle A \rangle = \int_H A(h) f(h) dh \tag{5.7}$$

It can be seen that the Fourier representation of the functions $A(h)$ and $f(h)$ will prove beneficial in evaluating the integral shown in Equation (5.7), because of the orthonormality of the Fourier basis.

Substitution of Eq. (5.4) into Eq. (5.7) yields expressions for the components of the local stiffness and compliance tensors in the sample frame that are dependent on the local state parameters ($\theta$ in 2-D composites and ($\Phi$,$\beta$) in 3-D composites). To denote this dependency, these components shall be denoted as $S_{abcd}(\theta)$ and $S_{abcd}(\Phi,\beta)$, respectively.

[4] For statistically homogeneous microstructures, ensemble averages are equal to the volume averages. All the microstructures considered in this study are assumed to be statistically homogenous.

Note that these functions can also be expressed in the same Fourier spaces that were used to represent the 1-pt distributions characterizing the internal structure of the material.

$$
\begin{aligned}
&S_{abcd}(\theta) = \sum_{l=0,2}^{\infty} {}_{abcd}\Xi_l \cos(l\theta), \\
&{}_{abcd}\Xi_l = \frac{2}{\pi}\int_0^{\pi/2} S_{abcd}(\theta)\cos(l\theta)\,d\theta \\
&S_{abcd}(\phi,\beta) = \sum_{l=0,2}^{\infty}\sum_{\mu=1}^{M(l)} {}_{abcd}\Xi_l^{\mu}\dot{k}_l^{\mu}(\phi,\beta), \\
&{}_{abcd}\Xi_l^{\mu} = \frac{2}{\pi}\int_0^{\pi/2}\int_0^{\pi/2} S_{abcd}(\phi,\beta)\dot{k}_l^{\mu}(\phi,\beta)\sin\phi\, d\phi\, d\beta
\end{aligned}
\tag{5.8}
$$

Computation of the $\Xi$ coefficients in Eq. (5.8) reveals that these coefficients are non-zero only for $l$ = 0,2,4. As an example, Table 1 lists the expressions for ${}_{abcd}\Xi_l$ in terms of $S_{ij}$.

The ensemble averages in the Eq. (5.8) for bounds (Eq. (3.9)) can be evaluated as

$$
\begin{aligned}
&2-D: \quad \langle S_{abcd} \rangle = \sum_{l=0,2}^{4} {}_{abcd}\Xi_l F_l \\
&3-D: \quad \langle S_{abcd} \rangle = \sum_{l=0,2}^{4}\sum_{\mu=1}^{M(l)} {}_{abcd}\Xi_l^{\mu} F_l^{\mu}
\end{aligned}
\tag{5.9}
$$

The major advantage of using the MSD framework is realized in Eq. (5.9). First, note that the ensemble averages needed to obtain the bounds (or estimate) require the use of only a finite number of terms in the Fourier expansion of the 1-pt distributions. In other words, the higher-order microstructure coefficients ($F$ coefficients for $l > 4$) do not have any influence on the ensemble averages for the properties of interest. We expect this important feature to carry over to other physical properties as well. The microstructure-property linkage expressed in Eq. (5.9) is invertible. The ensemble averages described by Eq. (5.9) denote hyperplanes in the Fourier space. If one selects a specific desired value

for the ensemble average for any of the compliance component, the intersection of Eq. (5.9) and the microstructure hull (Figure 6) denote the set of 1-pt distributions that would yield the desired ensemble average. Furthermore, the hyperplane defined by Eq. (5.9), when it intersects the hull depicted in Figure 6, dissects the hull into two regions – one region depicting the set of 1-pt distributions with an ensemble average inferior to the desired value, and the other region with an ensemble value superior to the desired value. Of course, when the hyperplane does not intersect with the hull, it implies that the specified value for the ensemble average is not feasible for the selected material system.

Further reflection on Eqs. (3.9), (5.7), and (5.9) reveals that iso-property hypersurfaces can be depicted for bounds or estimates of all effective properties. Figure 8 shows examples of iso-property surfaces for selected components of the effective compliance tensor for the class of 2-D composite systems studied in this paper. Note that multiple design objectives or constraints can be depicted simultaneously in the types of plots shown in Figure 8, identifying the set of all 1-pt distributions that are predicted to satisfy several design criteria.

In studies on selected classes of continuous fiber reinforced composites, appropriately weighted averages of the first-order bounds have been found to yield reasonably accurate estimates of the effective properties [57, 64]. The weights used in these models were found to be dependent on the type of fibers and matrix materials used [58]. In this study, it has been assumed that reasonably good estimates of the effective properties of the 2-D and 3-D composites being studied can be obtained using the following class of weighted average models (WAM) [64]:

$$C^{*}_{abcd} \approx \alpha C^{up}_{abcd} + (1-\alpha) C^{low}_{abcd} \tag{5.10}$$

where $\alpha$ is the weighting factor $(\alpha \in [0,1])$, and the superscripts 'up' and 'low' denote the respective upper and lower bounds for the stiffness component of interest.

It should be noted that advanced homogenization theories do currently exist, especially for the effective elastic properties of composite material systems. These higher-order theories (see e.g. [39, 46, 65]) require more detailed information on the spatial distribution of the reinforcing phase in the internal structure of the composite system, and have only been critically evaluated experimentally in a limited class of material systems (see [66] for application of higher-order theories to polycrystalline material systems). It is envisioned that the MSD framework will incorporate these theories in near future (the reader is referred to [47] for a demonstration of the incorporation of the higher-order theories in the MSD framework for polycrystalline material systems).

### 5.1.2. First-Order Failure Criteria

The development of a comprehensive theoretical model for the effective failure properties of a composite material system is significantly more complicated, and lags substantially behind the developments described earlier for their effective elastic properties. It is fully acknowledged that the development of robust linkages between the internal structure of the composite and the failure properties would require a sophisticated approach that takes into account the nature of the fiber-matrix interaction and a detailed description of the spatial distribution of the fiber reinforcement in the internal structure of the material. In the present study, however, we adopt a very simple model based on the Tsai-Hill description [60, 67, 68] and a consideration of only a limited number of failure

modes [57, 59], to estimate the failure strength of a unidirectional laminate in off-axis simple compression loading:

$$\sigma_{fail}(\theta)=\left(\frac{\cos^4\theta}{X^2}+\left(\frac{1}{S^2}-\frac{1}{X^2}\right)\cos^2\theta\sin^2\theta+\frac{\sin^4\theta}{Y^2}\right)^{-1/2}$$
$$X=V_f S_{fc},\quad S=S_{ms}\Big/\left(1-\sqrt{V_f}\left(1-G_m/G_{f12}\right)\right),\quad Y=S_{mc}\Big/\left(1-\sqrt{V_f}\left(1-E_m/E_{f2}\right)\right) \tag{5.11}$$

where $S_{fc}$ is the axial compressive strength of the fiber, $S_{ms}$ is the shear strength of the matrix, $S_{mc}$ is the compressive strength of matrix, and $\theta$ denotes the angle between the orientation of the fibers in the laminate subsystem and simple compression loading direction (usually defined in the sample reference frame). The effective strength of the composite is assumed to be given by volume averaging the failure strengths of the constituent laminate subsystems.

$$\sigma_{fail}(\theta)=\sum_{l=0,2}^{\infty}\Psi_l\cos(l\theta),\quad \psi_l=\frac{2}{\pi}\int_0^{\pi/2}\sigma_{fail}(\theta)\cos(l\theta)\,d\theta,\quad \left\langle\sigma_{fail}\right\rangle=\sum_{l=0,2}^{4}\psi_l F_l \tag{5.12}$$

Equations. (5.11) and (5.12) can be suitably modified for 3-D composites.

## 5.2. HOMOGENIZATION: POLYCRYSTALLINE METALS

In MSD, a polycrystalline material is treated essentially as a composite material, in which individual grains of different lattice orientations are considered as the constituents of the composite material system. The overall behavior of the material depends on the distribution of the crystallographic orientations inside the material.

### 5.2.1. ELASTICITY: POLYCRYSTALLINE METALS

The fourth-rank elastic stiffness of a cubic crystal in its own reference frame (aligned with the [100] directions) can be expressed as

$$\mathrm{C}^{\mathrm{c}}_{\mathrm{ijkl}}=\mathrm{C}_{12}\delta_{ij}\delta_{kl}+C_{44}\left(\delta_{ik}\delta_{jl}+\delta_{il}\delta_{jk}\right)+\left(C_{11}-C_{12}-2C_{44}\right)\sum_{r=1}^{3}\delta_{ir}\delta_{jr}\delta_{kr}\delta_{lr} \tag{5.13}$$

where $C_{11}$, $C_{12}$, and $C_{44}$ are material constants representing the independent elastic constants for cubic symmetry, and $\delta_{ij}$ represents the Kronecker delta function. The same elastic stiffness can be expressed in the fixed global reference frame (attached to the sample) as

$$C_{ijkl} = g_{ip} g_{jq} g_{kr} g_{ls} C^{c}_{pqrs} \tag{5.14}$$

where $g_{ij}$ represents the rotation matrix described in Eq. 3.13. This transformation can be represented conveniently as a set of Bunge angles [50], as described in Chapter 3.1.2. The upper bound theory[5] is employed to obtain the elastic stiffness of the polycrystal representing the material microstructure.

$$\overline{C}_{ijkl} = \iint_{M_c} f(g) C_{ijkl}(g) dg \tag{5.15}$$

In Eq. (5.15), *f(g)* represents the orientation distribution function (ODF) defined earlier . The integral in Eq. (5.15) is performed over the set, $M_c$, comprising all possible single crystal orientations (taking into account cubic symmetry of the crystals); this set is called the material set.

Note that for a given microstructure, the elastic constants needed for the design of the orthotropic thin plate in section 8.1 (namely $E_x$, $E_y$, $G_{xy}$, and $\nu_{xy}$) can be obtained from $\overline{C}_{ijkl}$, using established relations in literature.

### 5.2.2. PLASTICITY: POLYCRYSTALLINE METALS

Components are usually designed for performance within the elastic range, and the onset of plasticity is considered failure of the component. As the focus of the MSD is to

[5] As mentioned earlier, MSD framework is being extended to include 2-point statistics of the details of the microstructure; use of the higher order details of the microstructure will automatically facilitate use of a more refined homogenization theory.

exploit material anisotropy in design, anisotropic plasticity is considered. The anisotropic plasticity is considered in the form of Hill's anisotropic yield surface [60] with the orthotropic symmetry imposed.

Orthotropic Hill yield description [60] is used to assess the initiation of plastic deformation in the plate:

$$F\left(\sigma_{yy}-\sigma_{zz}\right)^2+G\left(\sigma_{zz}-\sigma_{xx}\right)^2+H\left(\sigma_{xx}-\sigma_{yy}\right)^2+2L\sigma_{yz}^2+2M\sigma_{zx}^2+N\sigma_{xy}^2=1 \qquad (5.16)$$

where F, G, H, L, M, and N are orthotropic yield strength parameters that depend on the details of the material microstructure. The overall approach taken here was to use a Taylor-type crystal plasticity model and extract the relevant properties for the design (F, G, H, L, M, and N) from the predictions of the crystal plasticity model for a given microstructure. The details of the crystal plasticity model [69] used in this study are briefly reviewed next, using a notation which is now standard in modern continuum mechanics. In particular, the deformation gradient is denoted by **F**, the velocity gradient by **L**, and the symmetric Cauchy stress by **T**.

Assuming small elastic stretches but large plastic deformations, the equation for stress at a material point in a single crystal is expressed as

$$\mathbf{T}^* = \mathbf{C}[\mathbf{E}^*],\ \mathbf{E}^*= \tfrac{1}{2}\left\{\mathbf{F}^{*\mathrm{T}}\mathbf{F}^*-1\right\},\ \mathbf{T}^* = \mathbf{F}^{*-1}\left\{\left(\det\mathbf{F}^*\right)\mathbf{T}\right\}\mathbf{F}^{*-\mathrm{T}} \qquad (5.17)$$

where **C** is the fourth order elasticity tensor described earlier (Eq. 5.14), and **F*** is an elastic deformation gradient defined in terms of the deformation gradient **F** and a plastic deformation gradient $\mathbf{F}^p$ with $\det\mathbf{F}^p = 1.0$ (plastic incompressibility), by

$$\mathbf{F}^* = \mathbf{F}\mathbf{F}^{p-1},\quad \det\mathbf{F}^* \succ 0 \qquad (5.18)$$

The plastic deformation gradient is, in turn, given by the flow rule

$$\dot{\mathbf{F}}^p = \mathbf{L}^p \mathbf{F}^p, \quad \mathbf{L}^p = \sum_\alpha \dot{\gamma}^\alpha \mathbf{S}_o^\alpha, \quad \mathbf{S}_o^\alpha = \mathbf{m}_o^\alpha \otimes \mathbf{n}_o^\alpha \tag{5.19}$$

where $\mathbf{m}_o^\alpha$ and $\mathbf{n}_o^\alpha$ are time-independent orthonormal unit vectors which define the slip direction and the slip plane normal of the slip system $\alpha$ in a fixed (initial) reference configuration, respectively, and $\dot{\gamma}^\alpha$ is the plastic shearing rate on this slip system. The plastic shearing rate on the slip system $\alpha$ is taken as

$$\dot{\gamma}^\alpha = \dot{\gamma}_o \left| \frac{\tau^\alpha}{s^\alpha} \right|^{1/m} sign\left(\tau^\alpha\right), \quad \tau^\alpha \cong \mathbf{T}^* \bullet \mathbf{S}^\alpha \tag{5.20}$$

where $\tau^\alpha$ and $s^\alpha$ are the resolved (Schmid) shear stress and the slip resistance associated with slip system $\alpha$, $\dot{\gamma}_o$ is a reference value of slip rate (typically set to 0.001 $s^{-1}$), and *m* is a slip rate-sensitivity parameter (for plastic deformation of metals at low homologous temperatures, this parameter is given a very small value, typically around 0.01, to approach rate-independent behavior). For the present problem, we are only interested in the yield properties. Consequently, $s^\alpha$ for all slip systems was assumed to be same and equal to $s_o$.

The most widely used approach to obtain the response of a polycrystal from the response of the individual grains is to use extended Taylor's assumption of iso-deformation gradient in all of the crystals comprising the polycrystal. Furthermore, if all grains are assumed to be of the same size, the Cauchy stress in the polycrystal can be taken as a simple number average of the Cauchy stresses in the various grains. Therefore, employing these assumptions, the macroscopic Cauchy stress in the polycrystal ($\bar{\mathbf{T}}$) can be expressed as

$$\bar{\mathbf{T}} = \frac{1}{N}\sum_{k=1}^{N}\mathbf{T}^{(k)} \tag{5.21}$$

where N is the number of crystals in the aggregate, and $\mathbf{T}^{(k)}$ is the Cauchy stress in the crystal (labeled (k)).

The crystal plasticity models are used to obtain the yield strength of the polycrystal in three specific stress states, namely, uniaxial stress in x-direction, uniaxial stress in y-direction, and equi-biaxial stress in x- and y- directions. Using these three yield strengths in the Hill's anisotropic yield function (Eq. 5.16), we can obtain values for three of the anisotropic yield parameters, namely, F, G, and H. Next, imposing a monotonic simple shear deformation in the x-y, x-z, and y-z planes on a polycrystal and obtaining the shear yield of the polycrystal, and using that value in the Hill's anisotropic yield function will provide a value for L, M, and N. Therefore, it is possible to use the Taylor-type polycrystal plasticity model and extract a set of values for all of the required anisotropic yield parameters in Hill's anisotropic yield function as described above. It should be noted that an alternative, and more refined, description of yield function was proposed by Barlat et al. [70, 71] for orthotropic polycrystalline materials. It was, however, found that the results for the present case studies were not sensitive to either choice of the yield function.

### 5.2.3. FRACTURE MECHANICS: POLYCRYSTALLINE METALS

It should be once again be emphasized that our interest here in fracture mechanics is not in developing new fracture models, but using existing fracture models to explore invertible microstructure-effective property linkages using known fracture models.

The *J*-integral was proposed by Rice [72] as a means of evaluating the crack driving force in the form of a path-independent line integral around 2D deformation fields of

linear or nonlinear elastic materials. In the case of an elastic material with monotonic loading, the *J*-integral has a precise physical meaning as the rate of total potential energy per unit crack tip advance [73]. The details of the formulation are described in Appendix C. For the simple case of crack in an isotropic linear elastic material, the critical value of the *J*-integral, denoted by $J_{Ic}$, is expected to match with $G_{Ic}$ defined as the elastic crack driving force in Griffith's theory [74] for purely elastic-brittle failure. The *J*-integral approach for evaluating the crack driving force is much more convenient as most modern finite element software are capable of evaluating this integral readily for complex geometries and loading conditions. Moreover, the *J*-integral approach can in principle be extended to incorporate nonlinear elasticity as well as some inelasticity (though limited to monotonic loading) [74]. However, once inelasticity is considered the *J*-integral is no longer the rate of total potential energy per unit crack tip advance and becomes a crack tip characterizing parameter.

In current design, the evaluation of the *J*-integral is accomplished using isotropic material behavior, neglecting largely the inherent material anisotropy in most engineered material systems. There has been a few recent efforts to include anisotropy into fracture mechanics by Zhao [73] and Tian [75], who focused on anisotropic bimaterials. Some models using the *J*-integral approach have incorporated inelasticity by considering it as an extension of nonlinear elasticity [74]. In the MSD approach, the complete set of all feasible anisotropic elastic stiffness tensors (corresponding to all feasible textures) can be identified, thus raising the possibility that one can select a texture that will minimize the *J*-integral for a given application. In this study, the *J*-integral is evaluated numerically using finite element methods in ABAQUS [76].

# CHAPTER 6. PROPERTY CLOSURES

An important consequence of having microstructure and properties defined in the spectral method is that their linkage can be inverted. It is worth remembering that the properties are influenced by only a finite subset of the Fourier representation of the 1-pt statistics of the microstructure. This feature permits us to evaluate the effective properties over a finite subspace of the microstructure hull and produce a properties closure that delineates the complete set of property combinations that are theoretically feasible in a given material system.

Property closures are not required for the MSD Design Tool; however they do provide a valuable tool that can be used to quickly evaluate materials systems to determine if the materials system under consideration can indeed provide the combination of properties that are required in a specific application. The use of property closures is somewhat similar to using Ashby [31] cross plots. The difference in the property closure and Ashby cross-plots is that the information in the property closure is rigorously tied to *physically realizable microstructures that can exhibit the specific combination of properties simultaneously*. Ashby cross-plots are compiled from a database where a single property was measured, while this does show that microstructures exists that achieve property X and property Y, there is no guarantee that *any* microstructure exists that may exemplify *both* property X and Y *simultaneously*. Therein lies the advantage of property closures based on the MSD framework, that microstructures exhibiting *multiple* properties simultaneously are *physically realizable*.

## 6.1. PROPERTY CLOSURES: COMPOSITES

It is now possible to construct property closures reflecting the complete set of combinations of specified effective properties for a given composite material system

using Eqs. (3.9) and Eq. (5.9) together with the microstructure hulls defined in Figure 6. Figure 8 depicts examples of elastic property closures for the material systems studied here.

As an example, Figure 9 shows an elastic property-failure property closure computed using the above simplistic model for the failure strength of composite.

### 6.2. PROPERTY CLOSURES: POLYCRYSTALLINE METALS

The property closures for polycrystalline metals with cubic-orthorhombic symmetries have been previously solved by Proust [37, 63, 77, 78]. The property closures are not used directly in the MSD-FE design tool, However these property closures are an integral part of a proposed design framework and are valuable to the designers in determining if a particular set of material properties are feasible in a given materials system.

# CHAPTER 7. MSD DESIGN TOOL

Using the MSD framework to create a design tool that bridges the gap between the material developer and the design engineer is the primary function of the MSD Design Tool. Once the design tool has been developed, it is the goal to be able to provide a straightforward design tool that allows the design engineers first to be aware of the impact that material anisotropy has on design and second to be able to exploit this material anisotropy in HCD. Case studies demonstrating the MSD Design tool are presented in Section 7.4.

The MSD Design tool consists of three major components, finite element tool for mechanical analysis, MSD homogenization codes that provide the effective properties to the finite element code, and the iSIGHT shell environment for optimization. Each component will be discussed in detail in the following sections.

## 7.1. iSIGHT

iSIGHT is a commercially available optimization software that is currently used in an array of industries including automotive, aerospace, and defense [79, 80]. Microstructure optimization using finite element methods was conducted within an iSIGHT (software from Engineous Software) environment. iSIGHT was used as a shell program to encompass all the MSD codes and ABAQUS for the performance evaluation. iSIGHT also has preprogrammed optimization routines that are convenient for designers. It should be noted that the optimization routines can readily be supplanted by other codes should a designer have a preferred optimization routine. The initial goal was to demonstrate that the MSD concept can be integrated with existing design tools, and for this purpose, the optimization routines in iSIGHT were used as they were provided.

The schematic for the MSD-iSIGHT optimization loop is shown in Figure 11. The algorithm is designed only to calculate properties and performances for microstructures that are feasible, meaning the microstructures exist within the microstructure hull. The algorithm used to determine whether the microstructure exists is given by Lyon and Adams [81] with a set of 4225 coefficients from single crystals.

Once the microstructure was determined to exist within the microstructure hull, the elastic and yield properties where determined. The scripting routines within iSIGHT are used to write the orthotropic elasticity constants and the anisotropic yield ratios into an ABAQUS input file. Once ABAQUS input file has been updated iSIGHT uses a batch file to call and run the ABAQUS job. When the job has completed the iSIGHT parses the ABAQUS data file for the reaction force on the fixed nodes, and the total plastic energy dissipated (PENER) at the nodes for the whole model. It was previously determined that the critical plastic energy dissipation of 0.6 (MPa) was used locally to determine when the material had yielded. This constant, was determined by the .02% offset method from the critical resolved shear stress. The critical resolved shear stress was taken as 100 (MPa), which was selected arbitrarily, because the load carrying capacity simply scales with this number. The critical value of plastic dissipation (PENER) was kept constant throughout the entire process, i.e. determining the yield parameters, and the point of yielding in the ABAQUS model. iSIGHT was used to interpolate the exact load the plate was experiencing when the yield was first detected in the plate. From this point the optimization process was used to determine the next set of microstructure coefficients.

### 7.1.1. Optimization Methods

iSIGHT has many preprogrammed optimization codes, and several codes where explored before settling on the generalized reduced gradient optimization (LSGRG2).

Previous work [4] with three dimensions had used a sequential quadratic programming (NLPQL) optimization routine that was found to terminate early in higher dimensions, often leading to erroneous results. The generalized reduced gradient optimization [82, 83] routine was determined to be the most robust and straightforward optimization routine to use. The convergence epsilon was set to 0.001 and the gradient step size was set to 0.01. The gradient step size is the largest step size allowed in the search algorithm. The convergence epsilon corresponds to an effectively zero gradient. When the search algorithm finds a gradient of less than the convergence epsilon three times consecutively, the optimization is determined to have converged. In a sense the gradient step size and convergence epsilon is an indication of the sensitivity of the performance to the ODF. The gradient step size is the distance from the point that was just evaluated to the next guessed microstructure. It was determined that the minimum step size had to be of the order of 0.01, otherwise the performance was insensitive to the microstructure and the optimization stopped due to a lack of a gradient.

### 7.2. FINITE ELEMENT TOOLS (ABAQUS)

Finite element tools are widely used in the design field, as such they are considered an as a highly important component in the construction and implementation of the MSD Design tool. The finite element component has a twofold purpose in being incorporated to the MSD Design Tool, 1) it provides a means of mechanical analysis for complex problems 2) it provides a familiar starting point to the design engineer.

In this work the finite element analysis tool that was interfaced with the MSD framework was ABAQUS [76]. ABAQUS was considered to be an ideal FE tool to incorporate due to the relative ease in incorporating customized material models. This was of particular importance in the verification of the work in this thesis. The case studies

discussed in section 7.4 were kept simple 1) because an analytical solution was known for the 2D plane stress problem and 2) to avoid additional complications associated with complex problems such as: mesh convergence, integration problems, and long running simulations.

Though the MSD design tool is capable of considering a wide range of crystal and sample symmetries, we have restricted our considerations here to cubic materials with orthorhombic sample symmetry. In these case studies, the geometry was set to be a thin plate with a circular hole that is loaded in in-plane tension. The orthorhombic sample symmetry allows for a reduced model, and therefore a 1/8 model was used for the analysis, as shown in Figure 10. The mesh was also refined near the circular hole where the stress concentration is present and where yielding occurs.

The models considered in this study were elastic-plastic problems where material anisotropy was considered for both elasticity and yielding. Elasticity is treated directly with an orthorhombic stiffness tensor. Plasticity was considered with no strain hardening (perfectly plastic). Plasticity as mentioned previously was considered to have a critical resolved shear stress of $\tau_{crss} = 100$ MPa.

The yielding criteria was considered to be Hill's orthotropic yield condition [84-87]. Detailed discussion of the yield description is presented in Chapter (5.2.2). It is important to note that there are other anisotropic yield models available and may provide equally valid results. In ABAQUS, the anisotropic yield is introduced by

```
*plastic
σy, ε0
*potential
```

```
R1, R2, R3, R4, R5, R6
```

where R1, R2, and R3 are the ratios of yielding in the principal direction normalized by $\sigma_y$, and R4, R5, and R6 are the ratios of shear yielding in the principal direction normalized by $\sigma_y\sqrt{3}$ [76]. The values for R1-6 are provided by the MSD code for plasticity.

The FE model treats the materials on the continuum level, which corresponds to a polycrystalline metal where the grain sizes are much smaller than the element sizes. The properties in ABAQUS are given as homogenized effective properties.

## 7.3. CUSTOM MSD CODES

Several customized computer codes are required to execute microstructure optimization using the MSD Framework. The first code verifies that the microstructure coefficients of interest correspond to physically realizable microstructures (i.e. they exist within the microstructure hull). Additional codes are required to calculate the effective properties of that microstructure. The following sections discuss the codes that are required in more detail.

### 7.3.1. MICROSTRUCTURE HULL

The microstructure hull code is an integral part of the inverse problem, if the microstructure does not exist then no matter what improvements are made in the models the design is worthless. The microstructure hull is the first and probably most important constraint. It also provides the reassurance that any improvements due to microstructure are in theory, physically realizable (assuming the accuracy of the material models are accurate enough).

The algorithm to determine whether the microstructure exist within the microstructure hull was given by Lyon [81]. The final code that was used was written by Proust and the source code is available [37]. Only minor modifications to this code were required for the optimization integration, these modifications were restricted to the read and write statements and have no bearing on the overall algorithm with the exception of the handling of the null vector (point consisting of all zeros, which is a valid microstructure coefficient), which was originally not addressed.

The MSD Design tool was setup and designed to run on a desktop computer, as many design engineers cannot afford the parallelized mainframes for design. The desktop PC in this study was a Dell Dimension 8200, 2.2 GHz Intel processor with 2 Gigabytes of RAM. The code used to determine whether the microstructure exists uses a set of 4225 coefficients from single crystals from an evenly discretized Euler space. The single crystal microstructures are described to $l$=4, $l$=6, and $l$=8 (with 3, 7 and 12 independent terms, respectively) depending on the level of approximation of the problem. The properly optimized code takes less than a minute on a desktop computer to determine whether or not a guessed set of microstructure coefficients are feasible. This is a substantial improvement over other codes available for convex hulls, such as Qhull, [88] which calculates the entire hull, and runs for approximately 24 hours for 7 dimensions, and did not run to completion for twelve dimensions even with a reduced input file (1000 single crystal coefficients).

The microstructure hull code has an input of the microstructure coefficients and in this case returns the maximum length of the vector from the null vector to the exterior of the microstructure hull. If the length of the initial point exceeds the maximum length, the

microstructure is infeasible and a new set of microstructure coefficients should be guessed.

### 7.3.2. HOMOGENIZATION

The MSD codes for effective properties, Eq. (5.7), are separate for elasticity and plasticity. The MSD homogenization codes were produced to provide effective property estimates based on the upper bounds for both effective properties [37]. Both codes accept microstructure coefficients as input variables so a single file was required for both elastic and plastic homogenization codes.

The property coefficients where separated from the codes so other materials may readily can be considered by simply changing material library files. The codes for elasticity and plasticity are shown in Appendix E and F, respectively

## 7.4. ASSEMBLY

The MSD-iSIGHT setup consisted of the iSIGHT optimization shell, microstructure hull code, MSD homogenization codes and the ABAQUS finite element. The codes listed were organized essentially in a linear fashion. Figure 15 is a general overview of the task arrangement. As mentioned previously, the microstructure coefficients were guessed in the iSIGHT environment, as long as the coefficients existed in or on the microstructure hull, the effective properties were calculated and the performance was evaluated. Figure 16 illustrates the input variables and optimization variables for the MSD framework.

File Parsing or reading the results from the MSD hull code, MSD homogenization, and ABAQUS files was an integral portion in completing the optimization loop. The file parsing from the MSD codes was straightforward, simply requiring iSIGHT to read the output results from the codes. Extracting the performance (load carrying capacity) was evaluated when PENER=0.6. ABAQUS was run in the mode standard and therefore had

time steps associated with the incremental nature for the solution. The time steps were allowed to vary, speeding the calculations for the elastic regime The complication comes from the difficulty that the time steps from model to model are not exactly the same, and that the solution at a time step where PENER=0.6 is not guaranteed. To overcome this inconvenience the values of PENER and the load carrying capacity were calculated for the steps immediately before PENER=0.6 and immediately after, the load carrying capacity was then linearly interpolated for the value of PENER=0.6. Since the time step is variable, the place in the ABAQUS output file is not identical from run to run, scripting can be used to find and interpolate the load carrying capacity for the critical value for plastic energy dissipated. The iSIGHT file parsing was used to read and interpolate the optimization variable, load carrying capacity.

Controlling the execution for ABAQUS was done using the command line and a batch code. The following is the batch code that was used:

```
del [job name].msg
del [job name].log
del [job name].sta
del [job name].com
del [job name].fil
del [job name].spc
del [job name].ipm
del [job name].mdl
del [job name].odb
del [job name].prt
del [job name].res
```

```
del [job name].stt
del [job name].lck
del abaqus.rpt
```

where the job name in square brackets are replaced with the job name. The downside to this method is that all the ABAQUS result files are deleted after the relevant information to design is read. This may be remedied but requires more overhead in the terms of a script that will move, rename, or otherwise archive files. This was not deemed to be a particularly critical step as the model is only reporting loads and plastic energy dissipation; it may become more important with more complicated models (longer execution times) where other parameters may be of interest, but are not the optimization variable. The detailed file parsing script is shown in Appendix G. The iSIGHT MDOL file which contains the complete description of the MSD framework in use for the hole in a plate problem is presented in Appendix H.

# CHAPTER 8. CASE STUDIES

This work uses three case studies to demonstrate the viability of the MSD framework. Although the case studies are relatively simple, the case studies show clearly the feasibility of the integrated MSD-FE environment in engineering design.

Holes and notches occur frequently in engineering design and cracks occur naturally in materials. Special attention is paid in designing components containing notches or holes, since it is well established that they have a major effect on design life of the components, especially in fatigue loading. Mechanical design handbooks [33, 35, 36] depict a number of charts providing estimates of stress concentration factors that depend on the geometry of the notch. However, in virtually all of the design handbooks, the material is assumed to possess isotropic mechanical properties. This practice, however, is in direct conflict with the trends in new materials development, where one of the major goals has been to enhance properties of the material in certain directions while sacrificing properties in other directions where they are not as needed (e.g. development of laminated composite systems). Anisotropy of the material is bound to play an extremely important role in highly constrained design (HCD) applications. In design of components with notches and holes, a relatively small reduction of the stress concentration factor can lead to a significant increase in the design life of the component (e.g. a 20% reduction in stress concentration factor can produce a 900% increase in the high-cycle fatigue life of a component made from SAE 4340 steel) [4].

## 8.1. HOLE IN AN ORTHOTROPIC PLATE SUBJECTED TO AN IN-PLANE LOAD

The hole in an orthotropic plate subjected to an in-plane tension was a problem that selected because an analytical solution exists for the plane stress case. The analytical solution that follows was used as verification that the finite element model was

approaching the plane stress solution for the thin plate. The elastic stress distribution around a circular hole in a thin orthotropic plate, was derived by Lekhnitskii [89] to be circumferential in nature for the plane stress case, and given by

$$\sigma_{\theta\theta} = \sigma^{\infty} \frac{E_{\theta}}{E_x} \left[ -\sqrt{\frac{E_x}{E_y}} \cos^2\theta + (1+n)\sin^2\theta \right] \tag{8.1}$$

$$n = \sqrt{\frac{E_x}{G_{xy}} - 2\nu_{xy} + 2\sqrt{\frac{E_x}{E_y}}} \tag{8.2}$$

$$\frac{1}{E_{\theta}} = \frac{\sin^4\theta}{E_x} + \left( \frac{1}{G_{xy}} - \frac{2\nu_{xy}}{E_x} \right) \sin^2\theta\cos^2\theta + \frac{\cos^4\theta}{E_y} \tag{8.3}$$

where θ is the angle measured from the x-axis, $\sigma^{\infty}$ is the stress applied at the edge of the plate (in the x-direction), $G_{xy}$ and $\nu_{xy}$ are shear modulus and Poisson's ratio in the x-y plane, and $E_x$ and $E_y$ are Young's moduli in the x- and y- directions, respectively. Note that only four elastic constants ($E_x$, $E_y$, $G_{xy}$, and $\nu_{xy}$) appear in this plane-stress design problem, and that their values are dictated by the details of the material microstructure.

Orthotropic Hill yield description [60] (Eq. 5.13) is used to assess the initiation of plastic deformation in the plate. Substituting the solution for the stress field around the hole (Eqs. 8.1-8.3) into where Eq. (5.13) is for plane stress, yields

$$\sigma_{\theta\theta}^2 \left\{ (G+H)\cos^4\theta + (F+H)\sin^4\theta + 2(N-H)\sin^2\theta\cos^2\theta \right\} = 1 \tag{8.4}$$

Note that, based on Eq. (5.13), the terms (G+H) and (F+H) can be related to uniaxial yield strengths of the material in x and y directions, respectively, and N can be related to the shear yield strength of the material in the x-y plane. Note also that the equi-biaxial strength of the plate loaded in x and y directions is related to (G+F) and therefore one can

derive an expression for H in terms of the uniaxial yield strengths in x and y directions and the biaxial yield strength.

In summary, the engineering performance of the plate in this design is controlled by four elastic parameters ($E_x$, $E_y$, $G_{xy}$, $\nu_{xy}$) and three plastic yield parameters (G+H, F+H, N-H). For given values of these seven parameters, Eqs. (8.1) - (8.4) along with Eq. (5.13) provide an expression for $\sigma^{\infty}$ as a function of θ. The load carrying capacity is simply determined by the minimum value of $\sigma^{\infty}$ that satisfies Eq. (8.4) anywhere in the range $\theta \in [0,90]$. The seven parameters listed above control the performance of the plate, and are in turn strongly dependent on the details of the microstructure. FE methods were used for the general case; the plane stress case was used for an analytical comparison to the MSD-FE results.

The plate considered in the finite element case is a thin plate with a small circular hole shown schematically in Figure 1. The critical dimensions of the plate are w=h, t=w/200, and the hole diameter, a=w/100 and was modeled as reduced 1/8 model along the lines of symmetry shown in Figure 10.

The microstructural design variable selected here is the one-point statistics (i.e. volume fractions) of the distribution of crystal lattice orientations (i.e. crystallographic texture). Therefore it is necessary to develop relationships between the macroscale elastic and plastic properties listed above and crystal orientations and their (statistical) distributions.

### 8.1.1. COMPOSITES

The MSD framework was also applied to continuous fibrous reinforced composites (CFRC) consisting of transversely isotropic fibers and an isotropic matrix. In this case

study, we restrict our attention to the fiber orientation distribution function and with a fixed volume fraction of fiber $\left(V_f = 0.5\right)$. The primary objective in this design (see Figure 1) is the maximization of the load carrying capacity. The plate must provide this load carrying capacity without failing. Thus, both elastic and composite failure are germane to the problem.

The materials system studied here is a carbon fiber (AS4) reinforced Shell epoxy matrix. The elastic properties for the AS4 carbon fiber are $E_{11}$= 234.6 GPa, $E_{22}$=13.8 GPa, $G_{12}$=13.8 GPa, and $G_{23}$=5.5 GPa [57]. The matrix is assumed to be isotropic and the elastic properties are given as E=2.94, and $\nu$=0.33 [68]. The Tsai-Hill failure criteria is used to predict failure, the important parameters are tensile strength of the fiber ($S_{fc}$=870 MPa), the shear strength of the matrix ($S_{ms}$=28.9 MPa), and the compressive strength of the composite ($S_{mc}$=50 MPa) as reported by Kalidindi and Abusafieh [57].

The solution for the composite hole in a plate used the analytical solution provided earlier. The potential improvement from the worst to best case scenario with the given materials system is a factor of 3.6. The highest load carrying capacity for the physics of the problem was a $\pm 36.5^{\circ}$ composite see Figure 13.

### 8.1.2. POLYCRYSTALLINE METAL

In this case study, we restrict our attention to only the crystal lattice orientation as a variable of the microstructure and their volume fractions (i.e. crystallographic texture).

The primary objective in this design (see Figure 1) is the maximization of the load carrying capacity. The plate must provide this load carrying capacity without plastic yielding (primary constraint). Thus, both elastic and yielding properties are germane to the problem.

The material system considered in this study is polycrystalline nickel. The single crystal elastic stiffness coefficients are $C_{11}$=246.5 GPa, $C_{12}$=147.3 GPa, and $C_{44}$=124.7 GPa [90]. The plastic properties stress ratios are calculated using an extended Taylor model [91] to determine the active slip systems for each uni-axial loading condition. The method is described in detail by Proust [37], and the yield parameters were determined by the .02% offset method from the critical resolved shear stress. The critical resolved shear stress was taken as 100 (MPa), which was selected arbitrarily, because the load carrying capacity simply scales with this number.

Starting from the random microstructure and using the generalized reduced gradient optimization method, the MSD-design tool discussed earlier in Chapter 7 was used to determine the maximum and minimum load carrying capacity for the thin plate with a circular hole.

The load carrying capacity was improved regardless of the how many Fourier coefficients were used to represent the microstructure, the results for the MSD predictions are presented in Table 3 in the MSD column. However the maximum predicted performance dropped from $1.38\,\tau_{crss}$ to $1.26\,\tau_{crss}$. The discrepancy was not unexpected and is discussed in the following chapter.

## 8.2. PRESSURE VESSEL WITH A PART THROUGH AXIAL FLAW

Textured metals are byproducts of the processing methods used to obtain the preform used to construct the final components. In the case of pressure vessels (particularly large pressure vessels) the preform is often from rolled plates (that are textured due to the processing), which are welded together. It is widely accepted that there will be cracks present in the pressure vessel as a consequence of the various fabrication steps involved in their manufacture. The inherent anisotropy of the elastic and plastic behavior of the

sheet (caused by the texture in the plate) should be expected to have a strong influence on the fracture behavior; this aspect is often overlooked. In this study, we looked at the elastic crack driving force in the sheet as a function of the inherent texture in the plate. For the present case study, the influence of plasticity and its anisotropy is not considered. This case study addresses a cylindrical pressure vessel with a part through axial flaw, shown schematically in Figure 12. The flaw is elliptical and located on the inner surface of the pressure vessel, it is oriented such that the length of the crack is oriented parallel with the cylinder axis. This configuration corresponds to the worst case scenario for crack location and orientation.

Brittle fracture of pressure vessels is catastrophic accompanied with disastrous effects in terms of loss of life, environmental effects, and in terms of lost time and materials. To avoid brittle failure the "leak before break" design philosophy is employed during the design of pressure vessels. This work does not supplant the leak before break design philosophy but instead illustrates that by exploiting material anisotropy through the control of the underlying texture and minimizing the elastic crack driving force for a given geometry and loading condition the pressures can be increased while maintaining the leak before break criteria. This will be accomplished using the integrated MSD-FE design tool mentioned previously.

The pressure vessel in consideration was assumed to be made from a cubic material (polycrystalline nickel) with orthotropic sample symmetry. The elastic properties for this case study are identical to the properties quoted for nickel in the hole in a plate case study, the single crystal elastic stiffness coefficients are $C_{11}$=246.5 GPa, $C_{12}$=147.3 GPa, and $C_{44}$=124.7 GPa [90]. Nickel was chosen for the material properties as it does have a

high degree of inherent elastic anisotropy. The choice for pure nickel is valid for high temperature corrosive environments. It is likely that in such a case the material of choice would actually be a nickel alloy, but more refined material properties where unavailable. The choice in materials properties can be refined for a more realistic model of performance.

The *J*-integral originally proposed by Rice [92] has been used to characterize the driving force in fracture. In the elastic regime the *J*-integral is path independent and has a clear and precise physical significance as the rate of potential energy release per unit crack tip advance[73]. This concept has seen wide use in analyzing fracture in linear fracture mechanics with both isotropy and anisotropy [73]. To a limited degree the approach has been extended for nonlinear fracture mechanics as well, however the nonlinear approach exceeds the current scope of the problem, though it is worth noting that this work can be directly extended to include yielding properties to consider more realistic crack growth rates.

The model from Parks and White [93] was selected from the set of reference models from ABAQUS as it was well established benchmark that has been thoroughly verified for the isotropic crack. The model is shown in Figure 12 as a 3D model of $1/8^{th}$ of the pressure vessel. The model was modified from isotropic elasticity to orthotropic elasticity (in cylindrical coordinates). No plasticity was considered in this case study. All other aspects of the reference model remained the same as the original reference model. The cylindrical coordinates for the material orientation was used to effectively model a rolled sheet that would have been formed to a cylindrical pressure vessel; perfect bonding was assumed.

The microstructure optimization variable is the polycrystalline metals are the first three Fourier coefficients of ODF (i.e. $F_4^{11}, F_4^{12}, F_4^{13}$) as these are the only ones that influence the elastic properties of the sheet. The performance variable to be optimized is the $J_1$-integral which is consistent with a tensile crack opening stress, and is the dominant loading type in a pressure vessel with the current crack configuration. The MSD framework for this problem was setup in exactly the same way it was set up for the case study involving the thin plate with a central circular hole. The main difference is that this case study involved a purely elastic response. The optimization method was the same as that used in the earlier case study, i.e. the generalized reduced gradient method with the same optimization criteria (convergence and minimum gradient).

The poles figures for the maximum and minimum *J*-integral are shown in Figure 19. The improvement in performance which entirely based upon the *J*-integral is an improvement of 31% improvement.

# CHAPTER 9. DISCUSSION OF RESULTS

The MSD framework was used in several case studies involving both polycrystalline metals and continuous fiber reinforced composites. These results are discussed in this chapter.

## 9.1. COMPOSITES

The MSD representation and framework were derived for the new class of materials, continuous fiber reinforced composites. The application of the MSD framework with simple homogenization models from literature and texts provide a framework to exploit the customizability of composites.

This is the first known technique that provides a method to optimize the fiber orientation distribution for composites. The analysis was kept at the 2-D level for composites; for the 2-D composites (laminates) the highest load carrying capacity was determined to be ($\theta = 36.5^{\circ}$) for the material system under consideration for both upper and lower bounds, and subsequently the WAM model. The estimated load carrying capacity however varies significantly with the consideration of the bounds, as can be seen by the peak values in Figure 9. It is important to note that optimal solution is dependant on the material system (effective properties) and the volume fraction of fibers. The load carrying capacity of composite has not been examined thoroughly to study the effects of the effective properties and volume fraction of fibers.

The test case study for CFRC is presented without additional verification and is left as a recommendation for future work.

## 9.2. POLYCRYSTALLINE METAL

The MSD Design tool was run on a desktop PC, in this study was a Dell Dimension 8200, 2.2 GHz Intel processor with 2 Gigabytes of RAM. The optimization methods

proved to be able to optimize the microstructure for the hole in a plate problem with a run time of 10.5 hours with the microstructure representation at *l*=8 in spherical harmonics. The optimization time was the shortest for *l*=4 at approximately 4 hours, which was expected as the number of variables is minimal. The optimization for l=6 was incrementally longer at roughly 7 hours. The bulk of the optimization time is spent evaluating the FEM model. The nearly linear increase in optimization times is not entirely representative of the complexity of the problem as some refinements in the tuning of the optimization were made. It is expected that the tuned optimization scheme would perform somewhat faster at lower Fourier representations (*l*=4 has 3 variables, *l*=6 has 7 variables, and *l*=8 has 12 variables). It should be cautioned that since the problem is largely elastic with small scale yielding, the bulk of the physics is captured at l=4, and higher order microstructure representations are refinements in the description of the yield surface.

The solutions given by the final optimization are in good agreement with earlier results based on analytical results [4, 81]. The results are tabulated in Appendix A.

The MSD calculations indicate the potential improvement (from worst case to best case scenario) is 26.7% which is a significant improvement particularly interesting when fatigue lifetimes are considered. The improvement from isotropic to case is only marginally improved over the worse case scenario, with a performance of $1.06\,\tau_{crss}$, which yields the surprising result of an improvement (isotropic to best case scenario) of 18.9%.

### 9.2.1. VERIFICATION

Verification of the model is important for the proof of concept. Two types of verifications can readily be considered 1) experimental and 2) an independent numerical model. There are several difficulties in experimental verification, first and foremost that the solution for the highest load carrying capacity is a texture that is not a readily known texture (i.e., rolling, or fiber textures) and the processing to achieve the prescribed optimal texture is, at this point, unknown. The upper bound assumption (simple volume fraction) homogenization method presents its own problems. The overall performance an experimental sample may not perform near the upper bound solution.

As the difficulties with the experimental verification leaves doubts as to how valid the verification would be, a numerical simulation was used for verification. The numerical verifications have the advantage that the same assumptions on the bounds can be employed, also many instantiations of the microstructure may be evaluated as the microstructure is by no means uniquely defined with $l$=4, 6, or 8 (3, 7, or12 Fourier coefficients respectively). The non-uniqueness of the microstructure however, is not critical as the higher order Fourier coefficients are only refinements of the initial coefficients. Therefore the MSD solution identifies a class of microstructures that have a similar performance metric.

The *independent* verification model was chosen to be a crystal plasticity model [94-96]. Crystal plasticity models are largely accepted in as being accurate for the average deformation behavior of polycrystalline metals and have been around for some fifty years [91]. The crystal plasticity model is a widely accepted model and is in use today. Crystal plasticity models continue to be a current research topics as well [94, 96-103]. This approach is accurate predicting the averaged texture evolution of grains experiencing

deformation; however they are not accurate in predicting lattice rotations for discrete crystals. The models are also very good at predicting stresses and strains in deforming metals where slip is the predominant deformation mechanism.

The complication is in that the crystal plasticity model requires discrete lattice orientations as opposed to Fourier coefficients of the ODF. Microstructures were reconstructed to have ODFs identical to the MSD solutions at $l$=4, 6, and 8 respectively. It is important to note that microstructures with the initial coefficients are not uniquely defined. As such, during the verification process multiple (twenty) microstructures were created. Figure 18 illustrates the several different instantiations for the ODF defined up to $l$=6 for the maximum performance of the hole in a plate. The pole figures on the bottom portion of Figure 18 are from ODFs with same initial microstructure coefficients (coefficients up to $l$=6); however the higher order coefficients (beyond $l$=6) are unconstrained. The reconstructed microstructures on the lower part of Figure 18 are shown to a high level of detail, at $l$=32. This means that simply a class of microstructures are identified that have a similar performance.

The verification FEM was done on twenty instantiations of microstructures with the constrained to having the Fourier coefficients that match the same predicted optimal solution. The results are presented in Table 3 where it is clear that the independent verification is converging with the MSD with increasing $l$. Predictions for microstructures defined to $l$=8 are within 5% of the crystal plasticity code.

The verification process indicates the MSD solution converges with the crystal plasticity model within an acceptable error when the microstructure is not completely defined. This indicates that a class of microstructures are identified that have a similar

performance metric. And the obvious conclusion is that the more details that are defined in the microstructure, the more the two models converge.

It should be noted that the verification models took approximately three times longer to complete than the initial MSD predictions. This suggests that the MSD technique is far less computationally intensive and may provide reasonable estimates for performance in much shorter timeframes.

Previous work by Parks and White verified the FEM model was in good agreement with experimental results [93]. The model only considers material behavior in the elastic regime. The crystal plasticity models have already been shown to converge with the MSD solutions in the elastic regime [4, 37]. No additional verification is presented for the pressure vessel with a part through axial flaw.

# CHAPTER 10. CONCLUSIONS

Microstructure Sensitive Design has been shown to be a useful tool for designing materials when the physics of the problem are well understood. It is readily apparent that the use of computers and models is necessary to consider designs where the microstructure is optimized to provide optimal performance of the overall component.

The case studies show an enriched design space when local anisotropy considered, showing significant room for improvement in the case studies presented. The development of a microstructure design tool has provided an additional that allows the designer an opportunity to further improve designs, particularly highly constrained designs and has the potential to make significant improvements with consideration of anisotropy.

MSD has been shown to be applicable to both cubic polycrystalline metals, and continuously reinforced fibrous composites. Combined with previous work by Proust on cubic and hexagonal closed packed metals [37], The MSD approach can be applied to a wide range of material classes.

The MSD approach has been shown that the accuracy of solutions is dependant on truncation of Fourier series and governing physics. Incorporating new governing physics will likely be of interest to address additional problems such as heat transfer, and magnetic properties; careful attention needs to be paid to the accuracy of the MSD solutions if truncations to the series are made.

MSD has identified a class of microstructures that provide a similar performance metric. A unique microstructure may not be determined when a truncation in the series is used though when the series sufficiently captures the physics, set of microstructures may be identified to have a similar performance. This non-uniqueness may actually be prove

to be beneficial by providing a broad set of microstructures that will meet the design requirements, from which the microstructure achieved by the easiest or cheapest processing route should have a performance similar to the optimal solution.

As a tool the MSD Framework can be readily incorporated into commercial design codes such as ABAQUS and iSIGHT. This means the MSD Framework can be readily incorporated into the existing design process without having to introduce a completely new set of tools to designers. This should result in quick incorporation in the design process.

MSD has promise providing faster forward models by using spectral representations without sacrificing accuracy from existing crystal plasticity models. With further development, considerable time savings is realized with MSD due to the unified mathematical framework used represent microstructures, properties and performance. It should also be realized that significant gains are made when simply the microstructure and effective property estimates are in the same mathematical framework and performance evaluation is done in finite element methods.

### 10.1. RECOMMENDATIONS FOR FUTURE WORK

One criticism of the work described here is that there has been no experimental verification presented. To date there has been no experimental verification due to the in ability to achieve the desired ODFs in samples of meaningful size. The inverse problem of determining processing routes to achieve materials with a specified ODF is a major problem to overcome, though if it can be achieved it will add credibility to the MSD approach. It is important to note that this work is currently in progress at Drexel University [17] and there has been some notable successes in applying spectral methods to the texture evolution of polycrystalline metals which is an important step on the way to

solving this inverse problem. If specified ODFs may be manufactured it will be possible to experimentally verify the predictions for optimal textures for specific engineering cases. Then it may become a challenge to ensure that the processing can be done economically to fully exploit material anisotropy commercially.

The experimental verification of the inverse problem of designing a composite structure with a specified fiber orientation distribution appears more tractable in the case of CFRC where more control is possible in the manufacture of the composite. In fact the part of the motivation behind expanding MSD to composites was the promise that it there may be an easier path to experimental verification of the MSD framework.

The MSD-FE framework should be expanded to incorporate saving the finite element output in a database, particularly if more information is desired from the model. This can readily be achieved in an *ad hoc* fashion by introducing a script that changes the model filenames sequentially after the file is parsed. In the longer term a more efficient method would be desirable, to avoid clutter in working directories. It should be noted that this is mostly a consequence of the optimization routine; most optimization methods fail to incorporate knowledge the designer has *a priori*. This can be addressed using more sophisticated optimization rules and databases for simpler problems however, more complicated problems may quickly reduce to having few if any "fundamental solutions."

This researcher recommends that the MSD design framework should be extended to fatigue and further into fracture mechanics where the contribution to the expanded design space can make a significant improvement, as mentioned previously a small improvement in yield strength can induce a large improvement in fatigue life. If the improved fatigue performance can be combined in reduction in stress concentration near a fracture the

improvements can be further magnified. This class of mechanics problems also addresses a larger group of designers that may find the MSD design framework a desirable tool.

The application of MSD to fracture should not be considered complete at this juncture. For completeness, the MSD design framework should be applied to a material with anisotropic elasticity and anisotropic plasticity. The problem also needs to be experimentally verified, which adds the additional complication that the route to "construct" a given ODF in a material needs to be addressed.

## LIST OF REFERENCES


1. Olsen, G.B., *Computational design of hierarchically structured materials.* Science, 1997. **277**(29): p. 1237-1242.

2. Olsen, G.B., *Pathways of discovery designing a new material world.* Science, 2000. **228**(12): p. 933-998.

3. Adams, B.L., A. Henrie, B. Henrie, M. Lyon, S.R. Kalidindi, and H. Garmestani, *Microstructure-sensitive design of a compliant beam.* J. Mech. Phys. Solids, 2001. **49**: p. 1639-1663.

4. Kalidindi, S.R., J.R. Houskamp, M. Lyons, and B.L. Adams, *Microstructure sensitive design of an orthotropic plate subjected to tensile load.* International Journal of Plasticity, 2004. **20**(8-9): p. 1561-1575.

5. Olson, G.B., *Computational design of hierarchically structured materials.* Science, 1997. **277**(29): p. 1237-1242.

6. Sigmund, O., *Materials with prescribed constitutive parameters: an inverse homogenization problem.* International Journal of Solids and Structures, 1994. **31**(17): p. 2313-2329.

7. Sheehan, N. and S. Torquato, *Generating microstructures with specified correlation functions.* Journal of Applied Physics, 2001. **18**(1): p. 53-60.

8. Sigmund, O. and S. Torquato, *Design of smart composite materials using topology optimization.* Smart. Mater. Struct, 1999. **8**: p. 365-379.

9. Sigmund, O. and S. Torquato, *Design of materials with extreme thermal expansion using a three-phase topology optimization method.* Journal of the Mechanics and Physics of Solids, 1997. **45**(6): p. 1037-1067.

10. Sigmund, O. and S. Torquato, *Composites with extremal thermal expansion coefficients.* Applied Physics Letters, 1996. **69**(21): p. 3203.

11. Sigmund, O., S. Torquato, and I.A. Aksay, *On the design of 1-3 piezocomposites using topology optimization.* Journal of Materials Research, 1998. **13**(4): p. 1038-1048.

12. Torquato, S., *Random Heterogeneous Materials*. 2002, New York: Springer-Verlag.

13. Torquato, S., *Modeling of physical properties of composite materials.* International Journal of Solids and Structures, 2000. **37**(1-2): p. 411-422.

14. Torquato, S. and G. Stell, *Microstructure of two-phase random media. V. The n-point matrix probability functions for impenetrable spheres.* The Journal of Chemical Physics, 1985. **82**(2): p. 980-987.

15. Torquato, S. and G. Stell, *Microstructure of two-phase random media. I. The n-point probability functions.* The Journal of Chemical Physics, 1982. **77**(4): p. 2071-2077.

16. Xu, B., F. Arias, S.T. Brittain, X.-M. Zhao, B. Grzybowski, S. Torquato, and G.M. Whitesides, *Making negative Poisson's ratio microstructures by soft lithography.* Advanced Materials, 1999. **11**(14): p. 1186-1189.

17. Kalidindi, S.R., M. Binci, D. Fullwood, and B. Adams, *Elastic Properties Closures Using Second-Order Homogenization Theories: Case Studies in Composites of Two Isotropic Constituents.* Submitted.

18. *Materials Research to Meet 21st Century Defense Needs*. 2003: National Research Council. 332.

19. McDowell, D.L., *Materials design: a useful research focus for inelastic behavior of structural metals.* Theoretical and Applied Fracture Mechanics, 2001. **37**(1-3): p. 245-259.

20. Shuaeib, F.M., A.M.S. Hamouda, M.M. Hamdan, R.S. Radin Umar, and M.S.J. Hashmi, *Motorcycle helmet: Part II. Materials and design issues.* Journal of Materials Processing Technology, 2002. **123**(3): p. 422-431.

21. Terry, J.C., *Materials and design in Gillette razors.* Materials & Design, 1991. **12**(5): p. 277-281.

22. Bendsoe, M.a.N.K., *Generating optimal topologies in structural design using a homogenization method.* Comp. Meth. Appl. Mechs. Eng., 1988. **71**: p. 197-224.

23. Brennan, J., *OptiStruct: A Topology Optimization Tool for Conceptual Design.* Cray Channels, 1994. **16**(2): p. 27-29.

24. Larsen, U.D., O. Sigmund, and S. Bouwstra, *Design and fabrication of compliant micromechanisms and structures with negative Poisson's ratio.* Journal of Microelectromechanical Systems, 1997. **6**(2): p. 99-106.

25. Silva, E., Carlos, Nelli and N. Kikchi, *Design of piezoelectric transducers using topology optimization.* Smart. Mater. Struct, 1999. **8**: p. 350-364.

26. Bruns, T.E. and O. Sigmund, *Toward the topology design of mechanisms that exhibit snap-through behavior.* Computer Methods in Applied Mechanics and Engineering, 2004. **193**(36-38): p. 3973-4000.

27. Sigmund, O., *Design of multiphysics actuators using topology optimization - Part I: One-material structures.* Computer Methods in Applied Mechanics and Engineering, 2001. **190**(49-50): p. 6577-6604.

28. Sigmund, O., *Design of multiphysics actuators using topology optimization - Part II: Two-material structures.* Computer Methods in Applied Mechanics and Engineering, 2001. **190**(49-50): p. 6605-6627.

29. Olson, G.B., *Pathways of discovery designing a new material world.* Science, 2000. **228**(12): p. 933-998.

30. Ashby, M.F., *Multi-objective optimization in material design and selection.* Acta Materialia, 2000. **48**(1): p. 359-369.

31. Ashby, M.F., *Materials Selection in Mechanical Design*. 2 ed. 1992: Butterworth-Heinemann. 502.

32. Iwata, S., T. Ashino, and S. Ishino, *Materials database for materials design.* Journal of Nuclear Materials, 1991. **179-181**(Part 2): p. 1135-1138.

33. *SAE Fatigue Design Handbook*. 3 ed, ed. S.o.A.E.F.D.a.E. Committee. 1997.

34. *Mechanics of Composite Materials*. 2 ed, ed. R.M. Jones. 1999.

35. *Handbook of Materials for Product Design*. 3 ed, ed. C. Harper. 2001: Mcgraw-Hill Professional.

36. *CRC Materials Science and Engineering Handbook*. 2001 ed, ed. J. Shackelford and W. Alexander. 2001, Boca Raton: CRC Press LLC.

37. Proust, G., *Identifying the Complete Space of Feasible Anisotropic Properties in Polycrystalline Microstructures*, in *Materials Science and Engineering*. 2005, Drexel University: Philadelphia, PA. p. 146.

38. Adams, B.L., A. Henrie, B. Henrie, M. Lyon, S.R. Kalidindi, and H. Garmestani, *Microstructure-sensitive design of a compliant beam.* Journal of the Mechanics and Physics of Solids, 2001. **49**(8): p. 1639-1663.

39. Beran, M.J., T.A. Mason, B.L. Adams, and T. Olsen, *Bounding elastic constants of an orthotropic polycrystal using measurements of the microstructure.* Journal of the Mechanics and Physics of Solids, 1996. **44**(9): p. 1543-1563.

40. Brown, W.F., *Solid mixture permittivities.* J. Chem. Phys., 1955. **23**: p. 1514-1517.

41. Kröner, E., *Bounds for effective elastic moduli of disordered materials.* J. Mech. Phys. Solids, 1977. **25**: p. 137-155.

42. Murat, F. and L. Tartar, *Optimality conditions and homogenization*, in *Non Linear Variational Problems*, A. Mariano, r. Unknown, and r. Unknown, Editors. 1985.

43. Garmestani, H., S. Lin, B.L. Adams, and S. Ahzi, *Statistical Continuum Theory for Large Plastic Deformation of Polycrystalline Materials.* Journal of the Mechanics and Physics of Solids, 2001. **49**(3): p. 589-607.

44. Lin, S. and H. Garmestani, *Statistical continuum mechanics analysis of an elastic two-isotropic-phase composite material.* Composites Part B: Engineering, 2000. **31**(1): p. 39-46.

45. Garmestani, H., S. Lin, and B.L. Adams, *Statistical Continuum Theory for Inelastic Behavior of a Two-phase Medium.* International Journal of Plasticity, 1998. **14**(8): p. 719-731.

46. Kröner, E., *Statistical modeling*, in *Modeling small deformation in polycrystals*, J. Gittus and J. Zarka, Editors. 1986, Elsevier: New York.

47. Adams, B.L., X.C. Gao, and S.R. Kalidindi, *Finite approximations to the second-order properties closure in single phase polycrystals.* Acta Materialia, 2005. **53**(13): p. 3563-3577.

48. Bunge, H., *Texture Analysis in Materials Science.* Butterworths, 1982.

49. Kreyszig, E., *Advanced Engineering Mathematics*. 8th ed. 1998, New York: Wiley, John & Sons, Incorporated.

50. Bunge, H.-J., *Texture analysis in materials science. Mathematical Methods*. 1993, Göttingen: Cuvillier Verlag.

51. Randle, V. and O. Engler, *Introduction to Texture Analysis. Macrotexture, Microstructure & Orientation Mapping*. 2000: Gordon and Breach Science Publishers.

52. Adams, B.L., D. Kinderlehrer, W.W. Mullins, A.D. Rollett, and S. Ta'asan, *Extracting the relative grain boundary free energy and mobility functions from the geometry of microstructures.* Scripta Materialia, 1998. **38**(4): p. 531-536.

53. Adams, B.L., S. Ta'asan, D. Kinderlehrer, I. Livshits, D.E. Mason, C.-t. Wu, W.W. Mullins, G.S. Rohrer, A.D. Rollett, and D.M. Saylor, *Extracting grain boundary and surface energy from measurement of triple junction geometry.* Interface Science, 1999. **7**(3-4): p. 321-338.

54. Wu, C.T., B.L. Adams, C.L. Bauer, D. Casasent, A. Morawiec, S. Ozdemir, and A. Talukder, *Mapping the mesoscale interface structure in polycrystalline materials.* Ultramicroscopy, 2002. **93**(2): p. 99-109.

55. Lambert, J., I. Cantat, R. Delannay, A. Renault, F. Graner, J.A. Glazier, I. Veretennikov, and P. Cloetens, *Extraction of relevant physical parameters from 3D images of foams obtained by X-ray tomography.* Colloids and Surfaces A: Physicochemical and Engineering Aspects, 2005. **263**(1-3): p. 295-302.

56. de Oliveira, L.F., R.T. Lopes, E.F.O. de Jesus, and D. Braz, *3D X-ray tomography to evaluate volumetric objects.* Nuclear Instruments and Methods in Physics Research Section A: Accelerators, Spectrometers, Detectors and Associated Equipment, 2003. **505**(1-2): p. 573-576.

57. Kalidindi, S.R. and A. Abusafieh, *Longitudinal and transverse moduli and strengths of low angle 3-D braided composites.* Journal of Composite Materials, 1996. **30**(8): p. 885-905.

58. Kalidindi, S.R. and E. Franco, *Numerical evaluation of isostrain and weighted-average models for elastic moduli of three-dimensional composites.* Composites Science and Technology, 1997. **57**(3): p. 293-305.

59. Chamis, C., C., *Mechanics of Composite Materials: Past, Present, and Future.* Journal of Composites Technology and Research, 1989. **11**(1): p. 3-14.

60. Jones, R.M., *Mechanics of Composite Materials*. 1975, New York: Hemisphere Publishing Corp.

61. Hill, R., *The elastic behavior of a crystalline aggregate.* Proceedings of the Royal Society of London. Series A, Mathematical and Physical Sciences, 1952. **65**: p. 349-54.

62. Paul, B., *Prediction of elastic constants of multiphase materials.* Trans. Metall. Soc. AIME, 1960(218): p. 36-41.

63. Proust, G. and S.R. Kalidindi, *Delineation of elastic and plastic yield property closures for face-centered cubic polycrystals using first order homogenization theories.* In preparation, 2005.

64. Kregers, A.F. and T.G. A., Mechanics of Composite Materials, 1979. **4**: p. 277-383.

65. Hashin, Z. and S. Shtrikman, *A variational approach to the theory of the elastic behaviour of multiphase materials.* Journal of the Mechanics and Physics of Solids, 1963. **11**(2): p. 127-140.

66. Mason, T.A. and B.L. Adams, *Use of microstructural statistics in predicting polycrystalline material properties.* Metallurgical and Materials Transactions A: Physical Metallurgy and Materials Science, 1999. **30**(4): p. 969-979.

67. Li, S., *Failure Criteria of Composites*. 2002.

68. Herakovich, C.T., *Mechanics of Fibrous Composites*. 1998, New York: John Wiley & Sons, Inc.

69. Kalidindi, S.R., C.A. Bronkhorst, and L. Anand, *Crystallographic Texture Evolution in Bulk Deformation Processing of Fcc Metals.* Journal of the Mechanics and Physics of Solids, 1992. **40**(3): p. 537-569.

70. Barlat, F., R.C. Becker, J.C. Brem, D.J. Lege, S.J. Murtha, Y. Hayashida, Y. Maeda, M. Yanagawa, K. Chung, K. Matsui, and S. Hattori, *Yielding description for solution strengthened aluminum alloys.* International Journal of Plasticity, 1997. **13**(4): p. 385-401.

71. Barlat, F., D.J. Lege, and J.C. Brem, *A six-component yield function for anisotropic materials.* International Journal of Plasticity, 1991. **7**(7): p. 693-712.

72. Rice, J.R., *A path independent integral and the approximate analysis of strain concentration by notches and cracks.* Journal of Applied Mechanics, 1968. **35**: p. 379-386.

73. Zhao, L.-G. and Y.-H. Chen, *On the contribution of subinterface microcracks near the tip of an interface macrocrack to the J-integral in bimaterial solids.* Int. J. Engng Sci., 1997. **35**(4): p. 387-407.

74. Anderson, T.L., *Fracture Mechanics: Fundamentals and Applications*. 2 ed. 1994: CRC Press.

75. Tian, W.-Y., K.-T. Chau, and Y.-H. Chen, *J-integral analysis of the interaction between an interface crack and parallel subinterface cracks in dissimila anisotropic materials.* international Journal of Fracture, 2001. **111**: p. 305-325.

76. ABAQUS, *Reference Manuals*. 2003, Hibbit, Karlsson, and Sorensen, Inc.

77. Proust, G. and S.R. Kalidindi, *Procedures for construction of anisotropic elastic-plastic property closures for face-centered cubic polycrystals using first order bounding relations.* JMPS, Submitted.

78. Proust, G., J.R. Houskamp, and S.R. Kalidindi. *Coupling of microstructure sensitive design with finite element codes: design of an orthotropic plate with a circular hole loaded in tension*. in *Plasticity 2005*. 2005. Kauai, Hawaii.

79. Engineous Software, I., *iSIGHT*. 2002, Engineous Software.

80. Inc., E.S., *iSIGHT Users Guide*. 2002.

81. Lyon, M. and B.L. Adams, *Gradient-based non-linear microstructure design.* Journal of the Mechanics and Physics of Solids, 2004. **52**(11): p. 2569-2586.

82. Lasdon, L., *Nonlinear and Geometric Programming - Current Status*, in *Annals of Operations Research*. 2001. p. 99.

83. Smith, S. and L. Lasdon, *Solving large sparse nonlinear programs using GRG.* ORSA, J. Comput, 1992. **4**: p. 1-15.

84. Hill, R., *Constitutive modelling of orthotropic plasticity in sheet metals.* Journal of the Mechanics and Physics of Solids, 1990. **38**(3): p. 405-417.

85. Hill, R., *Plastic anisotropy and the geometry of yield surfaces in stress space.* Journal of the Mechanics and Physics of Solids, 2000. **48**(6-7): p. 1093-1106.

86. Hill, R., *The theory of plane plastic strain for anisotropic metals.* Proceedings of the Royal Society of London. Series A, Mathematical and Physical Sciences, 1949. **198**(1054): p. 428-437.

87. Hill, R., *A theory of the yielding and plastic flow of anisotropic metals.* Proceedings of the Royal Society of London. Series A, Mathematical and Physical Sciences, 1948. **193**(1033): p. 281-297.

88. Barber, B.C., D.P. Dobkin, and H. Huhdanpaa, *The quickhull algorithm for convex hulls.* ACM Trans. Math. Softw., 1996. **22**(4): p. 469-483.

89. Lekhnitskii, S.G., *Anisotropic Plates*. 2 ed. 1968: Gordon and Breach. 534.

90. Hertzberg, R.W., *Deformation and Fracture Mechanics of Engineering Materials*. Fourth ed. 1996, New York: John Wiley & Sons, inc.

91. Taylor, G.I., *Plastic strain in metals.* Journal of the Institute of Metals, 1938. **62**: p. 307-324.

92. Adams, N.J.I. and H.G. Munro, *A single test method for evaluation of the J integral as a fracture parameter.* Engineering Fracture Mechanics, 1974. **6**(1): p. 119-132.

93. Parks, D.M. and C.S. White, *Elastic-Plastic Line-Spring Finite Elements for Surface-Cracked Plates and Shells.* Transactions of the ASME, Journal of Pressure Vessel Technology, 1982. **104**: p. 287-292.

94. Bronkhorst, C.A., S.R. Kalidindi, and L. Anand, *Polycrystalline plasticity and the evolution of crystallographic texture in FCC metals.* Philosophical Transactions of the Royal Society of London Series a-Mathematical Physical and Engineering Sciences, 1992. **341**(1662): p. 443-477.

95. Kalidindi, S.R., C.A. Bronkhorst, and L. Anand. *Crystallographic texture evolution in bulk deformation processing of metal*. in *Winter Annual Meeting of the American Society of Mechanical Engineers, Nov 25-30 1990*. 1990. Dallas, TX, USA: Publ by ASME, New York, NY, USA.

96. Van Houtte, P., L. Delannay, and S.R. Kalidindi, *Comparison of two grain interaction models for polycrystal plasticity and deformation texture prediction.* International Journal of Plasticity, 2002. **18**(3): p. 359-377.

97. Asaro, R.J., *Crystal Plasticity.* Journal of Applied Mechanics, 1983. **50**(4b): p. 921-934.

98. Bhattacharyya, A., E. El-Danaf, S.R. Kalidindi, and R.D. Doherty, *Evolution of grain-scale microstructure during large strain simple compression of polycrystalline aluminum with quasi-columnar grains: OIM measurements and numerical simulations.* International Journal of Plasticity, 2001. **17**(6): p. 861-883.

99. Kalidindi, S.R., *Modeling anisotropic strain hardening and deformation textures in low stacking fault energy fcc metals.* International Journal of Plasticity, 2001. **17**(6): p. 837-860.

100. Kocks, U.F., *Polyslip in polycrystals.* Acta Metallurgica, 1958. **6**(2): p. 85-94.

101. Li, D.S., H. Garmestani, and S. Schoenfeld, *Evolution of Crystal Orientation distribution coefficients during plastic deformation.* Scripta Materialia, 2003. **49**(9): p. 867-872.

102. Lin, G. and K.S. Havner, *On the evolution of texture and yield loci in axisymmetric deformation of F.C.C. polycrystals.* International Journal of Plasticity, 1994. **10**(5): p. 471-498.

103. Van Houtte, P., *Application of plastic potentials to strain rate sensitive and insensitive anisotropic materials.* International Journal of Plasticity, 1994. **10**(7): p. 719-748.

104. Adams, B.L., S.R. Kalidindi, and H. Garmestani. *Spectral representation of microstructure evolution in polycrystals*. in *Microstructure Modeling and Prediction During Thermomechanical Processing, Nov 4-8 2001*. 2001. Indianapolis, ID, United States: Minerals, Metals and Materials Society.

# APPENDIX A- TABLES

Table 1 Expressions for the spectral coefficients in the representation of compliance components of the laminate sub-components in the sample reference frame for the 2-D composites, computed from Eq. (22).

Elastic Property Fourier Coefficients for 2D Continuously Reinforced Composites

| | $l$=0 | $l$=2 | $l$=4 |
|---|---|---|---|
| $_{1111}\Xi$ | $\frac{1}{8}S_{11}+\frac{3}{8}S_{22}+\frac{1}{4}S_{12}+\frac{1}{2}S_{66}$ | $\frac{1}{4}S_{11}-\frac{1}{4}S_{22}$ | $\frac{1}{16}S_{11}+\frac{1}{16}S_{22}-\frac{1}{8}S_{12}-\frac{1}{4}S_{66}$ |
| $_{2222}\Xi$ | $\frac{3}{8}S_{11}+\frac{3}{8}S_{22}+\frac{1}{4}S_{12}+\frac{1}{2}S_{66}$ | $-\frac{1}{4}S_{11}+\frac{1}{4}S_{22}$ | $\frac{1}{16}S_{11}+\frac{1}{16}S_{22}-\frac{1}{8}S_{12}-\frac{1}{4}S_{66}$ |
| $_{3333}\Xi$ | $S_{22}$ | 0 | 0 |
| $_{2233}\Xi$ | $\frac{1}{2}S_{23}+\frac{1}{2}S_{12}$ | $\frac{1}{4}S_{23}-\frac{1}{4}S_{12}$ | 0 |
| $_{1133}\Xi$ | $\frac{1}{2}S_{23}+\frac{1}{2}S_{12}$ | $-\frac{1}{4}S_{23}+\frac{1}{4}S_{12}$ | 0 |
| $_{1122}\Xi$ | $\frac{1}{8}S_{11}+\frac{1}{8}S_{22}+\frac{3}{4}S_{12}-\frac{1}{2}S_{66}$ | 0 | $-\frac{1}{16}S_{11}-\frac{1}{16}S_{22}+\frac{1}{8}S_{12}+\frac{1}{4}S_{66}$ |
| $_{2323}\Xi$ | $S_{22}-S_{23}+\frac{1}{2}S_{66}$ | $\frac{1}{2}S_{22}-\frac{1}{2}S_{23}-\frac{1}{4}S_{66}$ | 0 |
| $_{1313}\Xi$ | $S_{22}-S_{23}+\frac{1}{2}S_{66}$ | $-\frac{1}{2}S_{22}+\frac{1}{2}S_{23}+\frac{1}{4}S_{66}$ | 0 |
| $_{1212}\Xi$ | $\frac{1}{8}S_{11}+\frac{1}{8}S_{22}-\frac{1}{4}S_{12}+\frac{1}{2}S_{66}$ | 0 | $-\frac{1}{16}S_{11}-\frac{1}{16}S_{22}+\frac{1}{8}S_{12}+\frac{1}{4}S_{66}$ |

Table 2 The microstructure coefficients for the optimized hole in a plate, with increasing microstructure representation.

| Microstructure Coefficient | Maximum | | | Minimum | |
|---|---|---|---|---|---|
| | $l=4$ | $l=6$ | $l=8$ | $l=4$ | $l=8$ |
| $F_4^{11}$ | -3.15 | -2.61 | -0.40 | 4.95 | 3.46 |
| $F_4^{12}$ | -0.99 | 2.07 | 0.40 | -1.35 | -0.14 |
| $F_4^{13}$ | -1.36 | 0.81 | -1.47 | -4.95 | -3.84 |
| $F_6^{11}$ | - | -1.04 | -2.34 | - | -1.40 |
| $F_6^{12}$ | - | 1.30 | -1.34 | - | -0.40 |
| $F_6^{13}$ | - | -1.56 | -3.13 | - | -3.23 |
| $F_6^{14}$ | - | -0.39 | 0.36 | - | 0.45 |
| $F_8^{11}$ | - | - | 0.21 | - | 8.57 |
| $F_8^{12}$ | - | - | -0.09 | - | -0.19 |
| $F_8^{13}$ | - | - | -4.57 | - | -4.77 |
| $F_8^{14}$ | - | - | -0.02 | - | -0.50 |
| $F_8^{15}$ | - | - | 4.28 | - | 6.60 |

Table 3 The predictions of the highest load carrying capacity for nickel. MSD predictions are shown with increasing microstructure representation ($l$). The FEM load carrying capacity is shown for twenty instantiations of reconstructed microstructures with their standard deviation in performance. The average error is the error of the MSD calculations with respect to the FEM predictions for the corresponding microstructures.

| Predictions of highest load carrying capacity | | | |
|---|---|---|---|
| Series Rank ($l$) | MSD $(\tau_{crss})$ | FEM $(\tau_{crss})$ | Average Error (%) |
| 4 | 1.38 | $1.01 \pm 0.05$ | 25 |
| 6 | 1.28 | $1.17 \pm 0.04$ | 9 |
| 8 | 1.26 | $1.24 \pm 1.5 \times 10^{-5}$ | 1.6 |

Table 4 The maximum and minimum performance of a pressure vessel with a part through axial flaw.

| Microstructure Coefficient | Minimum Performance | Maximum Performance |
|---|---|---|
| $F_4^{11}$ | -1.82 | 4.08 |
| $F_4^{12}$ | -1.61 | 2.11 |
| $F_4^{13}$ | -3.94 | 5.27 |
| $J$-Integral $\left(MPa/mm^2\right)$ | 1198 | 1565 |

## APPENDIX B- FIGURES

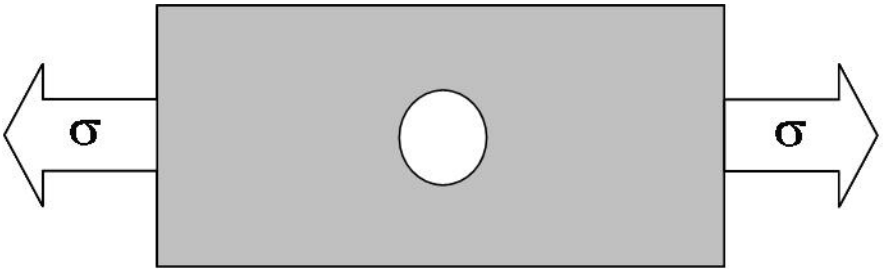


Figure 1 A plate with a circular hole, loaded in in-plane tension.

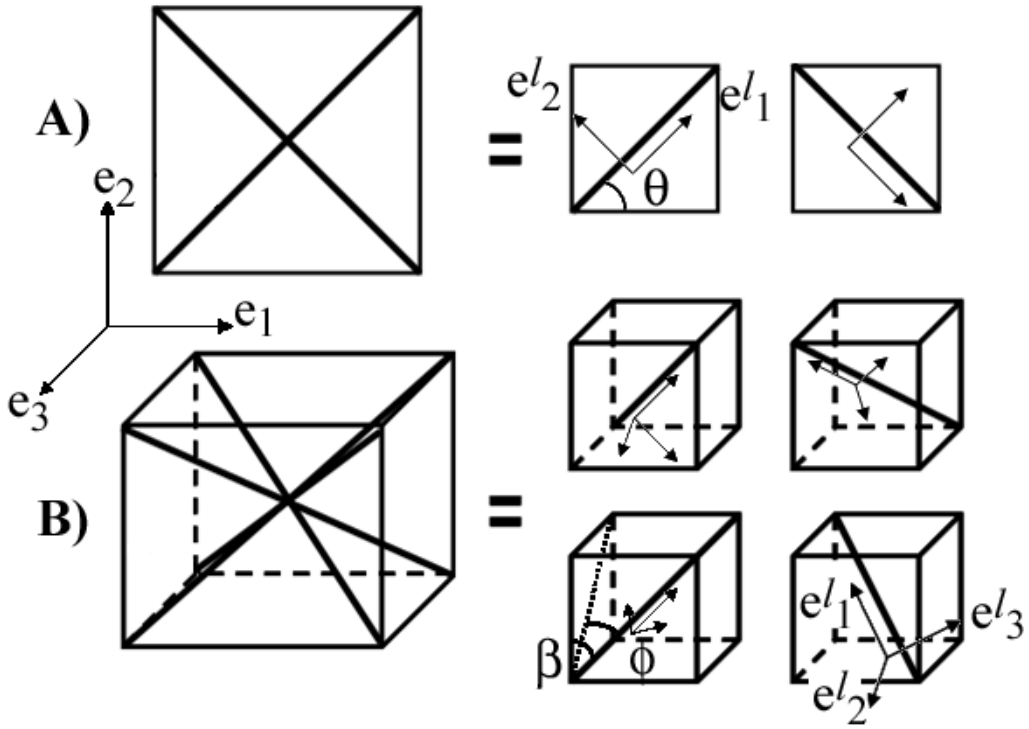


Figure 2 Idealization of a continuous fiber reinforced composite into unidirectional laminate sub-components (A) 2-D composites, (B) 3-D composites.

Figure 3 Earring in deep drawing of aluminum due to crystallographic texture. Compliments of Dr. Roger Doherty, Drexel University.

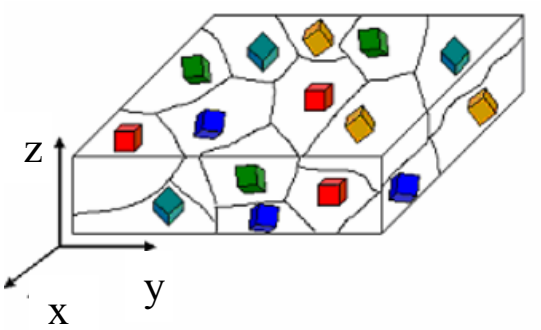


Figure 4 Schematically shows a polycrystalline metal; each grain may have an independent orientation.

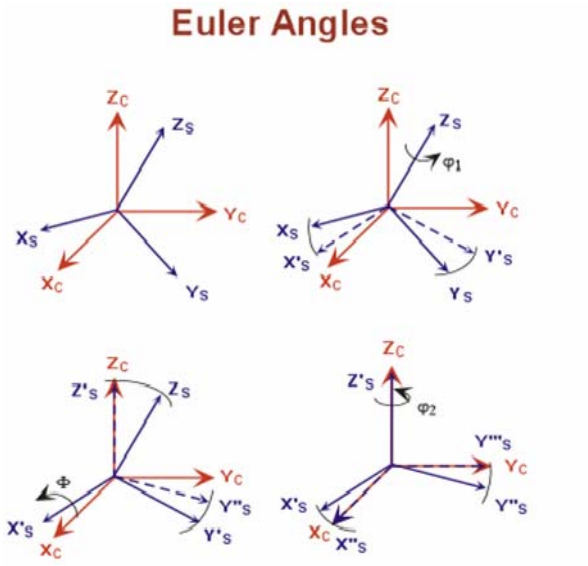


Figure 5 Euler angles describing the rotation of a crystal from the sample frame to the crystal frame in the series of $\varphi_1, \Phi, \varphi_2$.

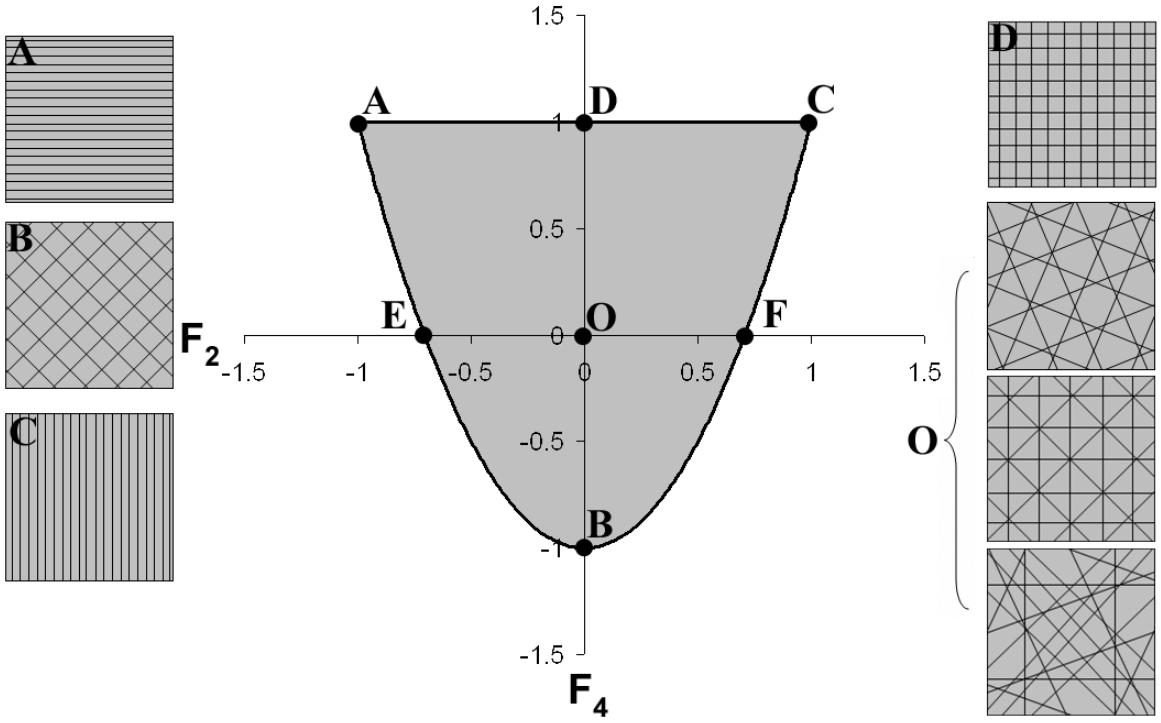


Figure 6 The microstructure hull for 2D transversely isotropic-orthorhombic materials. The hull is shown in the first two dimensions in Fourier space

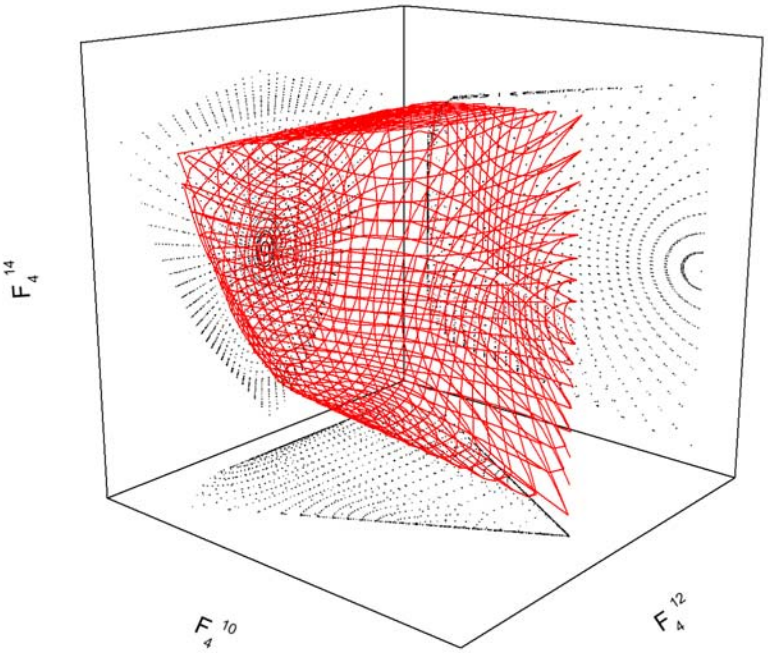


Figure 7 The first three non-zero coefficients for the cubic-orthorhombic symmetry.

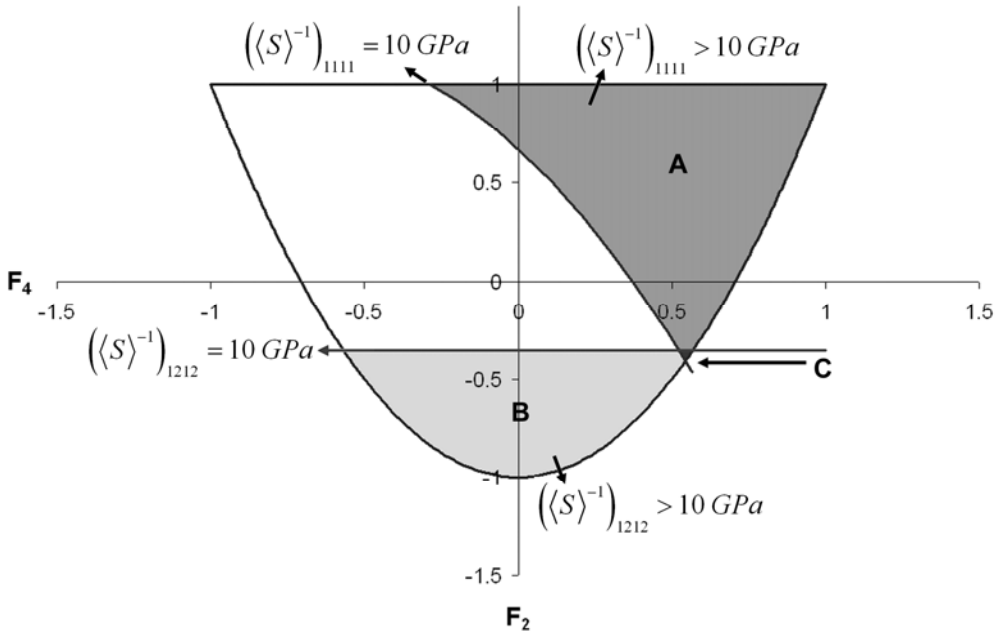


Figure 8 Isoproperty hypersurfaces delineating the set of microstructures in Fourier space that meet prescribed conditions.

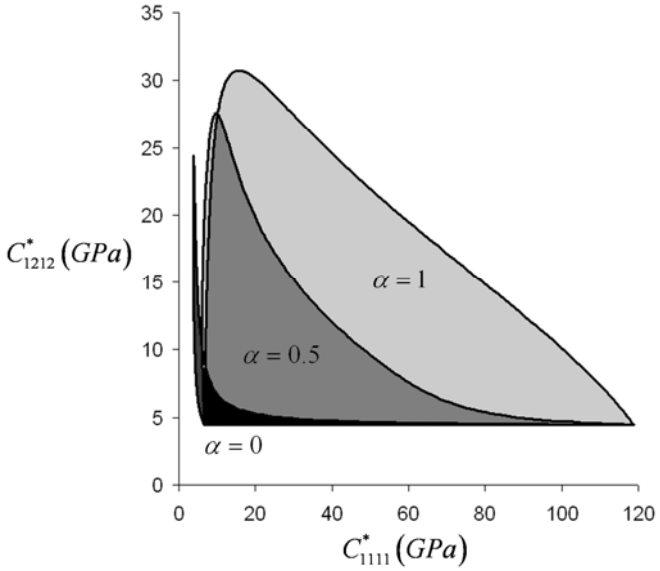


Figure 9 The property closure for the effective elastic properties $C^*_{1111}(GPa)$ and $C^*_{1212}(GPa)$ of the composite material system studied here. The material system studied was a AS-4 Carbon fiber [57] and epoxy [68] system with a fiber volume fraction ($V_f$) of 0.5, where $\alpha$ is the weighting factor of the upper bounds contribution to the properties.

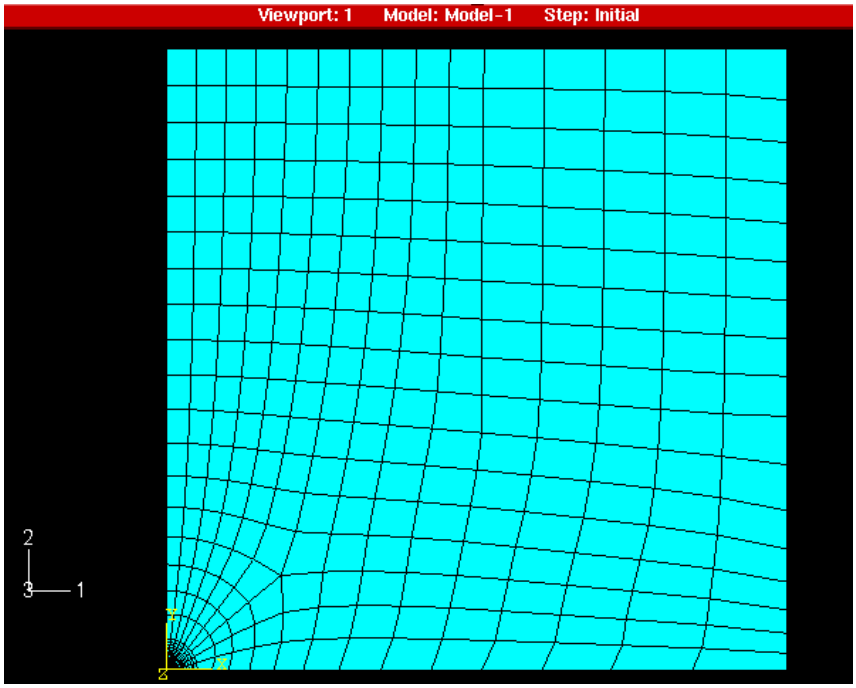


Figure 10 The finite element mesh for the 1/8 of the plate model with a circular hole.

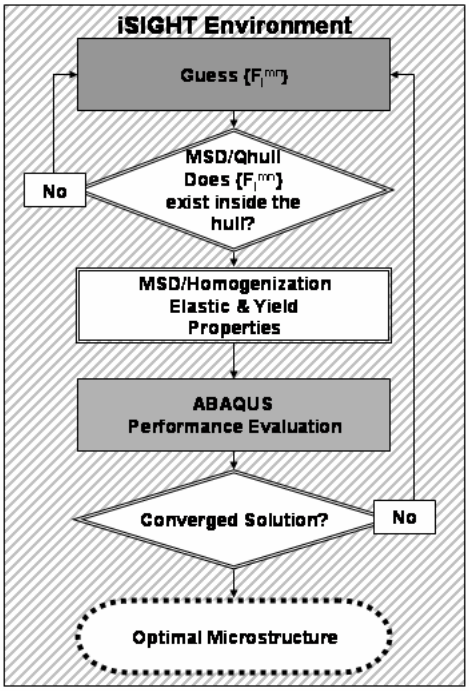


Figure 11 The flowchart for iSIGHT, MSD, ABAQUS microstructure optimization is shown above.

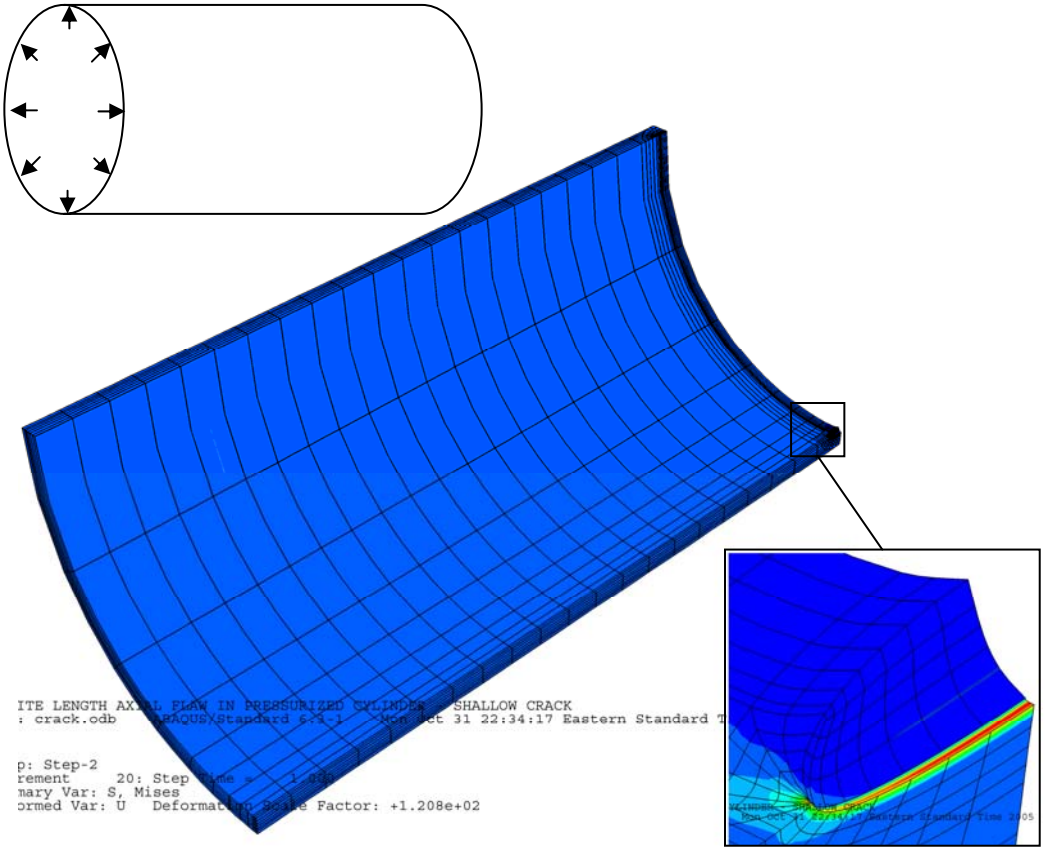

Figure 12 Schematically shows the cylindrical pressure vessel (upper left). The 1/8$^{th}$ model above is the ABAQUS example file (center), with the part through axial flaw show in detail (lower right).

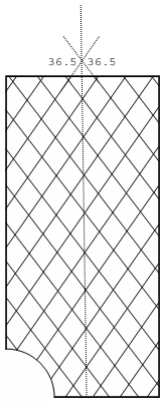

Figure 13 the optimal fiber orientation distribution for a composite with a volume fraction of ($V_f$=0.5) AS-4 and shell epoxy for a composite with a cirular hole.

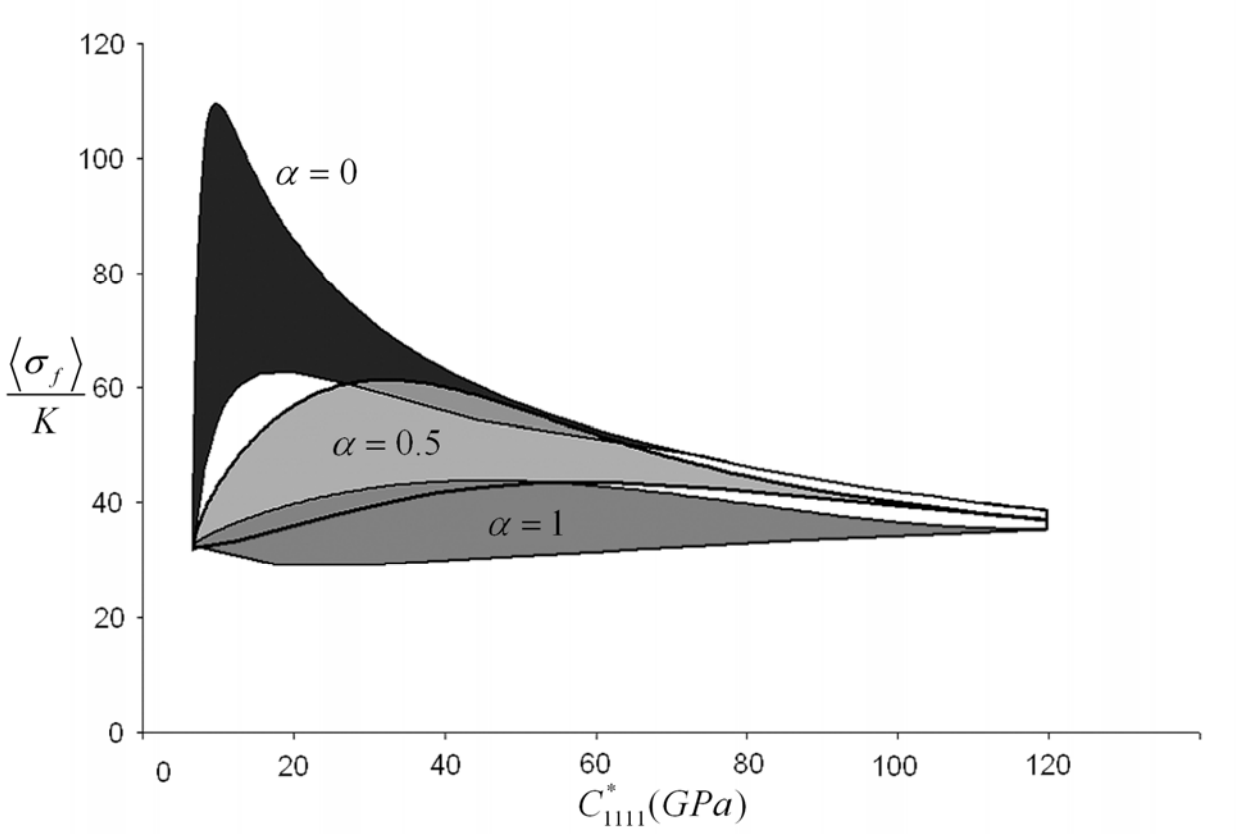


Figure 14 An example of a performance closure for a thin orthotropic plate containing a central circular hole and subjected to in-plane compression. Closures are shown for three different values of the interpolation parameter α in the WAM model, where the weighting factor of the upper bounds contribution to the properties is $\alpha$.

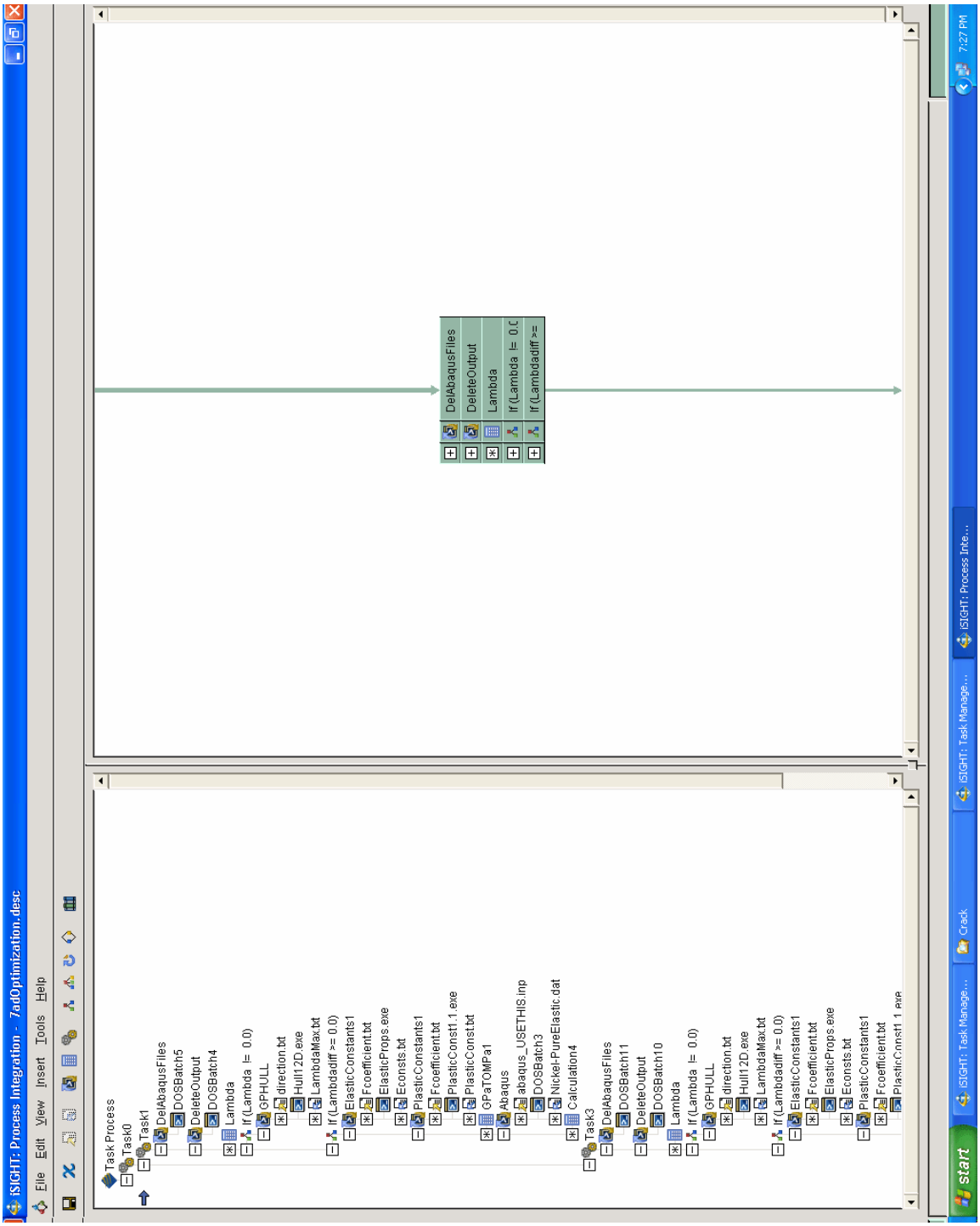


Figure 15 The iSIGHT shell for the optimization of the hole in a plate study.

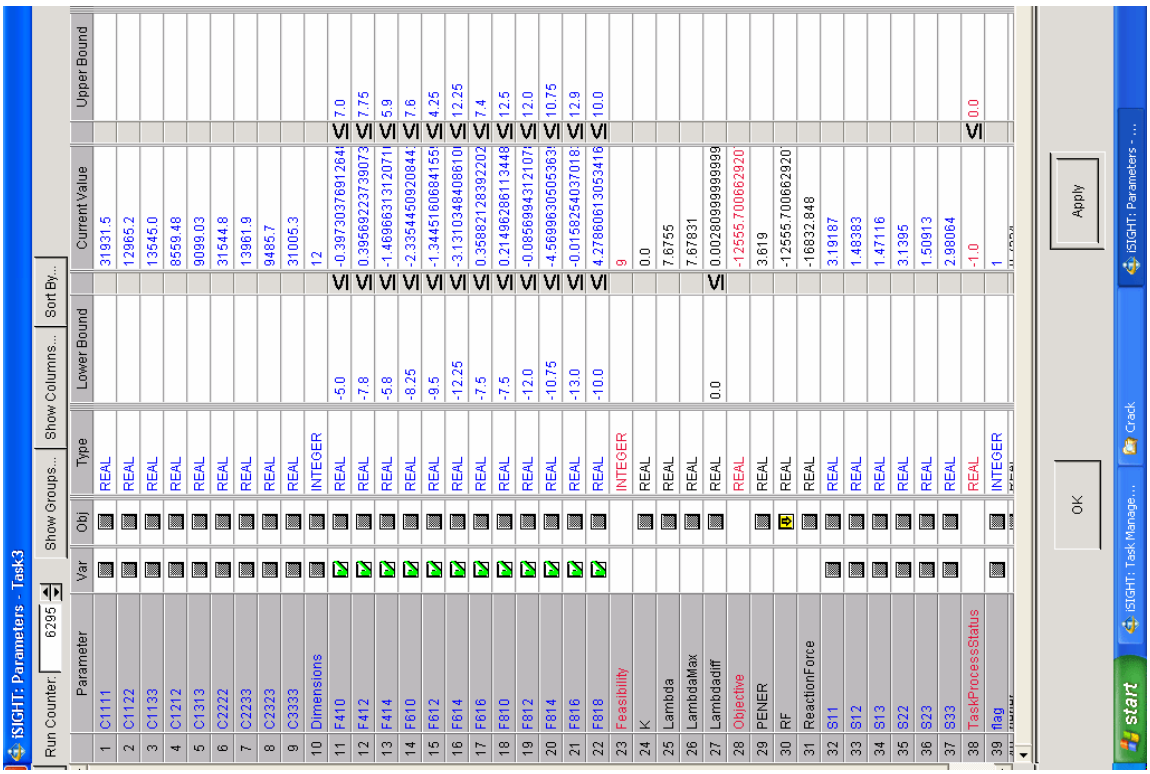


Figure 16 The iSIGHT list of parameters including: the optimization variables (Fourier coefficients), properties (elastic and plastic) and optimization objective (reaction force).

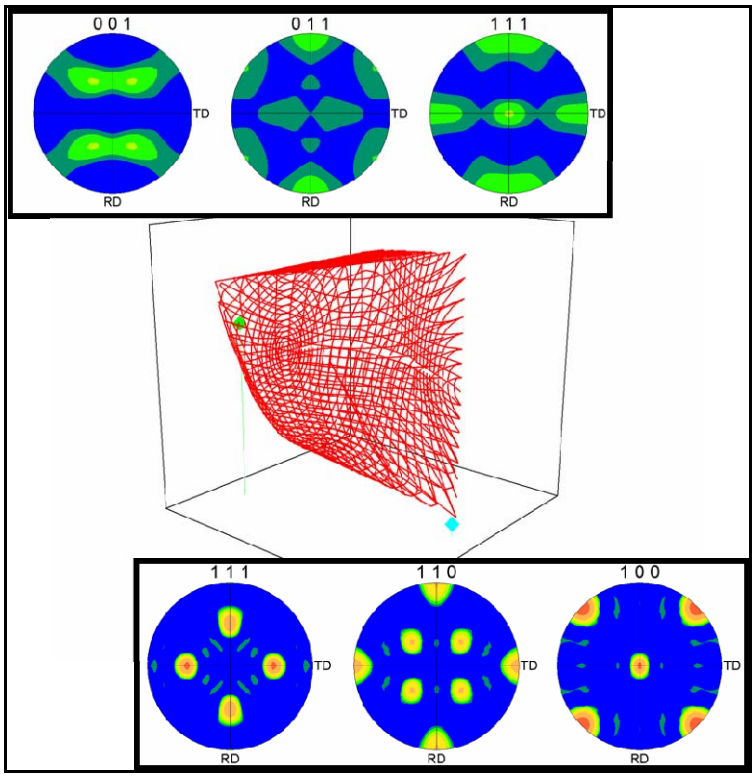


Figure 17 The optimal (highest load carrying capacity) texture is shown in pole figures (top) and in the first three non-zero dimensions of the microstructure hull (green). The minimum performance pole figures (bottom) and Fourier coefficient are shown (blue).

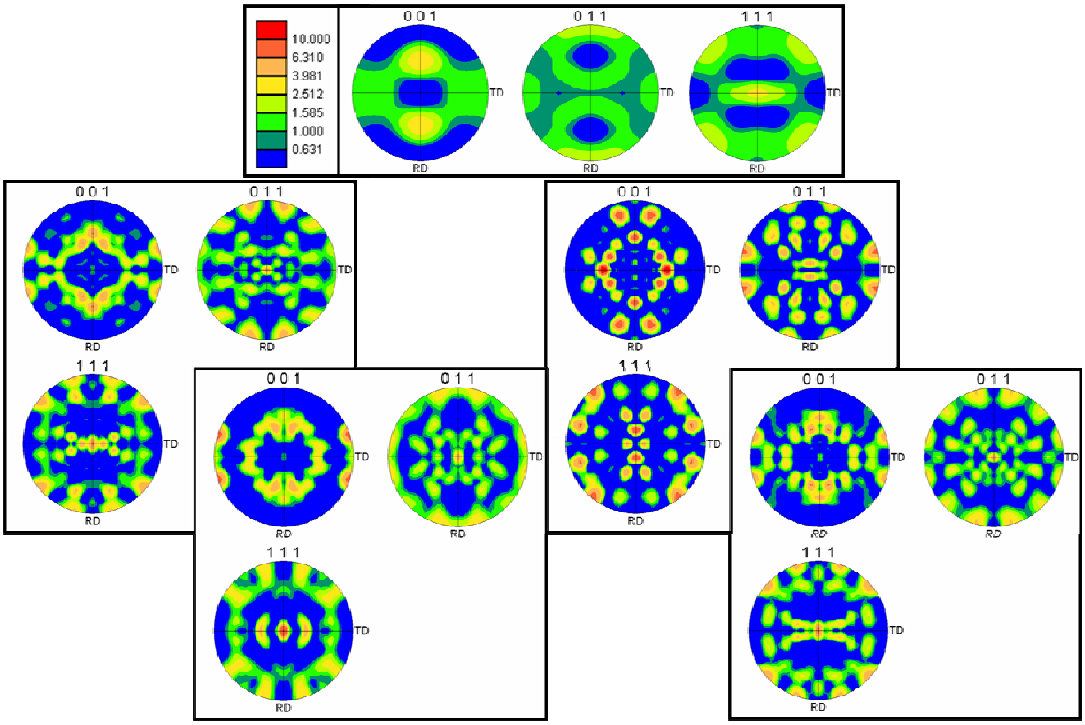


Figure 18 Several different instantiations of microstructures with the first seven identical coefficients.

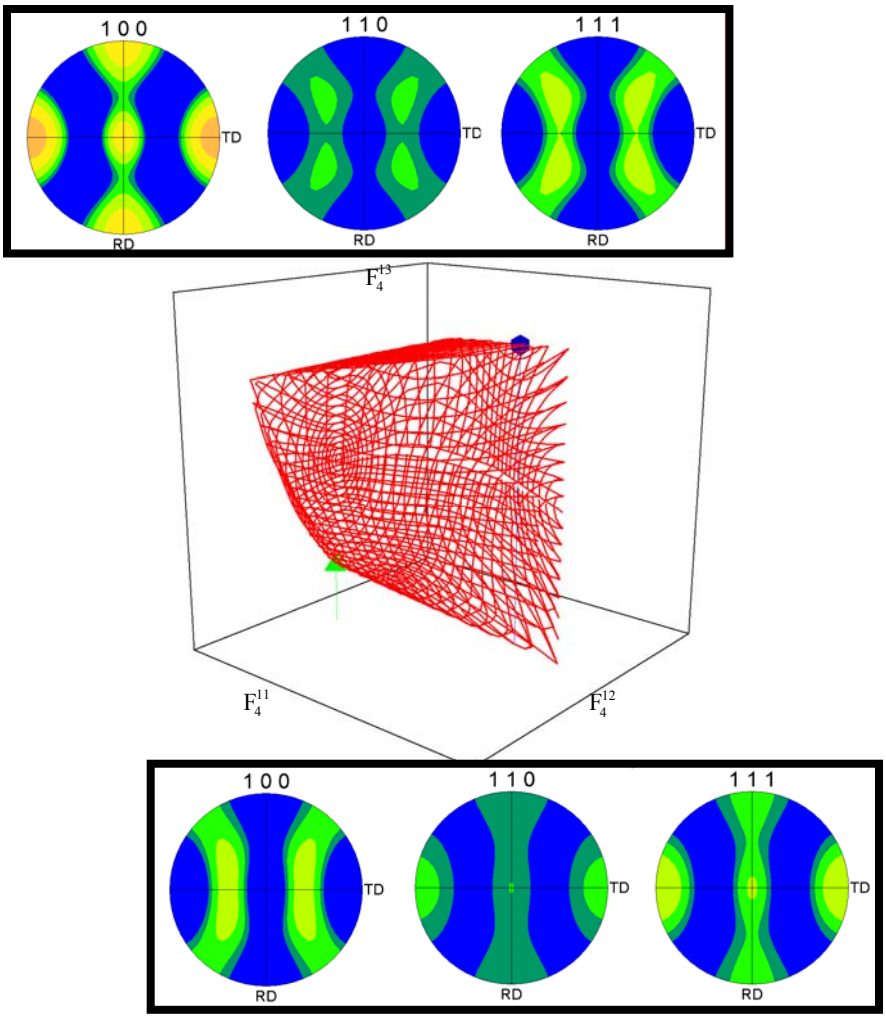


Figure 19 The pole figures for maximum *J*-integral (top and blue circle) and minimum *J*-integral (bottom and green triangle) are shown for the pressure vessel with a part through axial flaw.

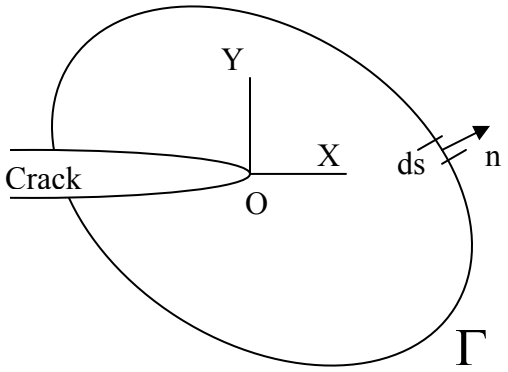


Figure 20 An elastic body containing a crack, the *J*-integral is calculated over the closed integral contour $\Gamma$.

# APPENDIX C J-INTEGRAL FORMULATION

Consider a nonlinear elastic body containing a crack, Figure 20 the *J*-integral is defined as

$$J = \int_{\Gamma} w dy - T_i \frac{\partial u_i}{\partial x} ds \tag{A.1}$$

Where

$$w = \int_0^{\varepsilon_{ij}} \sigma_{ij} d\varepsilon_{ij} \tag{A.2}$$

is the strain energy density,

$$T_i = \sigma_{ij} n_j \tag{A.3}$$

is the traction vector, $\Gamma$ is an arbitrary contour around the tip of the crack, n is the unit vector normal to $\Gamma$; $\sigma$, $\varepsilon$, and $u$ are the stress, strain, and displacement field, respectively. By tradition $\Gamma$ is taken as a smooth curve around the crack front.

Rice, J. R., 1968 [72], showed that the *J*-integral is a path-independent line integral and it represents the strain energy release rate of linear or nonlinear elastic materials:

$$J = \frac{d\Pi}{dA} \tag{A.4}$$

where $\Pi = U - W$ is the potential energy, the strain energy $U$ stored in the body minus the work $W$ done by external forces and A is the crack area.

The dimension of $J$ is

$$Dimension(J) = \frac{Energy}{Area} \tag{A.5}$$

For linear elastic materials, the *J*-integral is in fact the strain energy release rate, $G$, and both are related to the stress intensity factor K in the following fashion:

$$J = G = \begin{cases} \dfrac{K^2}{E} & \text{Plane Stress} \\ \dfrac{K^2}{E}\left(1-\nu^2\right) & \text{Plane Strain} \end{cases} \tag{A.6}$$

# APPENDIX D DERIVATION FOR CALCULATING FOURIER COEFFICIENTS FOR GENERAL SPHERICAL HARMONICS

Any function f(**g**) dependent on the lattice orientation g can be represented in Fourier series by generalized spherical harmonics:

$$f(g)=\sum_{l=0}^{\infty}\sum_{m=-l}^{+l}\sum_{n=l}^{+l}F_l^{mn}T_l^{mn}(g) \tag{A.1}$$

where $F_l^{mn}$ represent the Fourier coefficients of the function *f*(g) and $T_l^{mn}(g)$ are the generalized spherical harmonics. These harmonics for the complete set of orthonormal basis functions for SO(3) [104]. This representation is generalized for any crystal or sample symmetry. Using Euler angles defined by Bunge the generalized spherical harmonics are expressed as a function of $\varphi_1,\Phi,\varphi_2$ [48]

$$T_l^{mn}(g)=e^{im\varphi_2}P_l^{mn}(\cos\Phi)e^{in\varphi_1} \tag{A.2}$$

The $P_l^{mn}(\cos\Phi)$ function is an associated Legendre polynomial

$$\begin{aligned}P_l^{mn}(x)&=\frac{(-1)^{l-m}i^{n-m}}{2^l(l-m)!}\left[\frac{(l-m)!(l+n)!}{(l+m)!(l-n)!}\right]^{1/2}\\ &*(1-x)^{-\left(\frac{n-m}{2}\right)}(1+x)^{-\left(\frac{n+m}{2}\right)}\frac{d^{l-n}}{dx^{l-n}}\left[(1-x)^{l-m}(1+x)^{l+m}\right]\end{aligned} \tag{A.3}$$

The Legendre polynomial is purely real if m+n is even and purely imaginary if m+n is odd. Since the in fact form an orthonormal basis yields [48]

$$\iiint_{SO(3)}T_l^{mn}(g)T_{l'}^{*m'n'}(d)dg=\frac{\delta_{ll'}\delta_{mm'}\delta_{nn'}}{2l+1} \tag{A.4}$$

where $\delta_{ij}$ represents the Kronecker delta function. dg represents the invariant measure that can be expressed in a function of Euler angles

$$dg = \frac{1}{8\pi^2}\sin\Phi d\varphi_1 d\Phi d\varphi_2 \tag{A.5}$$

To determine the Fourier coefficient $F_l^{mn}$ for any function f(g), the procedure is as follows. Multiplying both sides of Eq. (A.1) by the conjugate of one of the spherical harmonic functions

$$f(g)T_{l'}^{*m'n'}(g) = \sum_{l=-0}^{\infty}\sum_{m=-l}^{+l}\sum_{n=-l}^{+l} F_l^{mn}T_l^{mn}(g)T_{l'}^{*m'n'}(g) \tag{A.6}$$

Eq. A.6 is then integrated on each side over SO(3) (or where symmetries are accounted for the FZ, SO(3)/G),

$$\iiint_{SO(3)} f(g)T_{l'}^{*m'n'}(g) = \sum_{l=-0}^{\infty}\sum_{m=-l}^{+l}\sum_{n=-l}^{+l} F_l^{mn}\iiint_{SO(3)} T_l^{mn}(g)T_{l'}^{*m'n'}(g)dg \tag{A.7}$$

Using the normalization from Eq. (A.4)

$$\iiint_{SO(3)} f(g)T_{l'}^{*m'n'}(g) = \sum_{l=-0}^{\infty}\sum_{m=-l}^{+l}\sum_{n=-l}^{+l} F_l^{mn}\frac{\delta_{ll'}\delta_{mm'}\delta_{nn'}}{2l+1} = \frac{F_{l'}^{m'n'}}{2l+1} \tag{A.8}$$

If the function f(g) represents the microstructure of a single state, it can be defined using Dirac's function $\delta(g-g_i)$ defined as

$$\iiint_{\Omega}\delta(g-g_i)dg = \begin{cases} 1 if g_i \in \Omega \\ 0 otherwise \end{cases} \tag{A.9}$$

Where $\Omega$ is the domain of single states. By substituting Eq. (A.9) into (A.8) for f(g) the Fourier coefficients for a single state can be evaluated [48] as

$$F_l^{mn} = (2l+1)T_l^{*mn}(g_i) \tag{A.10}$$

Using Eqs (A.2), (A.3), and (A.10), it can be shown the first term in the Fourier series is always equal to one, $F_0^{00} = 1$ for any texture.

If the microstructure is not a single state, and consists of multiple crystal orientations (as a polycrystal) the Fourier coefficients are in proportion to the volume fraction $(\alpha)$ of that state [48].

$$F_l^{mn} = (2l+1)\frac{\sum_j \alpha_j T_l^{*mn}(g)}{\sum_j \alpha_j}; \sum_j \alpha_j = 1$$

# APPENDIX E ELASTICITY HOMOGENIZATION SOURCECODE

The following is the source code for the effective elastic properties:

```
/*
//Elastic 1.0
//this code is used to calculate the upper bound values of all the
//components of the stiffness tensor of a cubic-orthorhombic material
//
//Elastic 1.1
//this code has been modified to be used with the Fourier coefficients
//of the microstructure taking into account the factor (2l+1)
//Gwenaelle Proust

//Elastic 2.0
//    This code has been updated:
//          Pi has be correctly defined
//          Format of code has compartmentalized
//          Code has been setup to calculate elastic stiffness for
//          multiple Fourier coefficients if desired.
//          Note this puts an integer (number of coefficient triplets)
//                in the input file before FCoefficients.
//          Column Headers are inserted in the output.txt file.
//Josh Houskamp 4/22/2005

//Elastic 3.0 5/23/2005
//This code calculates the elastic constants for any large number of
// coefficients.
*/
#include<fstream.h>
#include<iostream.h>
#include<istream.h>
#include<math.h>
#include<iomanip.h>
#define PI                    4*atan(1)

double MIN (double a, double b){
      if (a<b) return a;
      else return b;
}

int main(){
      char buffer[256];
      //Open the file for the microstructure coefficients
      double F[4];
      F[0]=1;                 //F000 is always egual to 1
      double coef[24];
      double consC[3], consS[3];

      //Reads the basic elastic Constants (C11,C12,C44,S11,S12,S44)
      ifstream elastic ("elastic.txt");
      while ( elastic.eof() ){
```

```
            elastic.getline(buffer,100);
      }
      elastic>>consC[0]>>consC[1]>>consC[2]>>consS[0]>>consS[1]>>\
            consS[2];
      elastic.close();

      //Reads the Property-Fourier Coefficients
      ifstream coeff ("coef.txt");
      if ( ! coeff.is_open()){
            cout<< "error opening coef file"; return (1);
      }
      while ( coeff.eof() ){
            coeff.getline(buffer,100);
      }
      for (int i=0; i<24;i++) coeff>>coef[i];
      coeff.close();

      //Reads Microstructure Coefficients (for more than one
      //microstructure)

      ofstream outputfile ("Econsts.txt");
      ifstream Fcoefficient ("Fcoefficient.txt");

      int NumCoeffs=1;
      if (! Fcoefficient.is_open()){
            cout << "Error opening Fcoefficient file"; return (1);
      }
      //
      ////Uncomment the following line
      Fcoefficient>> NumCoeffs ;

      if (outputfile.is_open()){
            outputfile<< "C1111\tC2222\tC3333\tC1212\tC1313\
                  tC2323\tC1122\tC1133\tC2233\n";
            for(int l=0;l<NumCoeffs;l++){
                  Fcoefficient >>F[1]>>F[2]>>F[3];
                  for (int i=1;i<4;i++) F[i]=F[i]/9;
//we divide the Fourier coefficients by 2l+1. in this case l=4 b/c only
//elastic properties
                  double A[6]; //A[0]=A1111; A[1]=A2222; A[2]=A3333;
                               //A[3]=A1212; A[4]=A1313; A[5]=A2323
                  for (int k=0;k<6;k++) A[k]=0;
                  for (int j=0; j<4; j++){
                        A[0]=A[0]+F[j]*coef[j];
                        A[1]=A[1]+F[j]*coef[j+4];
                        A[2]=A[2]+F[j]*coef[j+8];
                        A[3]=A[3]+F[j]*coef[j+12];
                        A[4]=A[4]+F[j]*coef[j+16];
                        A[5]=A[5]+F[j]*coef[j+20];
                  }
                  double C[9],S[6];
// Calculation of the volume average of all the stiffness and
//compliance components
                  for(int jj=0;jj<9;jj++) C[jj]=0;
                  for( jj=0;jj<6;jj++) S[jj]=0;
                  //C1111
                  C[0]=consC[1]+2*consC[2]+(consC[0]-consC[1]\
```

```
      -2*consC[2])*A[0];
//C2222
C[1]=consC[1]+2*consC[2]+(consC[0]-consC[1]\
      -2*consC[2])*A[1];
//C3333
C[2]=consC[1]+2*consC[2]+(consC[0]-consC[1]\
      -2*consC[2])*A[2];
//C1212
C[3]=consC[2]+(consC[0]-consC[1]-2*consC[2])*A[3];
//C1313
C[4]=consC[2]+(consC[0]-consC[1]-2*consC[2])*A[4];
//C2323
C[5]=consC[2]+(consC[0]-consC[1]-2*consC[2])*A[5];
//C1122
C[6]=consC[1]+(consC[0]-consC[1]-2*consC[2])*A[3];
//C1133
C[7]=consC[1]+(consC[0]-consC[1]-2*consC[2])*A[4];
//C2233
C[8]=consC[1]+(consC[0]-consC[1]-2*consC[2])*A[5];
//S1111
S[0]=consS[1]+0.5*consS[2]+(consS[0]-consS[1]-0.5\
      *consS[2])*A[0];
//S2222
S[1]=consS[1]+0.5*consS[2]+(consS[0]-consS[1]-0.5\
      *consS[2])*A[1];
//S3333
S[2]=consS[1]+0.5*consS[2]+(consS[0]-consS[1]-0.5\
      *consS[2])*A[2];
//S1122
S[3]=consS[1]+(consS[0]-consS[1]-0.5*consS[2])*A[3];
//S1133
S[4]=consS[1]+(consS[0]-consS[1]-0.5*consS[2])*A[4];
//S2233
S[5]=consS[1]+(consS[0]-consS[1]-0.5*consS[2])*A[5];

//Inversion of the volume average compliance tensor
double Sinv1111=0, Sinv2222=0, Sinv3333=0,\
      Sinv1122=0, Sinv1133=0, Sinv2233=0,\
      determinant=0;
determinant=S[0]*(S[1]*S[2]-S[5]*S[5])\
      -S[3]*(S[3]*S[2]-S[5]*S[4])+S[4]*(S[3]*S[5]\
      -S[1]*S[4]);
Sinv1111=(S[1]*S[2]-S[5]*S[5])/determinant;
Sinv2222=(S[0]*S[2]-S[4]*S[4])/determinant;
Sinv3333=(S[0]*S[1]-S[3]*S[3])/determinant;
Sinv1122=(S[4]*S[5]-S[3]*S[2])/determinant;
Sinv1133=(S[3]*S[5]-S[4]*S[1])/determinant;
Sinv2233=(S[5]*S[4]-S[3]*S[2])/determinant;

// Calculation of the off-diagonal bounds
double Cstar1122=0, Cstar1133=0, Cstar2233=0;
Cstar1122=MIN(C[6],Sinv1122)+sqrt(fabs(C[0]\
      -Sinv1111)*fabs(C[1]-Sinv2222));
Cstar1133=MIN(C[7],Sinv1133)+sqrt(fabs(C[0]\
      -Sinv1111)*fabs(C[2]-Sinv3333));
      //The following line corrected 4/18/05
```

```
                    Cstar2233=MIN(C[8],Sinv2233)+sqrt(fabs(C[1]-\
                          Sinv2222)*fabs(C[2]-Sinv3333));

                    //the output file order is: C1111, C2222, C3333,
                          // C1212, C1313, C2323, C1122, C1133, C2233
                    outputfile <<C[0]<<"\t"<<C[1]<<"\t"<<C[2]<<"\t"\
                                <<C[3]<<"\t"<<C[4]<<"\t"<<C[5]<<"\t"\
                                <<Cstar1122<<"\t"<<Cstar1133<<"\t"<<\
                                Cstar2233<<endl;
               }
          }
          Fcoefficient.close();
          outputfile.close();
          return (0);
}
```

# APPENDIX F PLASTICITY HOMOGENIZATION SOURCECODE

The following is the source code for the effective plastic properties:

Please note that this source code is limited to taking only up to *l*=8 coefficients. The logic is not in place to expand this code to higher orders of spherical harmonics automatically.

```
/*
//Version 1.0 Gwenaelle Proust
//This program calculates the yield strength for different orientations
//knowing the Euler angles
//of each orientation and the coefficient of the polynomial functions
//used to describe the Fourier coefficients
//use the Newton-Raphson with bisection (to be sure of the convergence)
//technique for the calculation of q
//this code has been modified to take into account the factor 2l+1 in
//the Fourier coefficients of the microstructure
//this code will need to be modified if one wants to go further than 12
//dimensions in the Fourier space

//Version 1.1 Josh Houskamp 6/1/2005
      //Fixed definition of Pi. (though its not used?)
      //Fixed spelling errors in comments.
      //The Fcoefficient.txt file now reads an integer (the number of
//Fourier coefficients to calculate properies for)
      //then the sets of (12) fourier Coefficients.
      //Rearranged order or read file statements to facilitate reading
//multiple Fcoefficients.
*/

#include<fstream.h>
#include<iostream.h>
#include<istream.h>
#include<math.h>
#include<iomanip.h>
#include"qimproved.h"   //file for the calculation of q with the NR
                        //method
#define PI  4*datan(1)  //3.1415926535897931

//function to calculate the yield strength for a specific orientation
//given the value of q for S11
double yieldS11(double coef[7][3][13], double F[13], int numterms,\
double q){
      double f=0;
      for (int in1=0;in1<=numterms; in1++){
            double x=1;
            double factor=0;
            for (int in2=0;in2<7;in2++){
```

```
                  factor=factor+(coef[in2][0][in1]-0.5*\
                  (coef[in2][1][in1]+coef[in2][2][in1]))*x;
                  x=q*x;
            }
            f=f+factor*F[in1];
      }
      return f;
}

//function to calculate the yield strength for a specific orientation
//given the value of q for S22
double yieldS22(double coef[7][3][13], double F[13], int numterms,\
double q){
      double f=0;
      for (int in1=0;in1<=numterms; in1++){
            double x=1;
            double factor=0;
            for (int in2=0;in2<7;in2++){
                  factor=factor+(coef[in2][1][in1]-0.5*\
                  (coef[in2][0][in1]+coef[in2][2][in1]))*x;
                  x=q*x;
            }
            f=f+factor*F[in1];
      }
      return f;
}

//function to calculate the yield strength for a specific orientation
given the value of q for S33
double yieldS33(double coef[7][3][13], double F[13], int numterms,\
double q){
      double f=0;
      for (int in1=0;in1<=numterms; in1++){
            double x=1;
            double factor=0;
            for (int in2=0;in2<7;in2++){
                  factor=factor+(coef[in2][2][in1]-0.5*\
                  (coef[in2][1][in1]+coef[in2][0][in1]))*x;
                  x=q*x;
            }
            f=f+factor*F[in1];
      }
      return f;
}

int main () {
      ofstream opp ("q.txt");
      //Open the file for the microstructure coefficients
      int numberterms=13;
      int NumOries;
      double F[13];
      F[0]=1; //F000 is always egual to 1
      //read the coefficients form the file coef
      //coefficients for the normal stress S11
      double coefS11[7][3][13];
      //coefficients for the normal stress S22
      double coefS22[7][3][13];
```

```
//coefficients for the normal stress S33
double coefS33[7][3][13];
//coefficients for the 3 shear stresses S12, S13, S23 in this
//order
double cshear[3][13];
ifstream coeff ("input.txt");
if (! coeff.is_open()){
      cout << "Error opening file"; return (1);
}
//while (! coeff.eof() ){
//    coeff.getline (buffer,100);
//}
ifstream fin("input.txt");
if (fin){
      for (int ab3=0;ab3<3;ab3++){
            for (int ab4=0;ab4<13;ab4++){
      //read the coefficients for calculation
                  for (int ab5=0;ab5<7;ab5++){
                  // of normal stress S11
                        fin>>coefS11[ab5][ab3][ab4];
                  }
            }
      }
      for (int a=0;a<3;a++){
            for (int b=0;b<13;b++){
                  for (int c=0;c<7;c++){
                  //read the coefficients for calculation
                        fin>>coefS22[c][a][b];
                        // of normal stress S22
                  }
            }
      }
      for (int d=0;d<3;d++){
            for (int e=0;e<13;e++){
                  for (int f=0;f<7;f++){
                  //read the coefficients for calculation
                        fin>>coefS33[f][d][e];
                  //of normal stress S33
                  }
            }
      }
      for (int g=0; g<3; g++){
            for (int h=0; h<13; h++){
            //read the coefficeints for the 3 shear stresses
                  fin>>cshear[g][h];
            }
      }
}
else{
      cout<<"Error with input.txt file"<<endl;
}
fin.close();

ifstream Fcoefficient ("Fcoefficient.txt");
ofstream outputfile ("PlasticConst.txt");
if (! Fcoefficient.is_open()){
      cout << "Error opening Fcoefficient.txt file"; return (1);
```

```
        }
        //if(! outputfile.is_open())cout << "Error opening
              //Fcoefficient.txt file"; return (1);
        outputfile <<"S11\tS22\tS33\tTau12\tTau23\tTau13\n";
        Fcoefficient>>NumOries;
        for(int k=0;k<NumOries;k++){

        Fcoefficient>>F[1]>>F[2]>>F[3]>>F[4]>>F[5]>>F[6]>>F[7]>>F[8]>>\
              F[9]>>F[10]>>F[11]>>F[12];
              //Fcoefficient.close();
              for (int i=1;i<4;i++) F[i]=F[i]/9;
                    //divide by 2l+1 for l=4
              for (i=4;i<8;i++) F[i]=F[i]/13;
                    //divide by 2l+1 for l=6
              for (i=8;i<13;i++) F[i]=F[i]/17;
                    //divide by 2l+1 for l=8
              char buffer[256];

              if (outputfile.is_open()){
                    double q;
                    double solution;

                    //FIND THE RIGHT VALUE OF q FOR THE NORMAL STRESS S11
                          //CONDITION: SIGMA22=SIGMA33
                    q=qcalculS11(coefS11,F,numberterms-1);
                    opp<<q<<endl;
                    solution=yieldS11(coefS11, F, numberterms-1, q);
                    outputfile <<solution<<"\t";

                    //FIND THE RIGHT VALUE OF q FOR THE NORMAL STRESS S22
                          //CONDITION: SIGMA11=SIGMA33
                    q=qcalculS22(coefS22,F,numberterms-1);
                    solution=yieldS22(coefS22, F, numberterms-1, q);
                    outputfile <<solution<<"\t";

                    //FIND THE RIGHT VALUE OF q FOR THE NORMAL STRESS S33
                          //CONDITION: SIGMA11=SIGMA22
                    q=qcalculS33(coefS33,F,numberterms-1);
                    solution=yieldS33(coefS33, F, numberterms-1, q);
                    outputfile <<solution<<"\t";
                    //CALCULATE THE NORMAL SHEAR STRESSES ORDER TAU12,
                          //TAU23, TAU 13
                    double shear[3];
                    for (int aa=0; aa<3; aa++) shear[aa]=0;
                    for (int bb=0; bb<3; bb++){
                          for (int cc=0;cc<13;cc++) shear[bb]=\
                                shear[bb]+F[cc]*cshear[bb][cc];
                          outputfile<<shear[bb]<<"\t";
                    }
                    outputfile<<endl;
              }
        }
        Fcoefficient.close();
        outputfile.close();
        return (0);
}
```

# APPENDIX G ISIGHT FILE PARSING

The following code is the ASCII version of the file parsing technique used to read the ABAQUS output file. Please note that this file will need to change if another model is used.

```
File Parse
PENER = 0.0
   ReactionForce = 0.0
   reactionforce = 0.0
   while ( $PENER  <  0.6 ) {
      find "THE FOLLOWING TABLE IS PRINTED AT THE NODES FOR ELEMENT
TYPE C3D8 AND ELEMENT SET" ignore
      find "MAXIMUM" ignore
      moveto word + 1
      read PENER as "%f"
      if ( $PENER  <  0.6 ) {
         pener = $PENER
         reactionforce = $ReactionForce
         ReactionForce = 0.0
      }
      find "THE FOLLOWING TABLE IS PRINTED FOR NODES BELONGING TO
NODE SET" ignore
      moveto line + 4
      ReactionForce = 0
      for ( i  =  0 ; $i  <=  49 ; i  =  $i + 1) {
         moveto word + 1
         read ReactionForceTemp as "%f"
         ReactionForce = $ReactionForce + $ReactionForceTemp
         if ( $PENER  <  0.6 ) {
            reactionforce = $ReactionForce
         }
      }
   }
   provide $reactionforce
   provide $pener
   provide $PENER
   provide $ReactionForce
```

# APPENDIX H ISIGHT MDOL FILE

This is the ASCII file description of the complete optimization of the hole in a plate case study.

```
MDOLVersion: 9.0
CompilerOptions: warn

Task Task0

   TaskHeader Task0
      Version: 1.0
      Evaluation: donotrun
      ControlMode: user
      RunCounter: 1
      BoundsPolicy: adjustvalue
      CheckPoint: unknown
   End TaskHeader Task0

   Outputs Task0
   End Outputs Task0

   Task Task1

      TaskHeader Task1
         Version: 1.0
         Evaluation: optimize GeneralizedReducedGradient
         ControlMode: user
         RunCounter: 6142
         BoundsPolicy: adjustvalue
         CheckPoint: unknown
      End TaskHeader Task1

      Inputs Task1
         Parameter: F410 Type: real InitialValue: 3.46074369675876
         Parameter: F412 Type: real InitialValue: -0.143433351842112
         Parameter: F414 Type: real InitialValue: -3.84449219014729
         Parameter: C1133 Type: real InitialValue: 14775.5
         Parameter: C2233 Type: real InitialValue: 10954.8
         Parameter: C1212 Type: real InitialValue: 6602.89
         Parameter: C1313 Type: real InitialValue: 11048.5
         Parameter: C2323 Type: real InitialValue: 10908.4
```

```
            Parameter: C1111 Type: real InitialValue: 31938.3
            Parameter: C2222 Type: real InitialValue: 32078.5
            Parameter: C3333 Type: real InitialValue: 27632.8
            Parameter: C1122 Type: real InitialValue: 10260.3
            Parameter: S11 Type: real InitialValue: 2.77665
            Parameter: S22 Type: real InitialValue: 2.8129
            Parameter: S33 Type: real InitialValue: 2.69567
            Parameter: S12 Type: real InitialValue: 1.39785
            Parameter: S23 Type: real InitialValue: 1.69562
            Parameter: S13 Type: real InitialValue: 1.70494
            Parameter: F610 Type: real InitialValue: -1.39948880240132
            Parameter: F612 Type: real InitialValue: -0.39798046721264
            Parameter: flag Type: integer InitialValue: 1 Description: "Flag tells the hull
bounds program to continue"
            Parameter: F614 Type: real InitialValue: -3.22610129852194
            Parameter: F616 Type: real InitialValue: 0.445090984535687
            Parameter: Dimensions Type: integer InitialValue: 12
            Parameter: F810 Type: real InitialValue: 8.57364442011326
            Parameter: F812 Type: real InitialValue: -0.186979154789191
            Parameter: F814 Type: real InitialValue: -4.77055852704273
            Parameter: F816 Type: real InitialValue: -0.498726533054286
            Parameter: F818 Type: real InitialValue: 6.59657383054447
         End Inputs Task1

         Outputs Task1
            Parameter: Lambda Type: real
            Parameter: LambdaMax Type: real
            Parameter: Lambdadiff Type: real
            Parameter: ReactionForce Type: real
            Parameter: K Type: real
            Parameter: PENER Type: real
            Parameter: reactionforce Type: real
            Parameter: pener Type: real
            Parameter: RF Type: real
         End Outputs Task1

         Calculations Task1
            Calculation Lambda
               Parameters
                  F410 F412 F610 F414 F612 F810 F614 F812 F616 F814
                  F816 F818 Lambda
               Statements
                  Lambda =
sqrt(F410^2+F412^2+F414^2+F610^2+F612^2+F614^2+F616^2+F810^2+F812^2+F81
4^2+F816^2+F818^2)
               End Statements
```

```
        End Calculation Lambda

        Calculation GPaTOMPa1
          Parameters
            C2323 C2233 C1212 C1122 C3333 C2222 C1313 C1133 C1111
          Statements
            C1111 = C1111*1000
            C1122 = C1122*1000
            C1133 = C1133*1000
            C1212 = C1212*1000
            C1313 = C1313*1000
            C2222 = C2222*1000
            C2233 = C2233*1000
            C2323 = C2323*1000
            C3333 = C3333*1000
          End Statements
        End Calculation GPaTOMPa1

        Calculation Calculation4
          Parameters
            reactionforce ReactionForce pener PENER RF
          Statements
            RF = ((ReactionForce-reactionforce)/(PENER-pener))*(0.6-
pener)+reactionforce
          End Statements
        End Calculation Calculation4
      End Calculations Task1

      SimCode GPHULL
        InputFiles GPHULL
          FileDescription directiontxt
            FileType: standard
            TemplateFile: "iSIGHT_direction.txt"
            InputFile: "direction.txt"
            Parameters
              F410 F412 F414 F610 F612 F614 F616 F810 F812 F814
              F816 F818
            Instructions
              require F810 F812 F814 F816 F818
              require F614 F616
              require F610 F612
              require F410 F412 F414
              moveto word + 1
              replace word with $F410 as "%f"
              replace word with $F412 as "%f"
              replace word with $F414 as "%f"
```

```
            replace word with $F610 as "%f"
            replace word with $F612 as "%f"
            replace word with $F614 as "%f"
            replace word with $F616 as "%f"
            replace word with $F810 as "%f"
            replace word with $F812 as "%f"
            replace word with $F814 as "%f"
            replace word with $F816 as "%f"
            replace word with $F818 as "%f"
         End Instructions
      End FileDescription directiontxt
   End InputFiles GPHULL

   OutputFiles GPHULL
      FileDescription LambdaMaxtxt
         FileType: standard
         OutputFile: "LambdaMax.txt"
         Parameters
            LambdaMax Lambda Lambdadiff
         Instructions
            find "Lambda =" ignore
            read Lambda as "%f"
            provide $Lambda
            find "=" ignore
            read LambdaMax as "%f"
            provide $LambdaMax
            Lambdadiff = $LambdaMax - $Lambda
            provide $Lambdadiff
         End Instructions
      End FileDescription LambdaMaxtxt
   End OutputFiles GPHULL

   SimCodeProcess GPHULL
      Program: "./Hull12D.exe"
      ProcessType: transient
      Environment: unrestored
      ElapseTime: 5m
      Prologue
         WriteInputSpecs: directiontxt
      Epilogue
         ReadOutputSpecs: LambdaMaxtxt
   End SimCodeProcess GPHULL

End SimCode GPHULL

SimCode ElasticConstants1
```

```
InputFiles ElasticConstants1
   FileDescription Fcoefficienttxt
      FileType: standard
      TemplateFile: "iSIGHT_Fcoefficient.txt"
      InputFile: "Fcoefficient.txt"
      Parameters
         F410 F412 F414 F610 F612 F614 F616
      Instructions
         require F614 F616
         require F610 F612
         require F410 F412 F414
         moveto word + 1
         replace word with $F410 as "%f"
         replace word with $F412 as "%f"
         replace word with $F414 as "%f"
      End Instructions
   End FileDescription Fcoefficienttxt
End InputFiles ElasticConstants1

OutputFiles ElasticConstants1
   FileDescription Econststxt
      FileType: standard
      OutputFile: "Econsts.txt"
      Parameters
         C1111 C2222 C3333 C1212 C1313 C2323 C1122 C1133 C2233
      Instructions
         moveto line + 1
         read C1111 as "%f"
         provide $C1111
         read C2222 as "%f"
         provide $C2222
         read C3333 as "%f"
         provide $C3333
         read C1212 as "%f"
         provide $C1212
         read C1313 as "%f"
         provide $C1313
         read C2323 as "%f"
         provide $C2323
         read C1122 as "%f"
         provide $C1122
         read C1133 as "%f"
         provide $C1133
         read C2233 as "%f"
         provide $C2233
      End Instructions
```

```
      End FileDescription Econststxt
   End OutputFiles ElasticConstants1

   SimCodeProcess ElasticConstants1
      Program: "./ElasticProps.exe"
      ProcessType: transient
      Environment: unrestored
      ElapseTime: 1m
      Prologue
         WriteInputSpecs: Fcoefficienttxt
      Epilogue
         ReadOutputSpecs: Econststxt
   End SimCodeProcess ElasticConstants1

End SimCode ElasticConstants1

SimCode PlasticConstants1
   InputFiles PlasticConstants1
      FileDescription Fcoefficienttxt
         FileType: standard
         TemplateFile: "iSIGHT_Fcoefficient.txt"
         InputFile: "Fcoefficient.txt"
         Parameters
            F410 F412 F414 F610 F612 F614 F616 F810 F812 F814
            F816 F818
         Instructions
            require F810 F812 F814 F816 F818
            require F614 F616
            require F410 F412 F414 F610 F612
            moveto word + 1
            replace word with $F410 as "%f"
            replace word with $F412 as "%f"
            replace word with $F414 as "%f"
            replace word with $F610 as "%f"
            replace word with $F612 as "%f"
            replace word with $F614 as "%f"
            replace word with $F616 as "%f"
            replace word with $F810 as "%f"
            replace word with $F812 as "%f"
            replace word with $F814 as "%f"
            replace word with $F816 as "%f"
            replace word with $F818 as "%f"
         End Instructions
      End FileDescription Fcoefficienttxt
   End InputFiles PlasticConstants1
```

```
   OutputFiles PlasticConstants1
      FileDescription PlasticConsttxt
         FileType: standard
         OutputFile: "PlasticConst.txt"
         Parameters
            S11 S22 S33 S12 S23 S13
         Instructions
            moveto line + 1
            read S11 as "%f"
            provide $S11
            read S22 as "%f"
            provide $S22
            read S33 as "%f"
            provide $S33
            read S12 as "%f"
            provide $S12
            read S23 as "%f"
            provide $S23
            read S13 as "%f"
            provide $S13
         End Instructions
      End FileDescription PlasticConsttxt
   End OutputFiles PlasticConstants1

   SimCodeProcess PlasticConstants1
      Program: "./PlasticConst1.1.exe"
      ProcessType: transient
      Environment: unrestored
      ElapseTime: 30s
      Prologue
         WriteInputSpecs: Fcoefficienttxt
      Epilogue
         ReadOutputSpecs: PlasticConsttxt
   End SimCodeProcess PlasticConstants1

End SimCode PlasticConstants1

SimCode Abaqus
   InputFiles Abaqus
      FileDescription abaqusUSETHISinp
         FileType: standard
         TemplateFile: "iSIGHT_abaqus_USETHIS.inp"
         InputFile: "abaqus_USETHIS.inp"
         Parameters
            C1133 C2233 C1212 C1313 C2323 C1111 C2222 C3333 C1122 S11
            S22 S33 S12 S23 S13
```

```
      Instructions
         require S11 S22 S33 S12 S23 S13
         require C1313 C2323 C1111 C2222 C3333 C1122 C1133 C2233 C1212
         find "*Elastic, type=ORTHOTROPIC" ignore
         moveto $Line_Start
         moveto line + 1
         delimiter ","
         replace word with $C1111
         replace word with $C1122
         replace word with $C2222
         replace word with $C1133
         replace word with $C2233
         replace word with $C3333
         replace word with $C1212
         replace word with $C1313
         moveto $Line_Start
         moveto line + 1
         replace word with $C2323
         find "*Potential" ignore
         moveto $Line_Start
         moveto $Line_Start
         moveto line + 1
         replace word with $S11
         replace word with $S22
         replace word with $S33
         S12 = $S12 * sqrt( 3 )
         S13 = $S13 * sqrt( 3 )
         S23 = $S23 * sqrt( 3 )
         replace word with $S12
         replace word with $S13
         replace word with $S23
      End Instructions
   End FileDescription abaqusUSETHISinp
End InputFiles Abaqus

OutputFiles Abaqus
   FileDescription NickelPureElasticdat
      FileType: standard
      OutputFile: "Nickel-PureElastic.dat"
      Parameters
         ReactionForce PENER reactionforce pener
      InstructionFile: "includedinMDOL1554082316.fdc"
   End FileDescription NickelPureElasticdat
End OutputFiles Abaqus

SimCodeProcess Abaqus
```

```
   ScriptLanguage: DOSBatch
   Script
      c: cd \Research\iSIGHT12d
      del Nickel-PureElastic.dat
      del Nickel-PureElastic.msg
      del Nickel-PureElastic.log
      del Nickel-PureElastic.sta
      del Nickel-PureElastic.com
      del Nickel-PureElastic.fil
      del Nickel-PureElastic.spc
      del Nickel-PureElastic.ipm
      del Nickel-PureElastic.mdl
      del Nickel-PureElastic.odb
      del Nickel-PureElastic.prt
      del Nickel-PureElastic.res
      del Nickel-PureElastic.stt
      del abaqus.rpy
      del Nickel-PureElastic.lck
      abaqus job=Nickel-PureElastic input=abaqus_UseThis.inp interactive
   End Script
   ProcessType: asynchronous
   Environment: unrestored
   ElapseTime: 1h 40m
   AsynchronousRun
      AsyncFile: "Nickel-PureElastic.sta"
      AsyncPattern: "THE ANALYSIS HAS COMPLETED"
      AsyncDelay: 0s
   End AsynchronousRun
   Prologue
      WriteInputSpecs: abaqusUSETHISinp
   Epilogue
      ReadOutputSpecs: NickelPureElasticdat
   AuxiliaryOutputFiles: "Nickel-PureElastic.msg"
                         "Nickel-PureElastic.log"
                         "Nickel-PureElastic.sta"
                         "Nickel-PureElastic.com"
                         "Nickel-PureElastic.fil"
                         "Nickel-PureElastic.spc"
                         "Nickel-PureElastic.ipm"
                         "Nickel-PureElastic.mdl"
                         "Nickel-PureElastic.odb"
                         "Nickel-PureElastic.prt"
                         "Nickel-PureElastic.res"
                         "Nickel-PureElastic.stt"
                         "abaqus.rpt"
End SimCodeProcess Abaqus
```

```
End SimCode Abaqus

SimCode DeleteOutput
   SimCodeProcess DeleteOutput
      ScriptLanguage: DOSBatch
      Script
         del results.txt
      End Script
      ProcessType: transient
      Environment: unrestored
      ReturnCodes: 1
      ElapseTime: 1s
   End SimCodeProcess DeleteOutput

End SimCode DeleteOutput

SimCode DelAbaqusFiles
   SimCodeProcess DelAbaqusFiles
      ScriptLanguage: DOSBatch
      Script
         del Nickel-PureElastic.msg
         del Nickel-PureElastic.log
         del Nickel-PureElastic.sta
         del Nickel-PureElastic.com
         del Nickel-PureElastic.fil
         del Nickel-PureElastic.spc
         del Nickel-PureElastic.ipm
         del Nickel-PureElastic.mdl
         del Nickel-PureElastic.odb
         del Nickel-PureElastic.prt
         del Nickel-PureElastic.res
         del Nickel-PureElastic.stt
         del Nickel-PureElastic.lck
         del abaqus.rpt
      End Script
      ProcessType: transient
      Environment: unrestored
      ReturnCodes: 1
      ElapseTime: 5m
   End SimCodeProcess DelAbaqusFiles

End SimCode DelAbaqusFiles

TaskProcess Task1
   Control: [
```

```
      Sequential [
         DelAbaqusFiles
         DeleteOutput
         Lambda
         If (Lambda  !=  0.0) [
            GPHULL
         ]
         If (Lambdadiff >= 0.0) [
            Sequential [
               ElasticConstants1
               PlasticConstants1
               GPaTOMPa1
               Abaqus
               Calculation4
            ]
         ]
      ]
   ]
End TaskProcess Task1

Optimization Task1
   PotentialVariables:
      F410 F412 F414 C1133 C2233 C1212 C1313 C2323 C1111 C2222
      C3333 C1122 S11 S22 S33 S12 S23 S13 F610 F612
      flag F614 F616 Dimensions F810 F812 F814 F816 F818
   Variables:
      F410 F412 F414 F610 F612 F614 F616 F810 F812 F814
      F816 F818
   VariableScaling
      Parameter: F410 ScaleFactor: 1.0
      Parameter: F412 ScaleFactor: 1.0
      Parameter: F414 ScaleFactor: 1.0
      Parameter: C1133 ScaleFactor: 1.0
      Parameter: C2233 ScaleFactor: 1.0
      Parameter: C1212 ScaleFactor: 1.0
      Parameter: C1313 ScaleFactor: 1.0
      Parameter: C2323 ScaleFactor: 1.0
      Parameter: C1111 ScaleFactor: 1.0
      Parameter: C2222 ScaleFactor: 1.0
      Parameter: C3333 ScaleFactor: 1.0
      Parameter: C1122 ScaleFactor: 1.0
      Parameter: S11 ScaleFactor: 1.0
      Parameter: S22 ScaleFactor: 1.0
      Parameter: S33 ScaleFactor: 1.0
      Parameter: S12 ScaleFactor: 1.0
      Parameter: S23 ScaleFactor: 1.0
```

```
      Parameter: S13 ScaleFactor: 1.0
      Parameter: F610 ScaleFactor: 1.0
      Parameter: F612 ScaleFactor: 1.0
      Parameter: flag ScaleFactor: 1.0
      Parameter: F614 ScaleFactor: 1.0
      Parameter: F616 ScaleFactor: 1.0
      Parameter: Dimensions ScaleFactor: 1.0
      Parameter: F810 ScaleFactor: 1.0
      Parameter: F812 ScaleFactor: 1.0
      Parameter: F814 ScaleFactor: 1.0
      Parameter: F816 ScaleFactor: 1.0
      Parameter: F818 ScaleFactor: 1.0
    InputConstraints
      Parameter: F410 LowerBound: -5.0 UpperBound: 7.0
      Parameter: F412 LowerBound: -7.8 UpperBound: 7.75
      Parameter: F414 LowerBound: -5.8 UpperBound: 5.9
      Parameter: F610 LowerBound: -8.25 UpperBound: 7.6
      Parameter: F612 LowerBound: -9.5 UpperBound: 4.25
      Parameter: F614 LowerBound: -12.25 UpperBound: 12.25
      Parameter: F616 LowerBound: -7.5 UpperBound: 7.4
      Parameter: F810 LowerBound: -7.5 UpperBound: 12.5
      Parameter: F812 LowerBound: -12.0 UpperBound: 12.0
      Parameter: F814 LowerBound: -10.75 UpperBound: 10.75
      Parameter: F816 LowerBound: -13.0 UpperBound: 12.9
      Parameter: F818 LowerBound: -10.0 UpperBound: 10.0
    PotentialObjectives:
      Lambda LambdaMax Lambdadiff ReactionForce K PENER reactionforce
pener RF F410
      F412 F414 C1133 C2233 C1212 C1313 C2323 C1111 C2222 C3333
      C1122 S11 S22 S33 S12 S23 S13 F610 F612 flag
      F614 F616 Dimensions F810 F812 F814 F816 F818
    Objectives
      Parameter: RF Direction: maximize Weight: 1.0 ScaleFactor: 1.0
    OutputConstraints
      Parameter: Lambdadiff LowerBound: 0.0 Weight: 1.0 ScaleFactor: 1.0

    OptimizePlan SeqQuadProg
      DefaultUpperBound: 1.0E15
      UseScaling: yes
      OptimizeStep Step1
        Technique: "Sequential Quadratic Programming - NLPQL"
        Prologue
          RestoreBestSolution: no
          RerunTask: no
        Epilogue
          RestoreBestSolution: no
```

```
            RerunTask: no
         Options
            FiniteDifference: 0.01
            UseRestarts: yes
      Control: [
         Step1
      ]

   OptimizePlan GeneralizedReducedGradient
      DefaultUpperBound: 1.0E15
      UseScaling: yes
      OptimizeStep Step1
         Technique: "Generalized Reduced Gradient - LSGRG2"
         Prologue
            RestoreBestSolution: no
            RerunTask: no
         Epilogue
            RestoreBestSolution: no
            RerunTask: no
         Options
            GradientStepSize: 0.01
      OptimizeStep Step2
         Technique: "Sequential Quadratic Programming - NLPQL"
         Prologue
            RestoreBestSolution: yes
            RerunTask: no
         Epilogue
            RestoreBestSolution: yes
            RerunTask: no
         Options
      Control: [
         Step1
         Step2
      ]

   OptimizePlan ReducedGradient
      DefaultUpperBound: 1E15
      UseScaling: yes
      Control: [
      ]
End Optimization Task1

TaskPlan Task1
   StopTaskPlanOnError: no
   Control: [
      SeqQuadProg
```

```
            GeneralizedReducedGradient
         ]
      End TaskPlan Task1

      DataStorage Task1
         Restore: no
         DataLog: "Final_12Dmax.db" Mode: append
         DataLookUp: "Task1.db"
         MatchMode: Exact
         Levels: all
         StoreGradRuns: yes
         StoreApproxRuns: yes
      End DataStorage Task1

   End Task Task1

   End TaskProcess Task0

   Optimization Task0
      Variables: none
      VariableScaling

      # PLAN TO BE CONFIGURED BY ADVISOR:
      OptimizePlan PriorityRankedPlan
         Control: [
         ]
   End Optimization Task0

   TaskPlan Task0
      StopTaskPlanOnError: no
      Control: [
         PriorityRankedPlan
      ]
   End TaskPlan Task0

   DataStorage Task0
      Restore: no
      DataLog: "Task0.db" Mode: overwrite
      DataLookUp: "Task0.db"
      MatchMode: Exact
      Levels: all
      StoreGradRuns: yes
      StoreApproxRuns: yes
   End DataStorage Task0

End Task Task0
```

# APPENDIX I- ABBREVIATIONS

| | |
|---|---|
| CFRC | Continuous Fiber Reinforced Composites |
| FE | Finite Element |
| FEM | Finite Element Methods |
| HCD | Highly Constrained Design |
| MSD | Microstructure Sensitive Design |
| ODF | Orientation Distribution Function |
| FZ | Fundamental Zone |

# VITA

Joshua Robert Houskamp
Born: Cortland, NY July 31, 1978
Citizenship: United States of America

| | |
|---|---|
| 2005-2001 | Graduate Student and Research Assistant<br>Drexel University, Philadelphia, PA<br>Obtained: Ph.D. in Materials Science and Engineering<br>Advisor: Dr. Surya R. Kalidindi |
| 2001 | B.S. Drexel University Materials Engineering<br>Materials Engineering Department |

Teaching Experience

| | |
|---|---|
| 2003 - 2003 | Recitation Instructor / Supplemental Teaching Assistant<br>Drexel University, Materials Science and Engineering Department<br>He taught the two recitation sections for the Fundamentals of Materials, a core requirement for all Drexel University undergraduate engineers. |

Scholarship
He received the Koerner Family Fellowship for the 2004-2005 Academic Year.

ORAU Postdoctoral Fellowship at Army Research L abs, Aberdeen MD

He established a scholarship in 2005 for students continuing studies in science and engineering in his former high school, Cincinnatus Central School. The scholarship is intended to ease the burden of buying science textbooks for the first year of school.

Publications

Kalidindi, S.R., J.R. Houskamp, M. Lyons, and B.L. Adams, *Microstructure sensitive design of an orthotropic plate subjected to tensile load.* International Journal of Plasticity, 2004. **20**(8-9): p. 1561-1575.

Kalidindi, S. R., J. R. Houskamp, *Application of the Spectral Methods of Microstructure Design to Continuous Fiber Reinforced Composites.* Journal of Composite Materials, 2005 ***Submitted***.